QUATERNARY DEPOSITIONAL HISTORY
OF A SHELF- MARGIN MINIBASIN,
NORTHERN GULF OF MEXICO

A Thesis

Presented to

the Faculty of the Department of Earth and Atmospheric Sciences

University of Houston

In Partial Fulfillment

of the Requirements for the Degree

Master of Science

In Geology

By

Tucker Conklin

May 2015

QUATERNARY DEPOSITIONAL HISTORY

OF A SHELF- MARGIN MINIBASIN,

NORTHERN GULF OF MEXICO

Tucker Conklin

APPROVED:

Dr. Julia S. Wellner

Chair of Committee

Dr. William Sager

Dr. Peter Emmet

Dr. Kenneth Abdulah

Dean, College of Natural Sciences and Mathematics

Acknowledgements

I would like to thank my advisor, Dr. Julia Wellner for the opportunity to work under her for my degree. I cannot thank her enough for all of the support and advice that she has given me. I would also like to thank Dr. Pete Emmet for his help in getting this project started, and for his guidance throughout the duration of my time here. I would like to extend my appreciation to Dr. William Sager, and Dr. Kenneth Abdulah (BHP Billiton) for providing excellent feedback and advice in all stages of this project. I would also like to thank my parents, Doug and Joyce Conklin, and my fiancé, Drew Barnhart for their continued support throughout these last two years.

QUATERNARY DEPOSITIONAL HISTORY
OF A SHELF- MARGIN MINIBASIN,
NORTHERN GULF OF MEXICO

A Thesis

Presented to

the Faculty of the Department of Earth and Atmospheric Sciences

University of Houston

In Partial Fulfillment

of the Requirements for the Degree

Master of Science

In Geology

By

Tucker Conklin

April 2015

Abstract

High-resolution 3D seismic data were used to study the evolution of a shelf-margin minibasin located approximately 160 km off of the coast of Louisiana. Depositional packages were delineated and classified based on observed changes in internal characteristics and lapout patterns. Reconstruction of the depositional history of the minibasin reveals information relating to how depositional styles and architecture change over time in response to eustasy, sediment supply, and salt tectonics.

Four shelf-margin deltas were identified and classified into two categories: unstable fluvial-dominated deltas, and stable wave-dominated deltas. Slope failure driven by continued uplift of two salt diapirs bounding the study area on both the eastern and western flanks caused numerous mass-transport complexes to redeposit sediment throughout the minibasin. Slope channels contained within the deltaic packages erode into the underlying substrate, and functioned as a shelf to slope sediment bypass mechanism. Deltaic packages are sometimes capped by muddy transgressive wedges. Prodelta muds and hemipelagic drape deposits also fill portions of the minibasin.

A sequence stratigraphic framework was used in order to relate the sediment packages to the sea-level record. Deltaic deposition occurred during lowstand periods, and accounts for the largest packages present in the minibasin. Muddy wedges were sometimes deposited during major transgressions, with high amplitude continuous sediment deposits forming during highstands. Fluvial-dominated deltas show signs of a higher sediment supply and rate, which is indicated by syndepositional internal deformation and greater sediment thicknesses. The wave-dominated deltas present are

stable, with no observed deformation. The constraining effects of the minibasin in relation to the depositional styles of the deposits were also examined. In this regard when compared to their open shelf-edge counterparts, the deltas present were more likely to develop shelf to slope bypass systems in the form of slope channel complexes, regardless of wave or fluvial influence.

Table of Contents

List of Figures

1. Introduction

Understanding the interplay between eustasy, sediment supply, and salt tectonics is imperative in order to understand the role and growth of shelf-margin settings. Morton and Suter (1996) stated that shelf-margin deltas are the primary means by which shelf margins prograde and sedimentary basins fill. Therefore, understanding shelf-margin deltas leads to understanding the shelf-edge setting. One area where shelf-margin data are plentiful is the northern rim of the Gulf of Mexico. This location provides a unique setting where all three factors, eustasy, sediment supply, and salt tectonics, can be observed to have directly affected shelf-margin systems. This is due to the high number of fluvial systems that have, and are currently, supplying sediment to the Gulf, and the presence of diapiric activity starting at the shelf margin. By studying buried deltaic systems using seismic data, we can also infer the interplay of base level and sediment supply on the formation of deltaic deposits.

Modern deltaic settings are easily accessible and have been studied thoroughly in the Gulf of Mexico (Sydow and Roberts, 1994; Abdulah et al., 2004; Anderson et al., 2004; Wellner et al., 2004; Wellner et al., 2006; Perov and Bhattacharya, 2011) and worldwide (e.g. Bhattacharya and Willis, 2001; Bhattacharya and Giosan, 2003; Saller et al., 2004; Adedayo et al., 2005; Olariu and Bhattacharya, 2006; Dixon et al., 2012). Many 2D seismic studies have looked at and characterized shelf margin deltas based on external geometries and well log data (Suter and Berryhill, 1985; Wellner et al., 2004; Abdulah et al., 2004). More recent studies by former University of Houston researchers analyzed internal characteristics of specific delta complexes using the same dataset as the one used in this study (Perov, 2009; Lee, 2010; Perov and Bhattacharya, 2011).

Understanding the role of the shelf margin in providing a link for sediment delivery from the shelf to the basin floor is essential. Dixon et al. (2012) discuss the process of predicting sediment delivery to the basin floor by analyzing the types of deltas found on the shelf margin. The particular setting in this study, in which shelf-margin deltas are deposited within a confined minibasin setting instead of an open-margin setting, could also help further the understanding of shelf-to-basin sediment transport.

The dataset used in this study is a 3D seismic volume covering the outer shelf of West Louisiana (Fig. 1). The use of high-resolution 3D seismic data presents quite a few advantages over 2D data. High frequency and tightly gridded lines allow for the calculation of accurate thickness maps. Seismic data volume properties can also be calculated for entire intervals. These techniques provide data that can shed light on both external characteristics and internal characteristics of sediment packages contained within the minibasin. The results and conclusions presented in this study serve several purposes: 1) To reconstruct the Quaternary history of a shelf-margin minibasin by characterizing the different types of sediment packages that have been deposited through the Quaternary; 2) To further understand the role of eustacy, sediment supply, and in this case, localized salt tectonics on shelf-margin deposition; 3) To examine the impact of constricting shelf-margin deposition within a confined minibasin; and 4) To examine the effects on sediment transport from shelf to basin when the shelf margin becomes confined.

2. Geologic Background

The study area is located approximately 160 km off of the coast of Louisiana in an area with numerous salt domes (Fig. 1 A). Modern water depths in the study area range from 80 – 270 m (Fig. 1 B). During the early Jurassic, a layer of salt known as the Louann Salt, was deposited due to intermittent flooding of the basin (Pindell, 1985). The absence of major river systems carrying sediment to the area further aided the deposition of the salt layer (Salvador, 1987). During the Miocene, seven large river systems, the Norma, Rio Grande, Carriso, Corsar, Houston, Red, and Mississippi, began supplying vast amounts of sediment to the Gulf (Konyukhov, 2008). The loading of sediment on top of the salt stimulated the vertical salt movement in the form of diapirs. This sediment loading, combined with the tilting of the salt layer, caused further diapiric activity to occur.

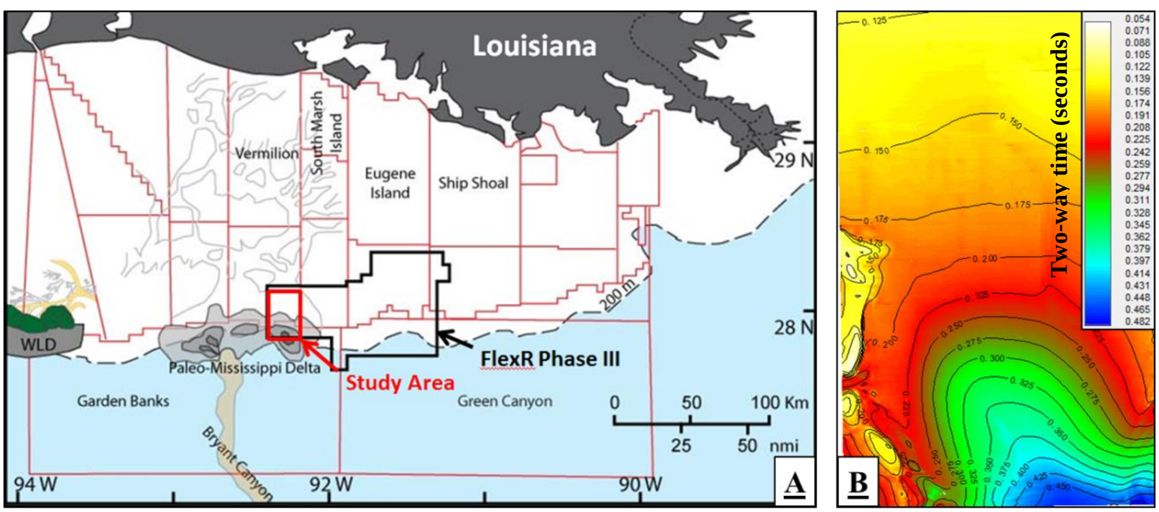

Figure 1. A) Location map showing the outline of the larger PGS dataset (FLEXR Phase III) in black, and the location of the smaller study area in red (Modified from Suter and Berryhill, 1985; Wellner et al., 2004). B) Bathymetry of the study area in two-way time in seconds.

The paleo-Mississippi river became the primary supply of clastic sediments to the study area starting in the Pliocene and continuing up to modern times (Galloway et al., 2011). Continued sediment loading and salt movement caused the shelf margin of the northern Gulf of Mexico to take its present-day shape. In the study area, there are two salt domes present that caused the initial formation of the minibasin, one in the southwest corner of the study area and one in the southeastern portion. The uplift of these diapirs has created an oval basin between the two uplifted areas (Fig. 2).

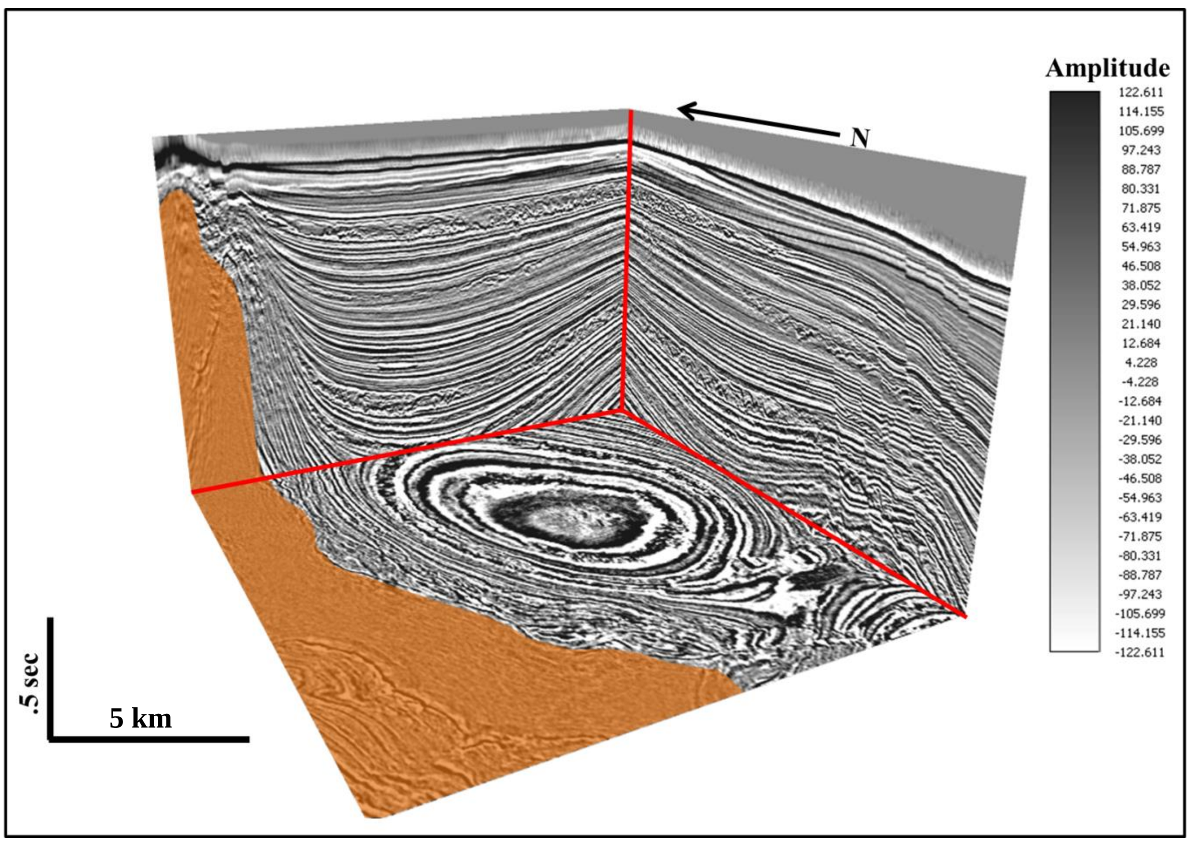

Figure 2. Inline (north to south), crossline (west to east), and timeslice at a depth of 2 seconds showing the location of one of the salt diapirs shaded in orange that cover the southwestern flank of the study area. Reflections filling the basin can be seen terminating against the salt.

3. Dataset and Methods

The 3D seismic dataset used in this study (Fig. 1) is part of a larger prestack time-migrated survey that was acquired by Petroleum Geo- Services and donated to the University of Houston. The total area of the cube is approximately 700 km^2 with inlines measuring 37 km and crosslines measuring approximately 19 km. The distance from inline to inline is 25 m, and 37.5 m from crossline to crossline. The survey was shot in an east to west direction and used bin dimensions of 12.5 x 40 m. The mean dominant frequency of the dataset is 33.5 Hz, which gives a vertical resolution in the data of roughly 16.5 m, and a horizontal resolution of 32.9 m (Rubio, 2010). A sound velocity of 1550 m/s was used to calculate rough estimates of thicknesses for various seismic packages.

The seismic dataset was analyzed using Kingdom 8.8 software suite which was donated to the University of Houston. Initial data inspection was done by standard data reconnaissance practices such as time slicing and cross section analyzation. Sediment packages were delineated by using horizon picking to interpret the tops and bases of packages based on lapout relationships and seismic reflection character as seen in strike and dip view. Each sediment package was then used as a building block to recreate the depositional history of the minibasin.

Six seismic facies were analyzed based on the work of Mitchum et al. (1977) and Berryhill et al. (1987), and were compared to those identified by Perov and Bhattacharya, (2011). These seismic facies were identified by similar seismic reflections being mappable in strike view, dip view, and map view (Sangree and Widmier, 1978). The classification of each seismic package was based on the seismic facies found within each unit. Isochron maps were generated for each sediment package in order to view the distribution of sediment for each individual unit, and to also locate the center of deposition for each unit. The thickest 40% of each package was then traced in order to outline each depocenter. These cores will be tracked throughout time later in the discussion section to see how they have migrated through time. Depocenter location also can aid in making references to where sediment was deposited in response to changes in sea level. Movement of depocenters towards the basin or towards the shelf can help to distinguish whether a package was deposited during periods of high, low, or transitioning base level.

The VATMIN attribute, which is an interval attribute that retains the most negative amplitude in the time range where both of the upper and lower surfaces have data, was calculated for most intervals. Minimum amplitude maps help identify deformation features as well as depositional features by highlighting changes in amplitude as some of these features do not show up as well in cross-section view. Proportional horizon slices were calculated through intervals of interest by dividing the package thickness into multiple, smaller intervals, and then using that interval thickness to obtain new horizon slices through one particular package (Fig. 3).

Sequence stratigraphic principles used in this study were based on pioneering work done by Vail et al. (1977) and Mitchum et al. (1977). Lapout relationships identified in seismic cross sections were used to help distinguish between three systems tracts. For this study three basic systems tracts are used, the highstand systems tract

(HST), lowstand systems tract (LST), and transgressive systems tract (TST). Key sequence stratigraphic surfaces can be placed between the systems tracts. The sequence boundary, which marks the transition from a high sea level to a falling and low sea level, is placed between the HST and the LST. The transgressive surface is placed between the TST and the LST, and the maximum flooding surface is placed at the base of the HST.

Deltaic packages are classified into one of two categories based on earlier work done by Porebski and Steel (2003, 2006). Unstable shelf-margin deltas are recognized by internal listric growth faults as well as rotational slides and slump features that can occur near the delta front. Stable shelf-margin deltas lack these deformation features and the clinoforms contained within them are generally more continuous in nature.

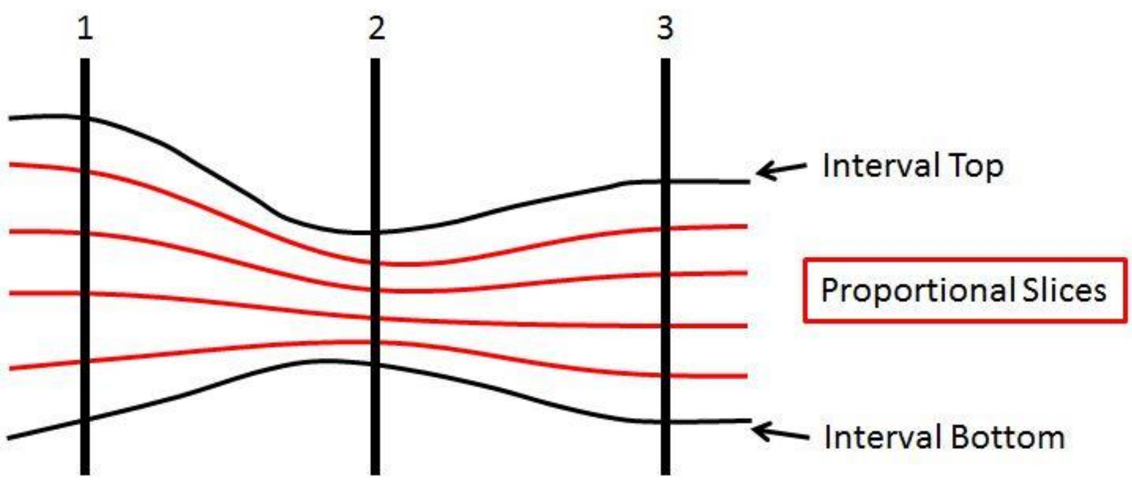

Figure 3. Cartoon displaying the creation of proportional horizon slices through an interval of interest. The interval thickness would in this case have been divided by 5 to obtain values to create four new slices. Then the new proportional value would be added on to the newest slice repeatedly to create multiple, new slices. At location 1 the thicknesses between each new horizon is the same, as is true for locations 2, and 3.

4. Results

4.1 Seismic Facies 1

Seismic facies 1 (SF1) shown in Figure 4 is interpreted as unstable shelf-margin deltaic sediments. It is made up of high amplitude oblique tangential clinoforms that dip gently to the south. Strike-view profiles of this facies show subparallel continuous reflections that conform to the shape of the minibasin. SF 1 tends to have an erosional bottom surface with reflectors either downlapping against this surface or gently grading into subparallel continuous reflections in the southernmost portion of the study area. Internal, syndepositional deformation is present in the form of listric growth faults also observed by Perov and Bhattacharya (2011). Perov and Bhattacharya also determined that the maximum height and length of the clinoforms found in SF 1 are 100m and 7km respectively. Well-log data from their study also showed upward-coarsening, funnel-shaped features similar to those found in sandy, prograding deltaic sequences. Volume amplitude minimum maps of this facies show slump-type concentrations of the higher amplitude sediments found near the southern ends of the deltas.

4.2 Seismic Facies 2

Seismic facies 2 (SF 2) shown in Figure 4 is interpreted as stable shelf-margin deltaic sediments. In dip view this facies is represented by medium to low amplitude, gently dipping clinoforms. Strike-view reflections are parallel to sub-parallel, and continuous. The base of SF 2 is erosional in some places of the study area, but to a lesser degree than the base of SF 1. Reflections downlap against the top of underlying SF 6 units, and this lapout is best seen in dip view. Well-log data shown in the Lee (2010) study display upward fining parasequences in this facies, with the overall unit composition being represented by a silty to muddy lithology.

4.3 Seismic Facies 3

Seismic facies 3 (SF 3) is interpreted as sandy, slope channels. Dip view of the slope channels show high-amplitude sub-parallel reflections that lap out against the erosional base. The channels are best seen in strike view, where the v- shaped erosion is easily observed, and where they cut into the underlying facies. Seismic reflections found within the erosional channels have a low continuity, and have a somewhat chaotic pattern in certain areas. The contact between SF 3 and the facies above is sinuous, and as observed by Perov and Bhattacharya (2011), bulges directly over the center of the channels. The amplitudes of the SF 3 units are the highest found in the study area, and, since they usually erode into, and are also overlain by lower amplitude reflections, have an exaggerated contrast between the surrounding units.

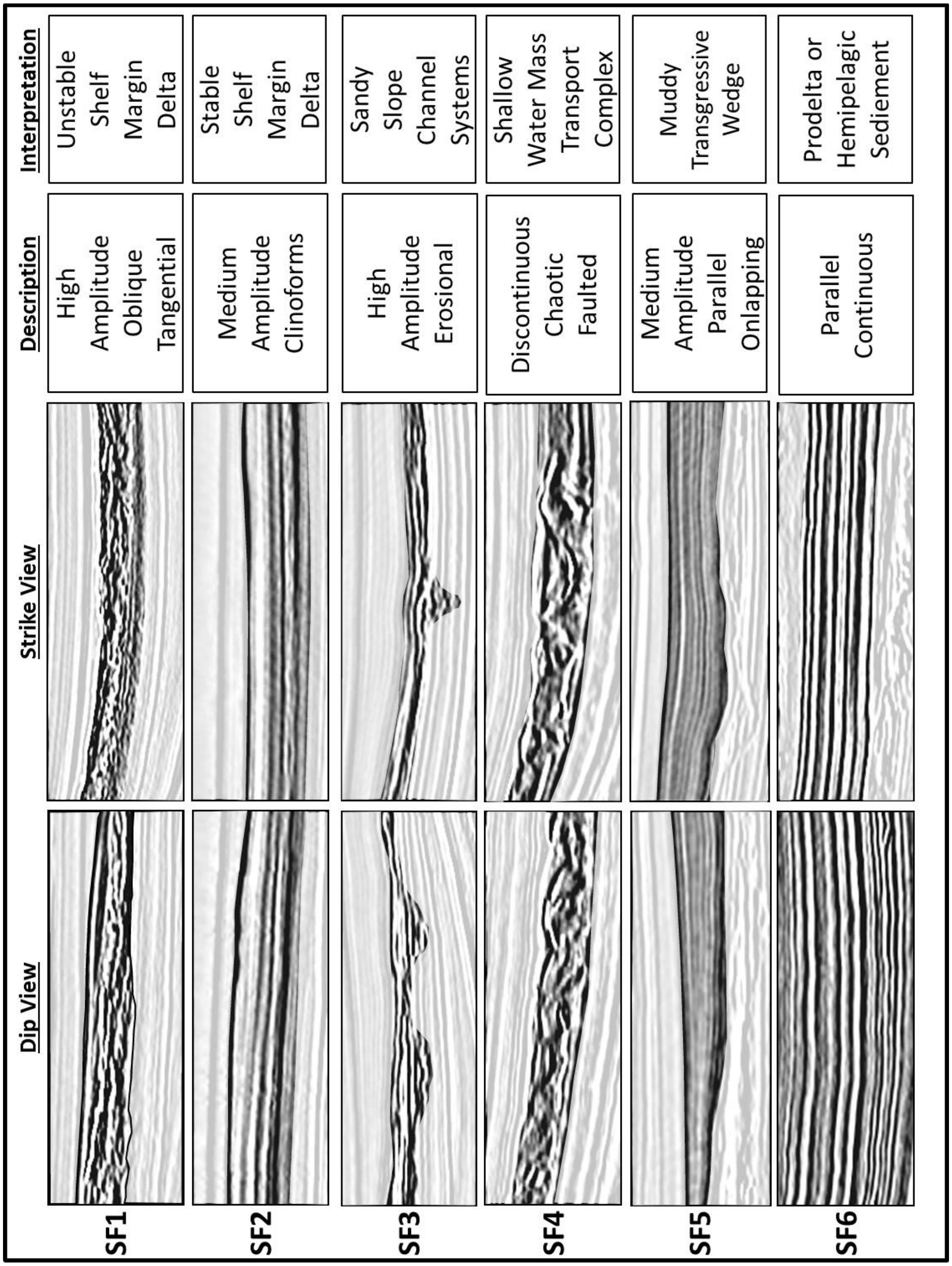

Figure 4: Six seismic facies used in this study labeled SF 1- SF 6. The facies are shown in dip view, strike view, and contain a brief description and interpretation.

4.4 Seismic Facies 4

Seismic facies 4 (SF 4) resembles a shallow-water mass-transport complex (MTC) units and would have been deposited in paleo-water depths of less than 250 m. Medium to low amplitude, discontinuous, chaotic reflections dominate SF 4 in dip view. Stratified, rotated fault blocks are also visible. Dip-view reflections of SF 4 appear similar to strike view. Multiple SF 4 units are found in the study area, and have deformed in multiple directions. The lateral margins of the features have erosional walls. Displacement of the sediment is most likely simulated from the vertical movement of either of the salt diapirs in the minibasin, as all of the features originate at or near them. The top of the facies is rugose in nature. These shallow-water MTCs are similar in style to their deep-water counterparts studied by Posamentier and Kolla (2003), and Moscardelli et al. (2006).

4.5 Seismic Facies 5

Seismic facies 5 (SF 5) is interpreted as a muddy, transgressive wedge of sediment that sits on the distal flanks of a shelf-margin delta. Dip-view reflections are medium to low amplitude reflections and are parallel to sub-parallel. Reflections converge and offlap to the north, and are slightly diverging to the south. The converging and onlapping to the north, and divergence of reflections to the south create a wedge that always thickens towards the southern portion of the study area. SF 5 always onlaps against either SF1 or SF 2.

4.6 Seismic Facies 6

Seismic facies 6 (SF 6) also shown in Figure 4 is interpreted as prodelta or hemipelagic sediment. The reflections appear similar in dip view and strike-view, and dip gently according to the shape of the basin. They are medium to low amplitude reflections and are parallel continuous in nature. SF 6 reflections show downlapping reflections at the base, and are sometimes truncated at the top.

Depositional packages have been labeled A through N with A being the youngest and N being the oldest. In order to discuss the filling of the basin in order, Package N is described first.

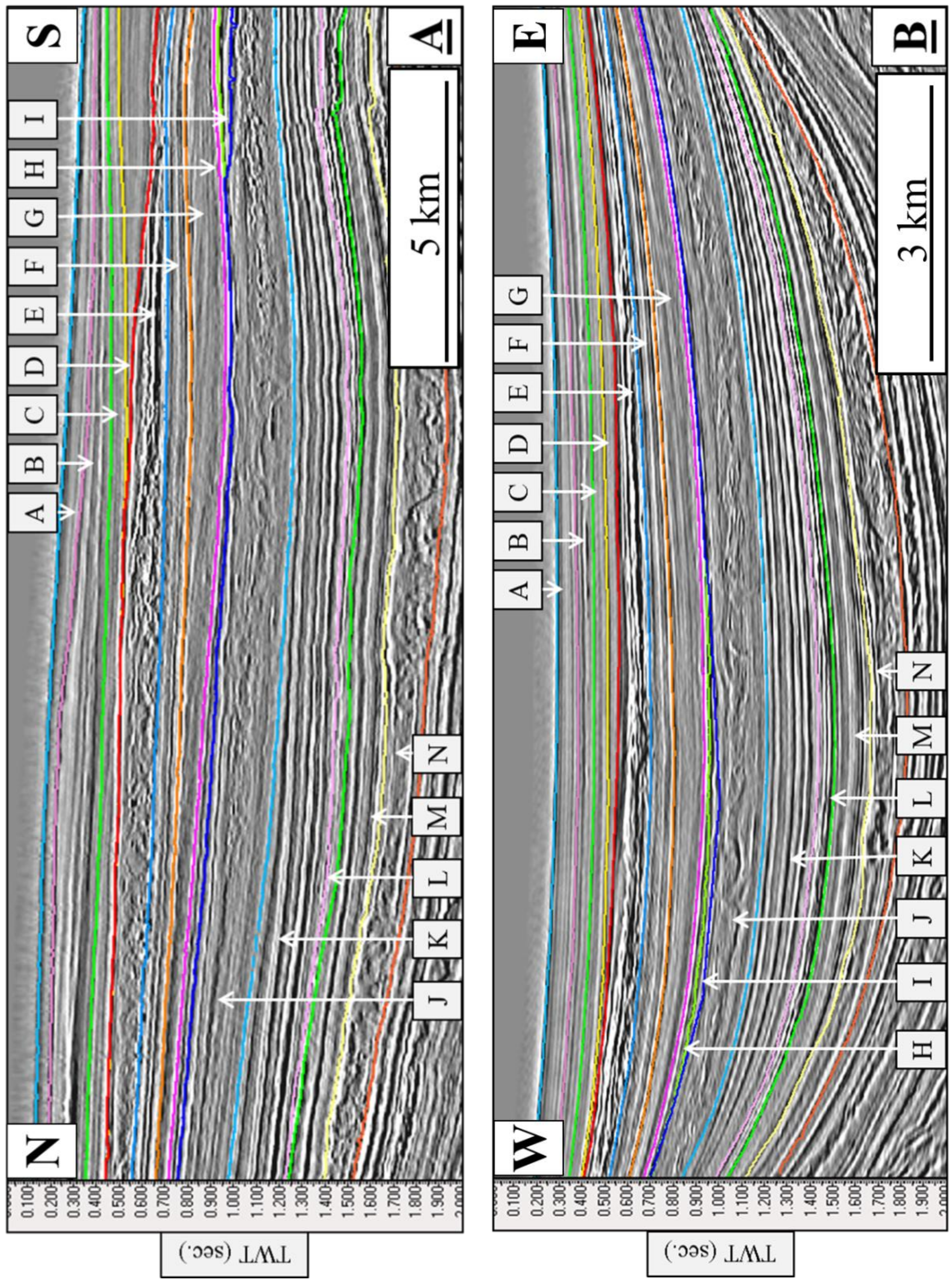

Figure 5. A) Inline showing location of sediment package intervals labeled A-N. B) Crossline showing location of sediment package intervals labeled A-N. Picked horizons are represented by the colored lines and mark the tops and bases of the packages.

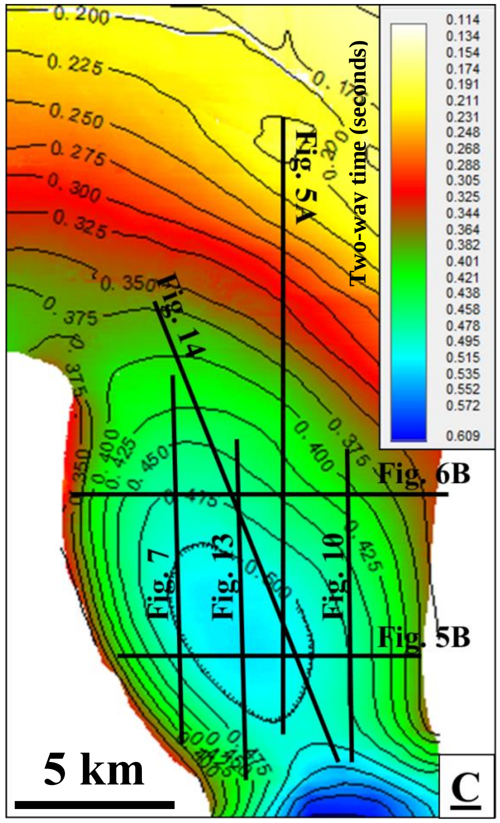

Figure 5. C) Time structure map of the bottom of Package B showing the location of various seismic lines shown in multiple figures.

4.7 Package N

Package N is dominated by two SF 4 chaotic deformed features described in Figure 4 and interpreted as shallow-water MTCs. These two complexes are sources from opposite sides of the minibasin and grow towards each other as shown in Figure 6 A. The separation of the two features creates multiple depocenters for the package which eventually grow into a single depocenter that is somewhat split, and the resulting thin spot is easily seen on the crossline shown in Figure 6 B, and in Figure A2-10. Each MTC

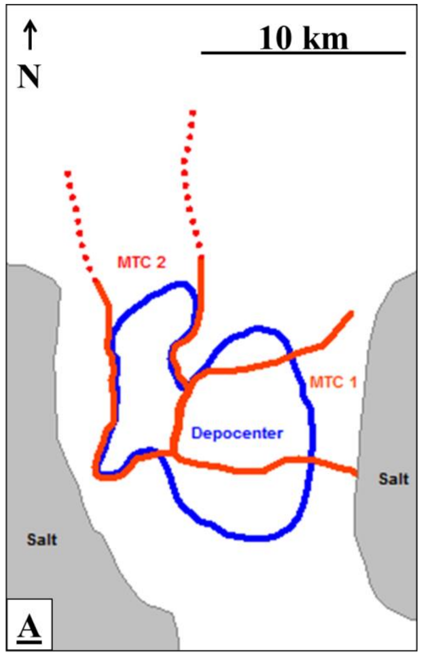

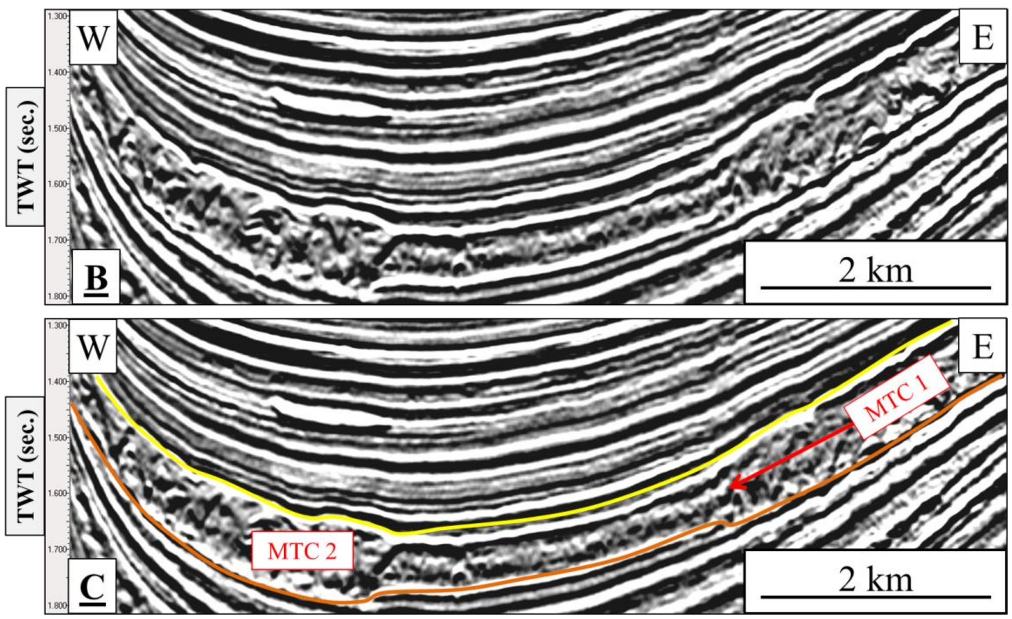

Figure 6. A) Interpretation of Package N showing the location of the two shallow water MTCs that make up the thickest sections of the package. B) Crossline from west to east of Package N. C) Interpreted crossline from west to east of the two MTCs found in Package N labeled in red. The bottom of Pacakge N is marked by the orange line, and the top in yellow. The red arrow next to MTC 1 represents the direction of transport for it. Two-way time in seconds is shown on the left. The locations of Figure 6 B and C are shown in Figure 5 C.

has its own depositional axis. The thickest parts of Package N can be attributed to the deformed sediments carried in by the two shallow water MTCs. Horizon slices shown in Figure 16 show that the eastern MTC 1 formed earliest. Figure 16 A, which shows the bottom 20% of the package, shows a well-developed eastern MTC, which has already formed the eastern portion of the depositional core of the unit. MTC 2 does not cut into the base of the package as far as MTC 1 does, and only shows localized deformation into the deepest parts of the package. The growth of MTC 2 down into the center portion of the minibasin can be seen in Figure 16 B and Figure 16 C. Evidence present also shows that MTC 2 started out as two separate bodies, one originating on the northern slope of the minibasin and one closer to the center of the minibasin. The two bodies eventually deformed into a single complex.

4.8 Package M

Package M made up entirely of SF 6 sits on top of the multiple shallow-water MTC units. The core of the package sits in the deepest part of the minibasin and conforms to the same shape. Sea level would have been high during the deposition of this unit and the shoreline would have been far to the north of the study area. Suspended sediment would have been carried to the deep waters present here and, eventually settled onto the seafloor of the study area. The parallel continuous seismic reflections that are contained within the package can be seen in Figure 7.

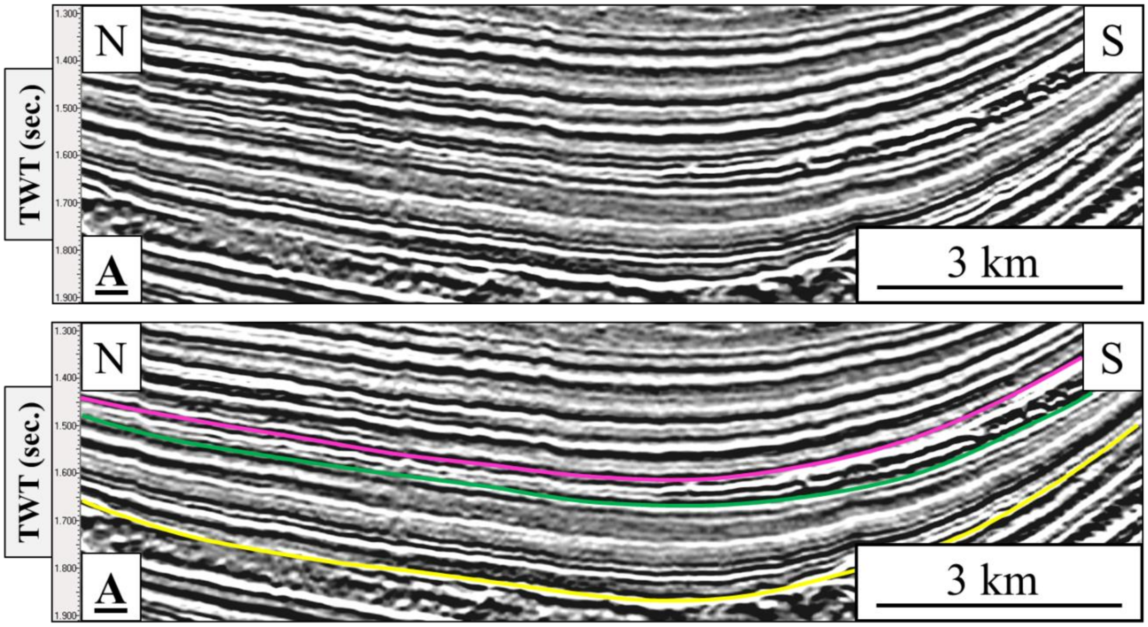

Figure 7. A) Cross-section from north to south showing the parallel continuous reflections of packages M, L, and K, as well as the small deformation feature contained within the southern portion of Package L. B) Interpreted cross-section from north to south with the base of Package M represented in yellow, the base of Package L in green, and the base of Package K in pink.

4.9 Package L

Package L is composed mostly of parallel continuous SF 6, however it is broken out from the surrounding packages due to a small SF 4 MTC feature originating from the western salt dome which deformed a small amount of sediment down the western slope of the basin. This small, deformation feature can be seen in Figure 7, and is localized to the very far southwestern corner of the minibasin.

4.10 Package K

Package K consists entirely of parallel continuous SF 6 reflections, and is the thickest deposit of its kind. This unit was created most likely by suspended sediment settling on the sea floor, with little to no deposition occurring during transitional and low sea- level periods. The dips of the reflections take the shape of the basin similar to Package M, as they would have formed from suspended sediment falling to the sea floor and conforming to the pre-existing shape of the basin. The location of the depocenter can be seen in Figure 16**.**

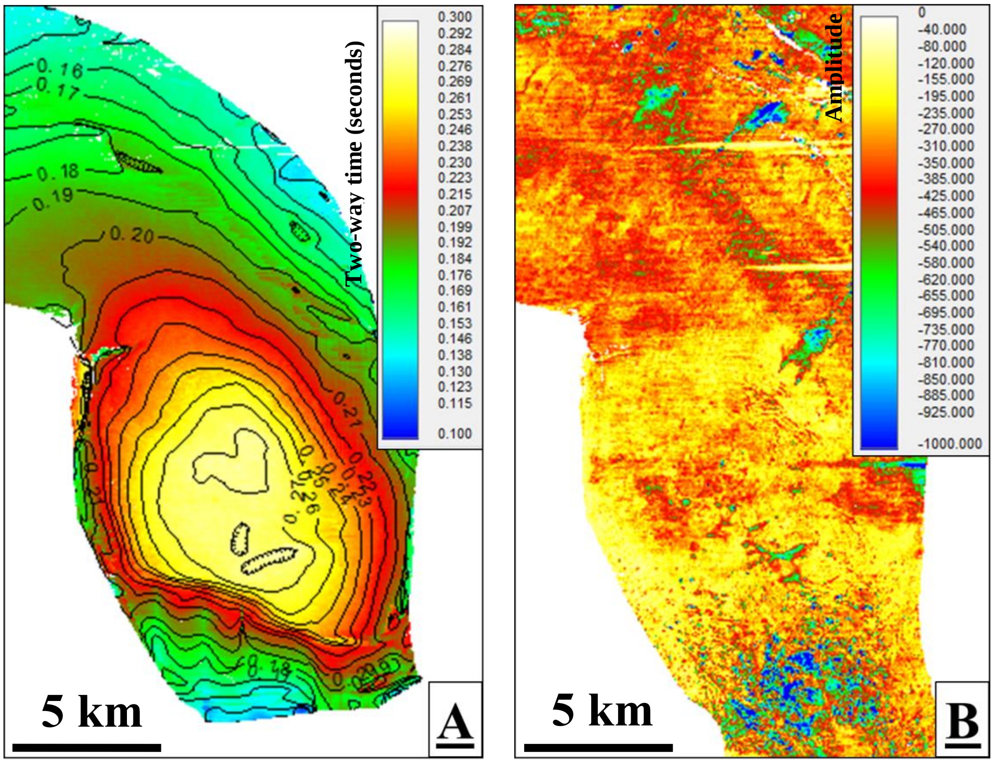

Figure 8. A) Isochron map showing the thickness of Package J. Thickness in two-way time is shown in the top right. B) VATMIN map of Package J which highlights varioations in amplitudes and concentrations. The scale in the top right represents changes in amplitude.

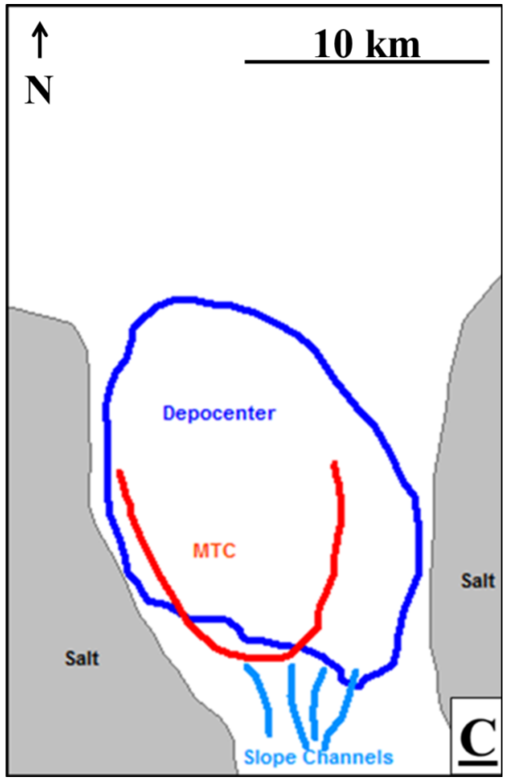

Figure 8. C) Interpretation of Package J highlighting the core of deposition, location of the MTC contained within it, and the location of minor slope channels at the southern end of the study area.

4.11 Package J

Progradational clinoforms began the formation of Package J. High sedimentation rates in the study area during a period of low sea-level caused syndepositional listric growth faults to occur, similar to the deltaic deformation described by Lee (2010), Perov and Bhattacharya (2011), Owens (2011), and Akhun (2013). Figure 8 A shows that deposition of the delta was mainly constrained to the ovoid minibasin, and little to no deposition occurred on the shelf to the north. Erosion into the underlying sediment occurred and can be seen in Figure 5 A. Progradation of the delta was interrupted by a localized SF 4 shallow-water MTC deposit which reworked a small part of the already deformed package. The location of the localized MTC is shown in Figure 8 C. Following the deformation of the MTC, sediment continued to prograde into the minibasin and was deposited on the distal end of the MTC. Erosional slope channels formed as a result of the high flux of sediment which served to transport sediment to the south towards the deeper basin. The delta package was formed due to a high fluvial influence, which is often associated with the syndepositional deformation which occurred, and reached a maximum thickness of about 190-200 m.

4.12 Package I

Package I, consisting of SF 5 transgressive wedge, was deposited on the distal edge of Package J. The location of the depocenter for Package I can be seen in Figure 16. Sediment would have backfilled over top of the southern end of the delta complex causing the lapout of the reflections seen in Figure 5 to terminate against the delta. Package I thickens slightly to the south, which would have occurred due to increased accommodation space there. It distribution can be seen in Figure A2-6.

4.13 Package H

A thin layer of suspended sediment settled in the basin following the transgression which created Package J. Package H, consisting of SF 6, caps both the muddy transgressive wedge to the south and the deformed deltaic package in the central area of the study area.

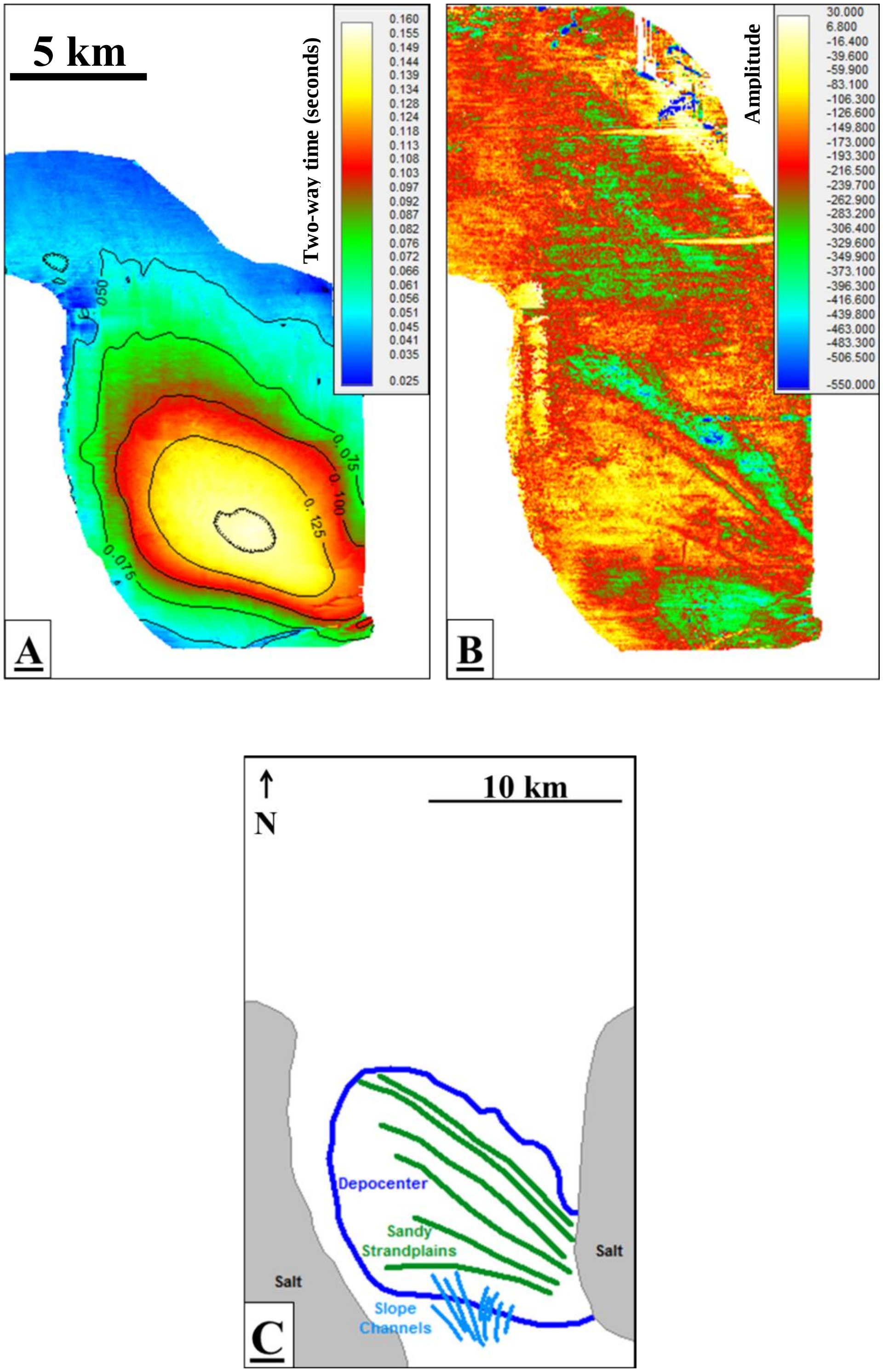

Figure 9. A) Isochron map of Package G with thickness in TWT (sec.) displayed in the top right. B) VATMIN map of Package G highlighting changes in amplitude with amplitude shown on the scale in the top right. C) Interpretation of Package G.

4.14 Package G

Package G, composed of SF 2, is a stable shelf-margin delta, and has a maximum thickness of about 110 m. Figure 9 A shows the thickness distribution of the thinnest delta found in the minibasin. It is concentrated in the southern area of the minibasin with little to no deposition occurring to the north. Medium to low-amplitude clinoforms can be seen prograding to the south in Figure 5 A. This delta shows signs of wave-domination, due to the parallel, continuous and linear internal clinoform geometry, (Figure 10) and also lacks the internal deformation associated with fluvial-dominated deltas in this area**.** Linear, high-amplitude bands seen in Figure 9 B are interpreted as strand plains, and would have formed from wave energy deflecting sediment along the slope. Minimally erosive slope channels can be seen in cross section, and show up at the southern end of Figure 9 B as slightly more negative amplitudes.

4.15 Package F

Overlying the stable delta is a unit composed of SF 6 parallel continuous reflections. The depocenter for Package F is shown in Figure 16. Perov and Bhattacharya (2011), interpreted this unit to have formed during the period of increasing accommodation, when the rate of sediment supply was high enough to maintain the normal regression of the shoreline. The top of this unit has been eroded by overlying slope channels.

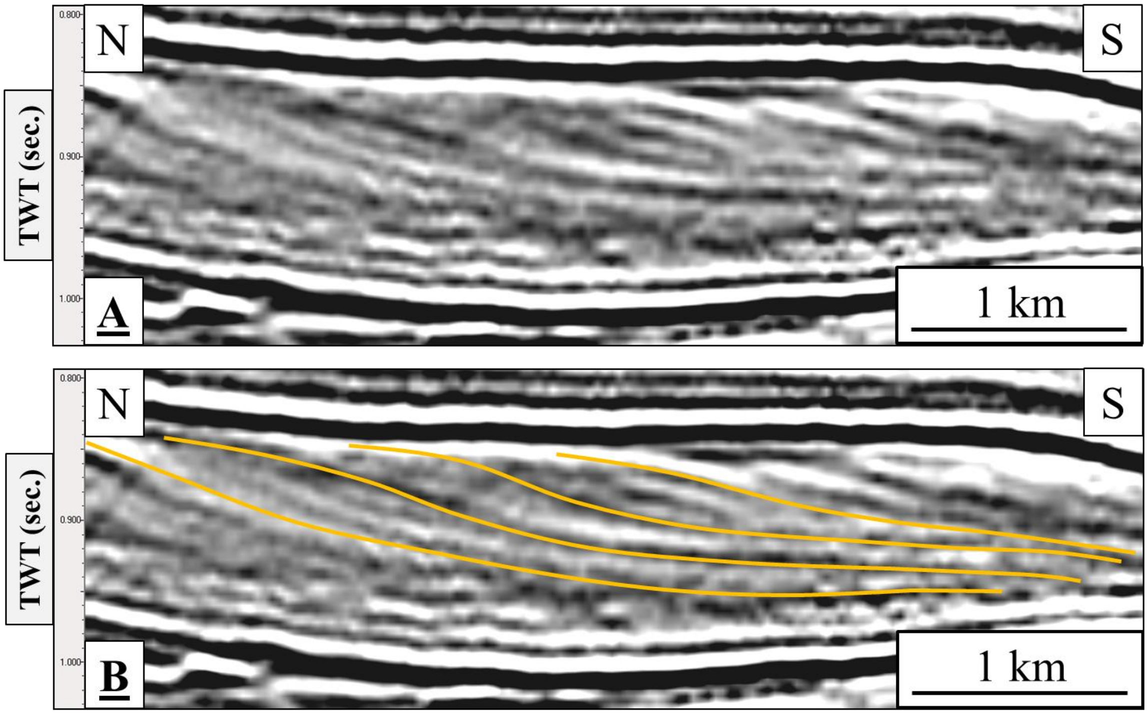

Figure 10. Cross-section of Package G highlighting parallel clinoform geometries in orange. Two-way time in seconds is shown on the left.

4.16 Package E

Package E is primarily composed of an SF 1 unstable shelf-margin delta unit. Clinoforms cut by listric growth faults prograde into the center of the basin. Perov and Bhattacharya (2011) came to the conclusion that this forced-regressive delta complex reflects higher rates of sea- level fall than other lowstand periods. This deformed delta is associated with a high level of fluvial influence which will be discussed later. An erosional slope channel network, highlighted in Figure 11 B by their negative amplitudes formed at the latter portion of the low sea- level period. These slope channels are outlined in Figure 11 C in blue. Uplift of the western salt dome caused remobilization of sediment deposited during this time and formed an MTC, composed of SF 4 that cut across the northwestern outline of the minibasin as shown in Figure 11 C**.** The maximum thickness of Package E is about 140 m. Based on the maximum change in sea level compared to modern times, shown in Figure 15, the paleo shoreline at the time of deposition of this unit was located slightly north of the minibasin, and is shown in Figure 11 C.

4.17 Package D

As sea level rose, sediment backfilled over the southern portion of Package E forming a SF 5 wedge unit. Low-amplitude reflections that lapout to the north against Package E can be seen in Figure 5 A, and Figure 5 B. These reflections are slightly diverging to the south, which indicates that the package thickens in that direction.

4.18 Package C

Capping Package D and Package E are parallel continuous reflections described as SF 6. This package is similar in nature to older packages composed of SF 6, however it also includes a downlapping feature interpreted as a muddy prodelta belonging to a highstand delta lobe which originates to the north of the study area. The thickest portion of this package can be seen in Figure 16. Maximum amplitudes in map view (Fig. A3-2) a high-amplitude concentration in the eastern portions of the minibasin. The thickest part of this unit however, is mostly represented by low-amplitude reflections.

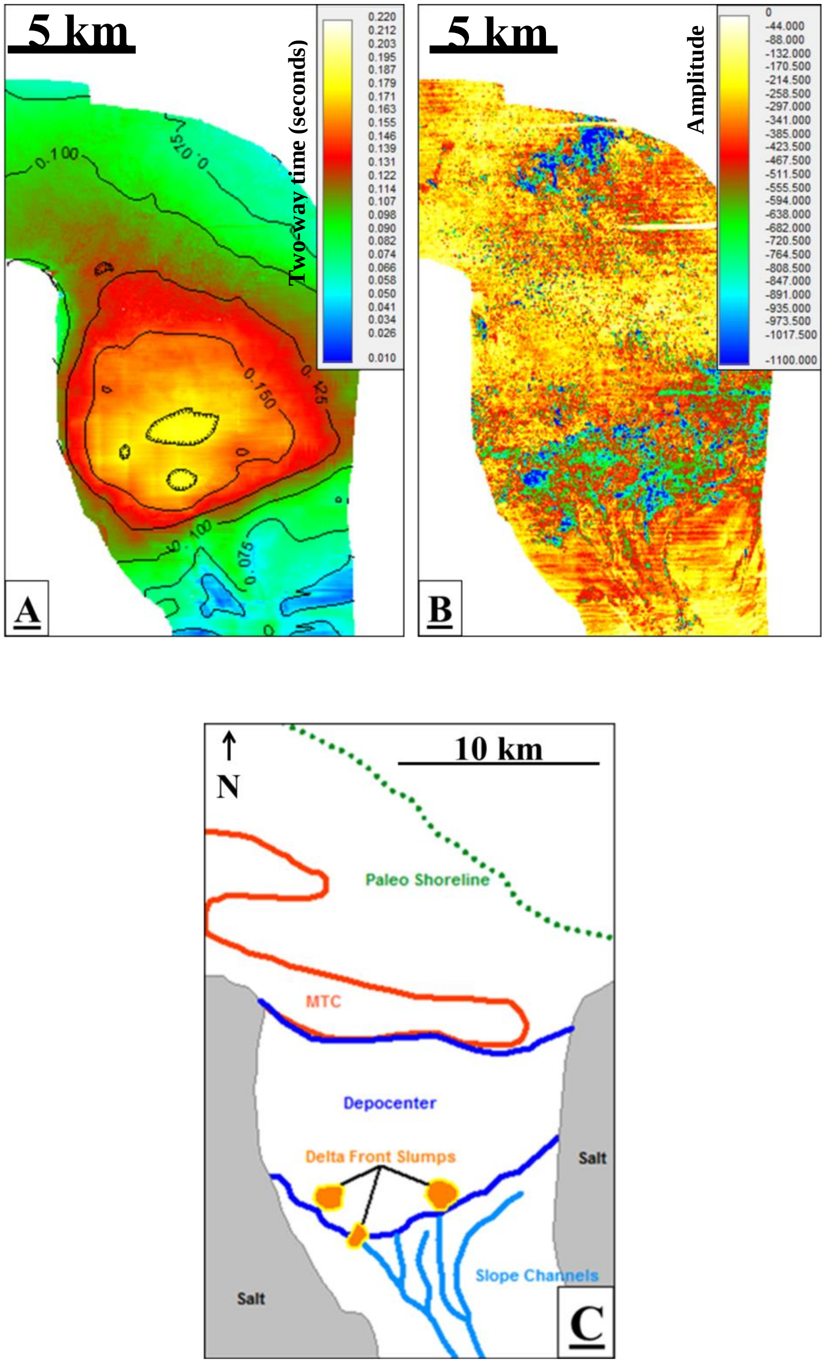

Figure 11. A) Isochron of Package E showing the thickness of the unit across the minibasin. B) VATMIN map of Package E showing differences in amplitude across the minibasin. C) Interpretation of Package E showing the core of deposition, the location of the SF 4 unit, delta front slumps, and erosional slope channel networks.

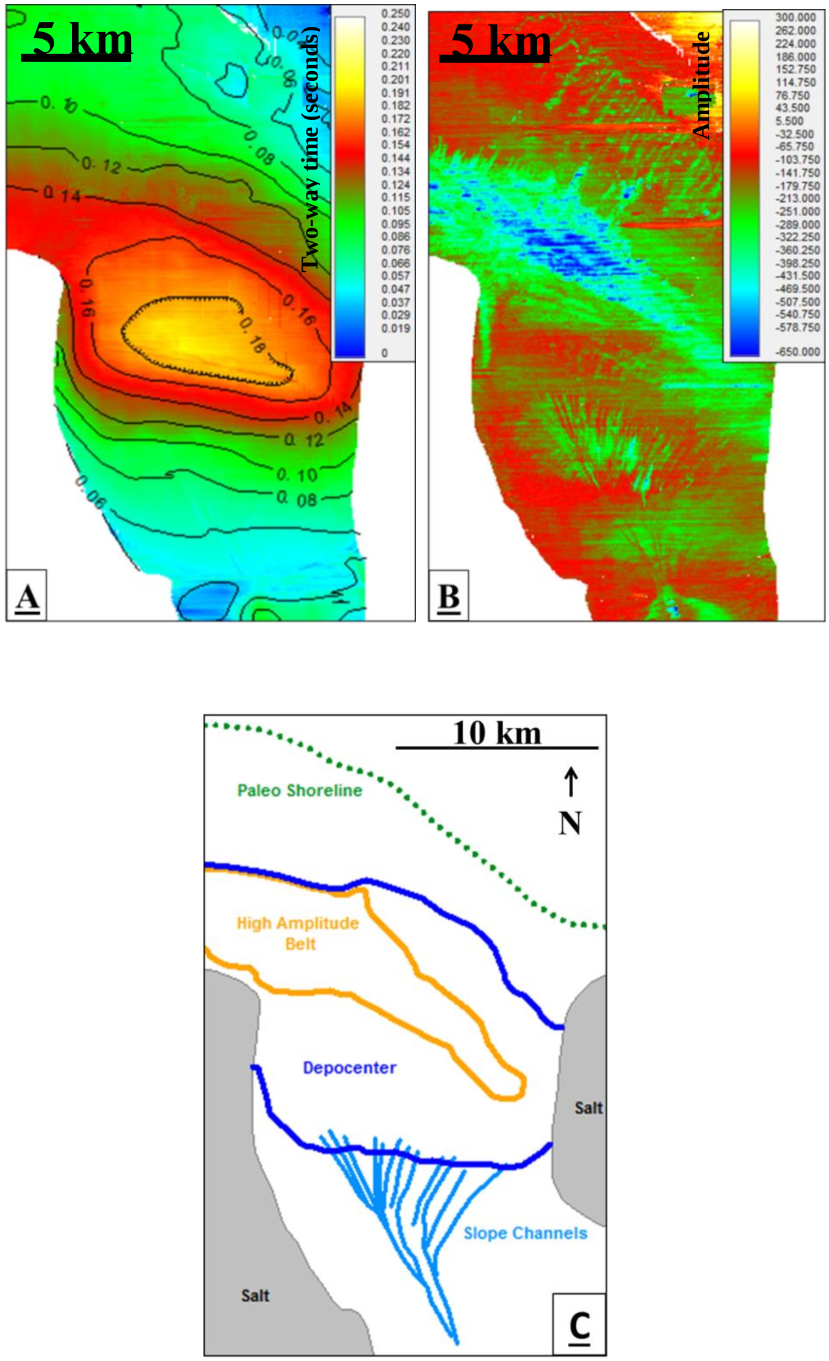

Figure 12. A) Isochron map of Package B showing the thickness of the unit across the minibasin. B) Minimum amplitude map of Package B. C) Interpretation of Package B showing the core of deposition outlined in blue, a concentration of high amplitude features outlined in gold, location of sandy slope channels outlined in light blue, and the location of both salt domes in gray. The approximate location of the shoreline at the time of deposition is represented by the dotted green line.

4.19 Package B

A stable shelf-margin deltaic unit composed of SF 2 is labeled as Package B. The youngest delta in the study area progrades to the south and reaches a maximum thickness of about 170 m. The thickness of the unit is shown in Figure 12 A. Highlighted in Figure 12 B, is the difference in amplitudes contained within the delta. A high-amplitude concentration, also outlined in Figure 12 C, can be seen deposited in a single, linear strandplain like feature at the northern boundary of the minibasin. The depositional style of the delta resembles a wave-dominated delta, due to the linear deposition style, and parallel clinoform geometry, similar to Package G. A high-amplitude, line source system can also be seen in Figure 12 B, feeding the delta complex. This source of sediment is found close to where the paleo-shoreline (Figure 12 C) would have been located at the time of deposition of Package B. While this shows that the sediment in the delta is possibly fluvial sourced, the depositional style of the package still resembles that of a wave-dominated delta. Slope channels, barely visible in cross section can also be seen in Figure 12 B. The channels are outlined in Figure 12 C, along with the rest of the features described within the delta package.

4.20 Package A

Package A, composed of an SF 5 wedge unit, is the youngest package found in the study area. Deposition of the unit began by backfilling the accommodation created to the south by the deposition of Package B, however this unit, unlike other similar units, filled this space and began to aggrade over top of the main body of the underlying delta

(Figure 13). The thickness and distribution of sediment for this unit is shown in Figure A2-1.

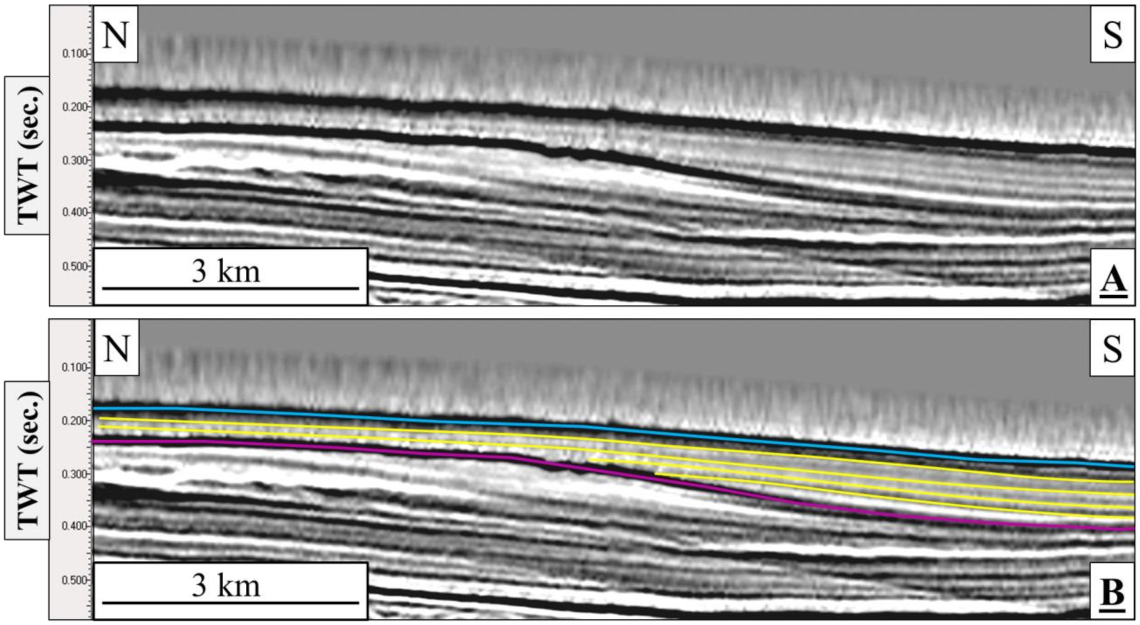

Figure 13. A) Uninterpreted inline of Package A. B) Interpreted inline showing the upper surface (blue) and lower surface (pink) of Package A. Internal, backfilling reflections are highlighted in yellow.

4.21 Sequence Stratigraphy

Without precise dates constrained by drilled core data, it is impossible to directly tie packages to the global sea-level record. However, by working backward from present day, and by comparing the units to similar studies in the area (Suter and Berryhill, 1985), it is possible to make assumptions about the timing of the deposition of the units found in the minibasin. Previously described lapout characteristics, along with previous work (Porebski and Steel, 2003; Anderson et al., 2004) led to categorizing the deltaic packages as LST deposits. Deltas formed during a period of high sea level are almost always confined to the shelf, particularly in the area of interest where the shelf can reach lengths upwards of 175 km. Therefore, HST deposits in the study area resemble SF 6 where sediment is only deposited when it falls out of suspension, or, in the case of Package C, a prodelta feature from a northern delta reaches the shelf edge, with the main body of the delta deposited to the north. SF 5 packages are interpreted as being deposited during TSTs due to their lapout relationships and locations compared to their overlying and underlying units. Figure 14 A and Figure 14 B displays the relationships of the packages based on their classifications as systems tracts.

By working backwards, the lowstand delta found in Package B correlates to oxygen isotope Stage 2 as shown in Figure 15. This puts the highstand deposit found beneath it as being deposited during Stage 5, with the Package E delta correlating to the Stage 6 lowstand as previously concluded by Perov and Bhattacharya (2011). The Package F HST would have been deposited during Stage 7, with the underlying lowstand delta studied by Lee (2010), during Stage 8. The HST underneath the Stage 8 delta correlates to the Stage 9 highstand, with the fourth delta, Package J, deposited during the lowstand of Stage 10.

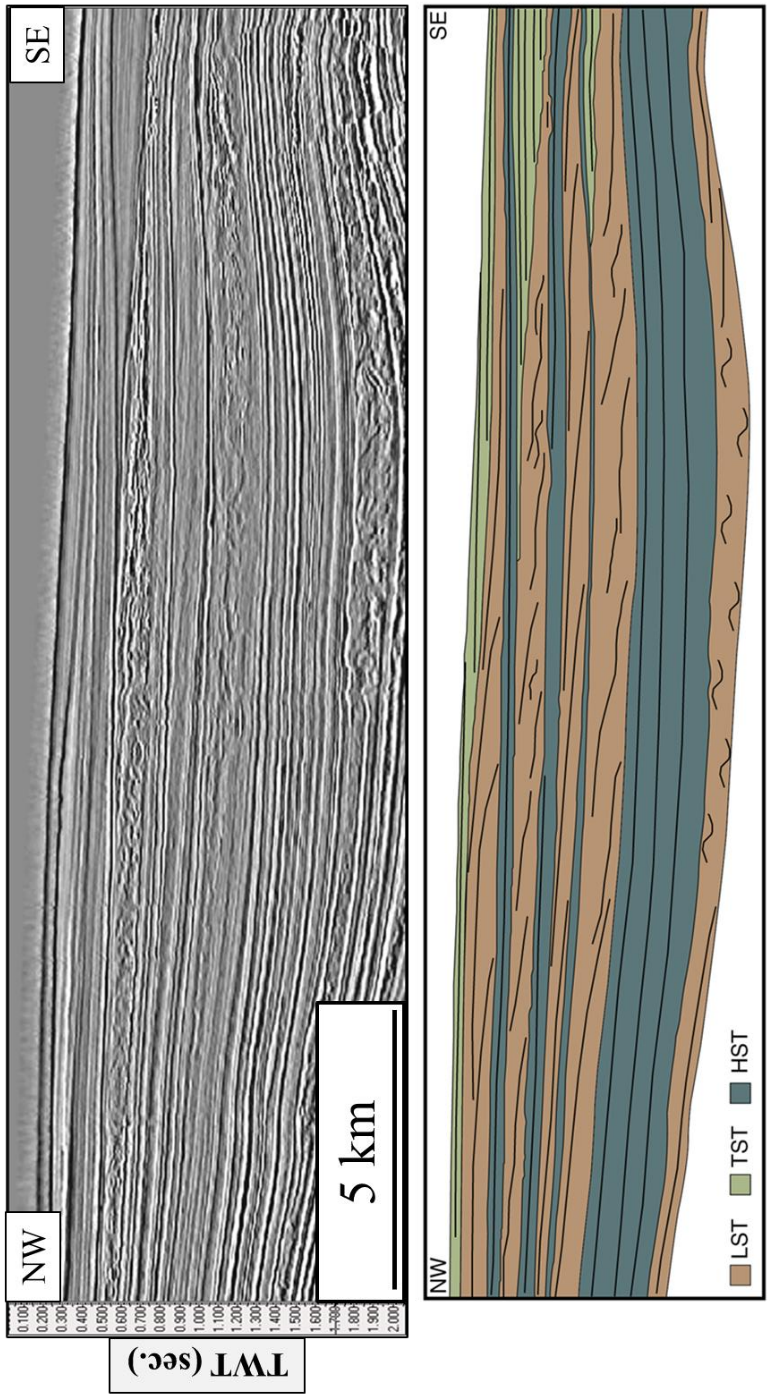

Figure 14. A) Uninterpreted arbitrary line running northwest to southeast through the center of the minibasin with its location shown in **Figure 5 C**. Time on the left of the figure is measured in TWT (sec.). B) Interpreted line of **Figure 14 A** showing the classification of each package as one of three systems tracts, LST, TST, or HST and their relationships to one another.

Packages K, L, and M resemble, and are subsequently classified as highstand deposits, however they are all much thicker than any of the younger similar deposits. With a setting of this nature, sediment delivered to the shelf edge could have very easily been diverted to another minibasin and deposited in another location, with no sediment reaching this study area during lowstand periods, therefore these units along with Package N are not correlated to the sea-level record. These thickened deposits could represent multiple highstands, with no deposition during multiple lowstands, therefore Package J is as far back as possible to relate packages to oxygen isotope stages in this way, as shown in Figure 15.

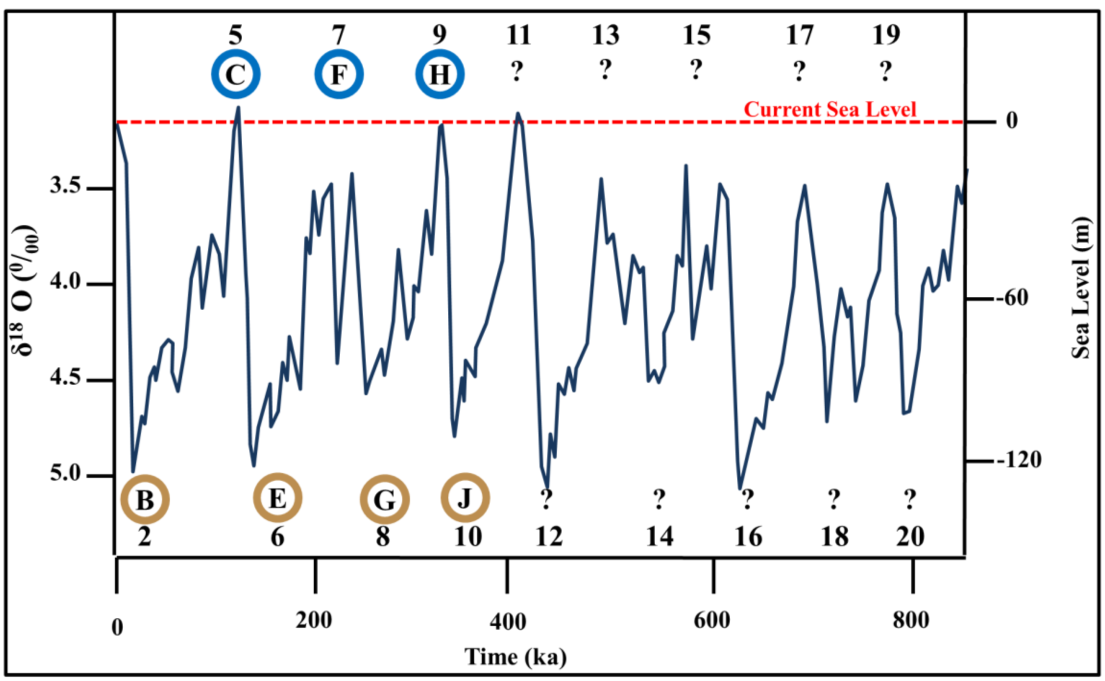

Figure 15. Sea-level curve shown in dark blue with the bottom axis corresponding to time, the left axis corresponding to $\delta\ ^{18}O\ (^{0}/_{00})$, and the right axis showing change in sea-level in relation to the current global sea- level. The numbers at the bottom represent the lowstand oxygen isotope stages, and the letters in brown represent the package from this study which correlates to each lowstand. Blue circled letters at the top correspond to highstand packages from this study. Highstand stages are odd numbered stages, and are numbered at the top (Modified from Lisiecki and Raymo, 2005).

Since it is impossible to make assumptions past Package J, it is impossible to determine the timing of the oldest packages in this study. Deposition of Package N could have taken place 450 ka, 650 ka, or much longer ago than that. Since only the highstand and lowstand stages are numbered in this system, the three TST packages do not correlate to a specific stage, but rather would be placed between stages during the rapid sea- level rises. Package A would have been deposited starting at the conclusion of stage 2, and continuing up to present day, since we are currently undergoing a transgression. Package D correlates to the transgression between stages 6 and 5. The oldest TST, Package I, would have been deposited during the rise in base level between stages 10 and 9.

5. Discussion

The packages outlined in this study follow a cyclic pattern that can be seen in Figure 16. During falling and low base-level periods, deltas prograde from the shelf and reach the shelf margin study area. They form the thickest deposits and are labeled as LST in Figure 16 and Figure 14 B. These deltaic packages mainly sit in, or close, to the center of the minibasin. The youngest lowstand deposit, Package B, is located slightly farther north of other similar deposits, and a portion of the depocenter is located to the north of the southwestern salt dome. It is plausible that some of the sediment which formed this delta was delivered to the west of the study area, but this cannot be confirmed since the western portion of the depocenter is located outside of it.

Following lowstand delta deposition, sediment occasionally backfills the accommodation space created and forms a wedge of muddy sediment on the southern edges of the deltas. Three TST deposits are found in the study area (Package A, Package D, and Package I). Their depocenters are shown in green in Figure 16. Two of the lowstand deposits, Package G and Package N, do not have transgressive wedges associated with them. One possible reason is that they are not present due to shorter transgressive periods which did not provide sufficient time for deposits to form that would be thick enough to be seen in this 3D seismic survey or, perhaps, did not provide enough time for deposits to even begin to form. Package G, associated with oxygen isotope stage 8 (Figure 15) is followed by the shortest transgressive period, where as the transgressions associated with Package A, Package D, and Package I have a higher rise in sea- level, and also occur over a slightly longer period. A third explanation for the lack of a transgressive wedge could be that they were simply deposited to the south of the study area and we simply cannot see them due to the location of the dataset.

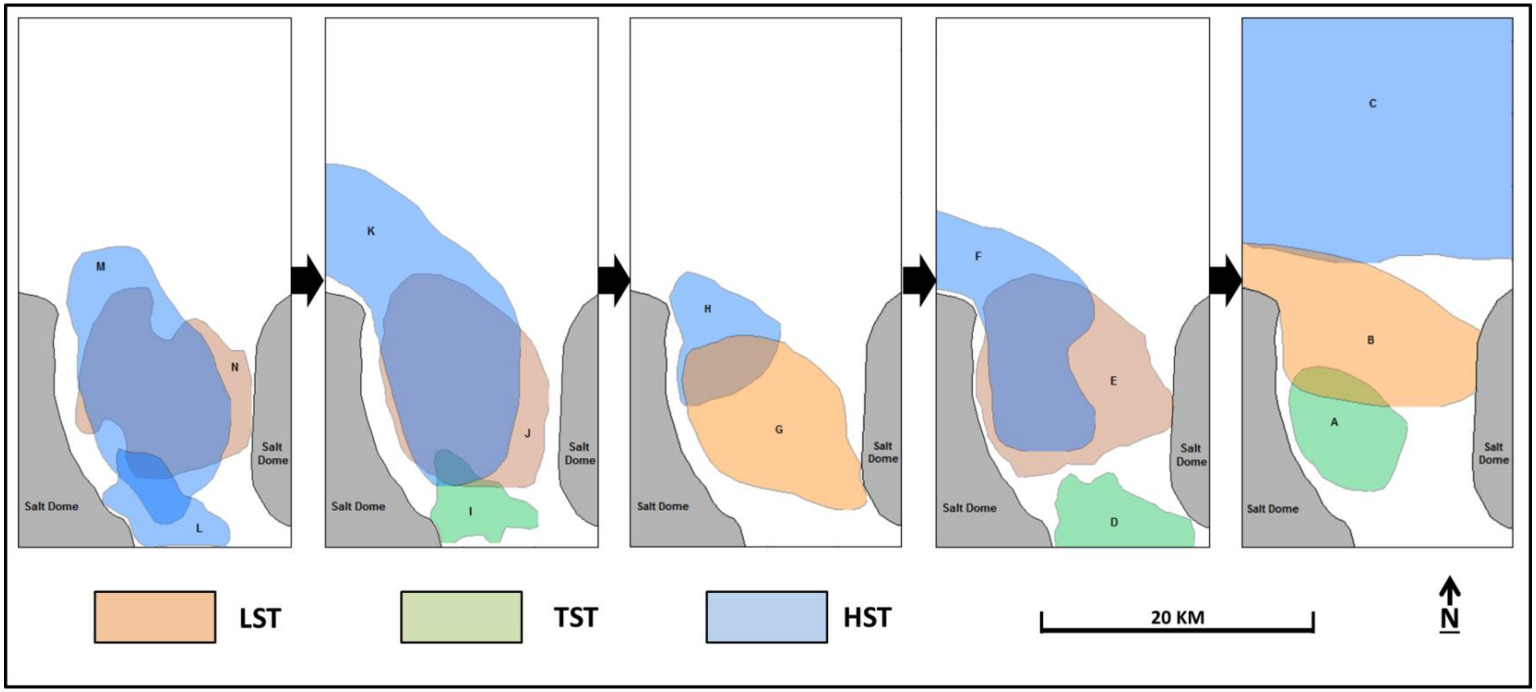

Figure 16. Cartoon showing the location of each package's depocenter. The packages are labeled A through N and are arranged in groups of 2 or 3. The oldest packages are shown on the left and the youngest packages on the right. The color of each package relates to the systems tract which they are associated with, and is the same color scheme used in Figure 10 B. Lowstand packages made from stable deltas are orange compared to the brown that the deformed lowstands are colored. Each depocenter was drawn by

Following deposition during a transgression, sediment would settle out of suspension, or in the case of Package C, prodelta muds would reach the study area from highstand deltas located on the shelf to the north. These deposits are shown in blue in Figure 16. All but the youngest of the HST deposits are concentrated in the center of the minibasin. They also tend to spill into the previously discussed accommodation space created by the continued uplift of the western salt dome. Package C is an exception since the thickest portion of it is located in the northern part of the study area. Sediment was deposited in the minibasin during the most recent highstand, and the depocenter location anomaly can most likely be attributed to the presence of additional prodelta sediments that reached the study area from the north.

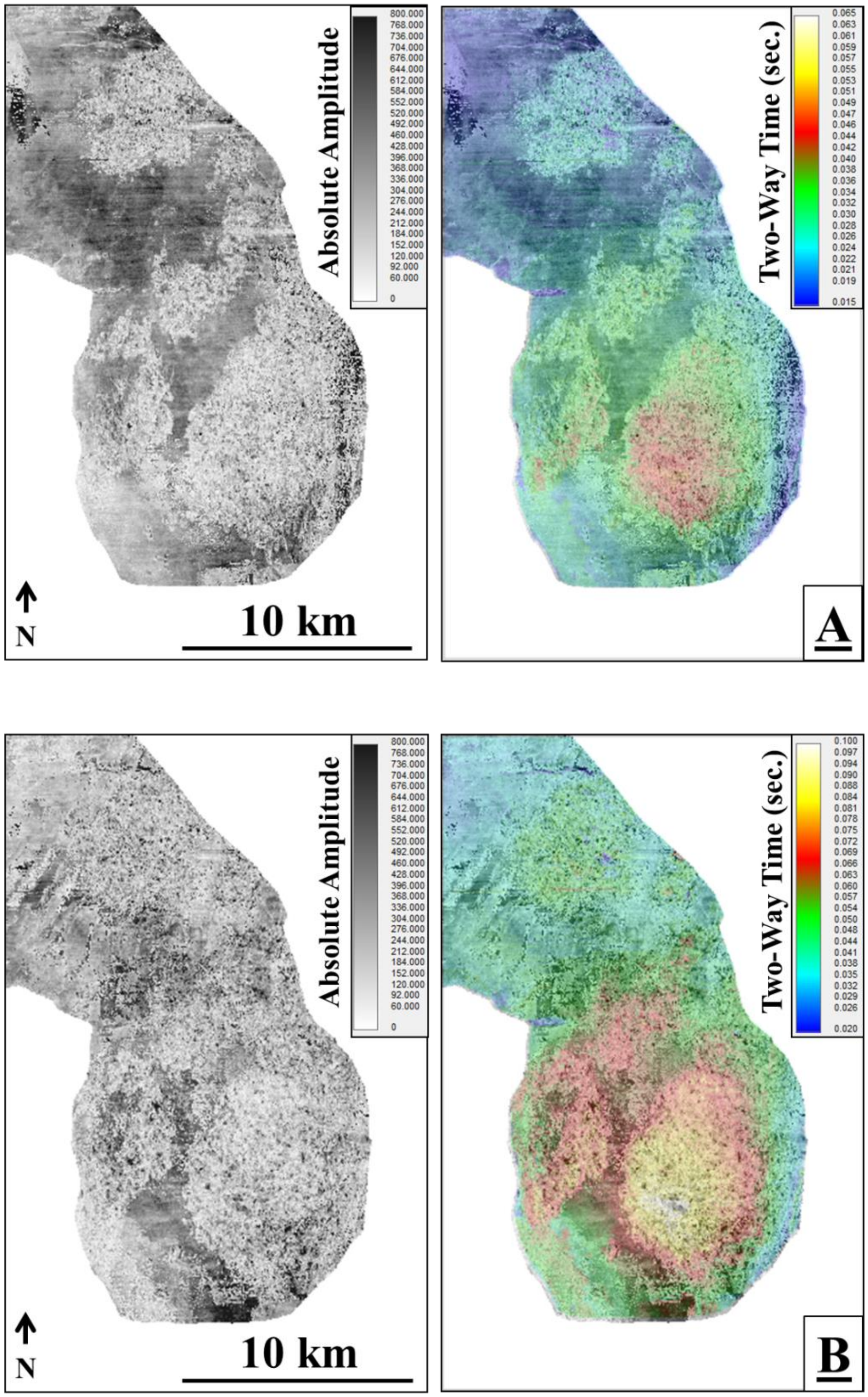

Figure 17. Three horizon slices of Package N showing the absolute amplitudes of the slice on the left, and the amplitudes plus the interval thickness in two-way time (sec.) overlaid on the right of each. A) Slice taken 20% up from the base of Package N. B) Slice taken 40% up from the base of Package N.

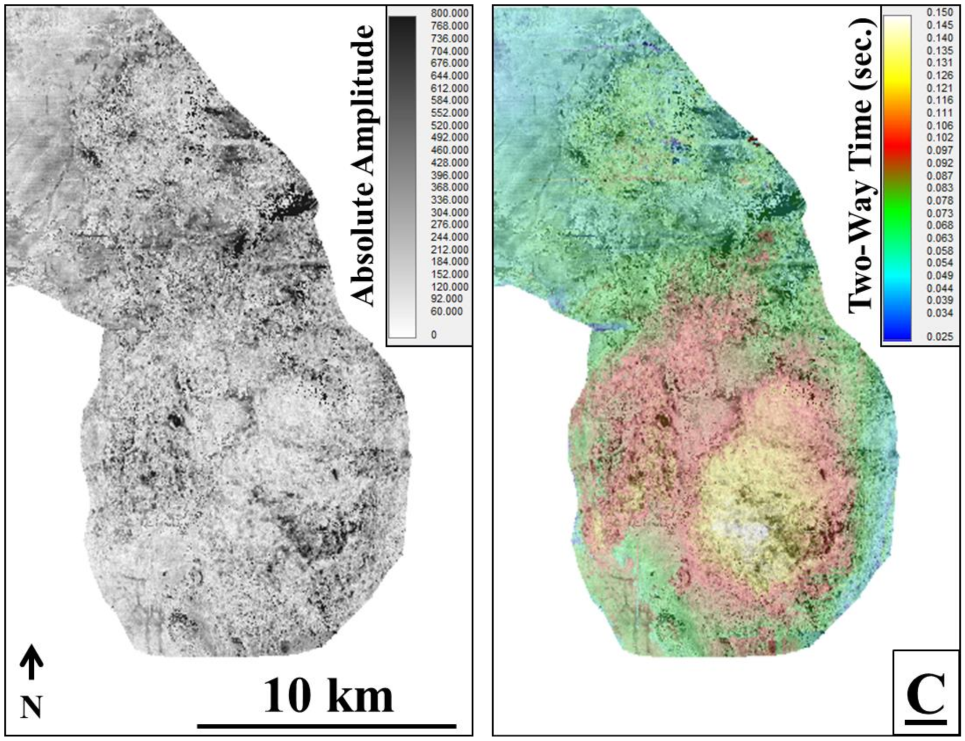

Figure 17. C) Slice taken 60% up from the base of Package N.

5.1 Salt Tectonics and Deformation Causes

Evidence shows that the two salt diapirs shown in Figure 2 were actively growing vertically throughout the filling of the basin, and that at least the western salt dome is still moving vertically today. Slope failure and the reworking of previously deposited sediment by shallow water MTCs are evidence of the salt movement throughout the history of the minibasin. The “U” shape of reflections and their fan-shaped cross-sectional geometries seen in Figure 5 B show that uplift continued during deposition which increased the slope of previous deposits. The geometry of the asymmetric horizons in Figure 5 B also indicate that the western salt dome is responsible for more uplift than the eastern salt dome, as the horizons dip greater to the west than they do to the east.

While most MTCs form further down the slope and have been studied using various geophysical methods, (e.g. Bull et al., 2009; Posamentier and Kolla, 2003; Frey-Martinez et al., 2005), and in outcrop, (Lucente and Pini, 2003), diapiric movement at the shelf edge is a sufficient mechanism to cause slope failure. While there are no shallow-water MTCs in the youngest sediment packages to indicate that the salt systems are still active, continued creation of accommodation at the northern tip of the southwestern salt dome shows that at least one salt diapir continues to grow vertically. Figure 2 shows the lateral termination of seismic reflections against the salt domes.

Two types of deformation features are present in the basin, salt tectonic-induced MTCs and sediment supply-driven deformed deltaic packages. Package N provides a prime example of shallow-water MTCs generated by the vertical movement of salt diapirs. Figure 17 A clearly shows a shallow-water MTC (MTC 1) deforming sediment directly down the gradient created by the eastern salt diapir. Another MTC carries sediment into the minibasin from the northwest, with the cause of deformation attributed to the western salt diapir. Figure 18 A and Figure 18 B show an example of the sediment supply-driven deformation found in the minibasin. Conversely, the package found in Figure 18, deformed as an entire unit, unlike the multiple MTCs which slump down the diapir created gradients. High amounts of sediment flowed into the minibasin from the northwestern inlet, and overloaded the system causing internal faulting and delta front

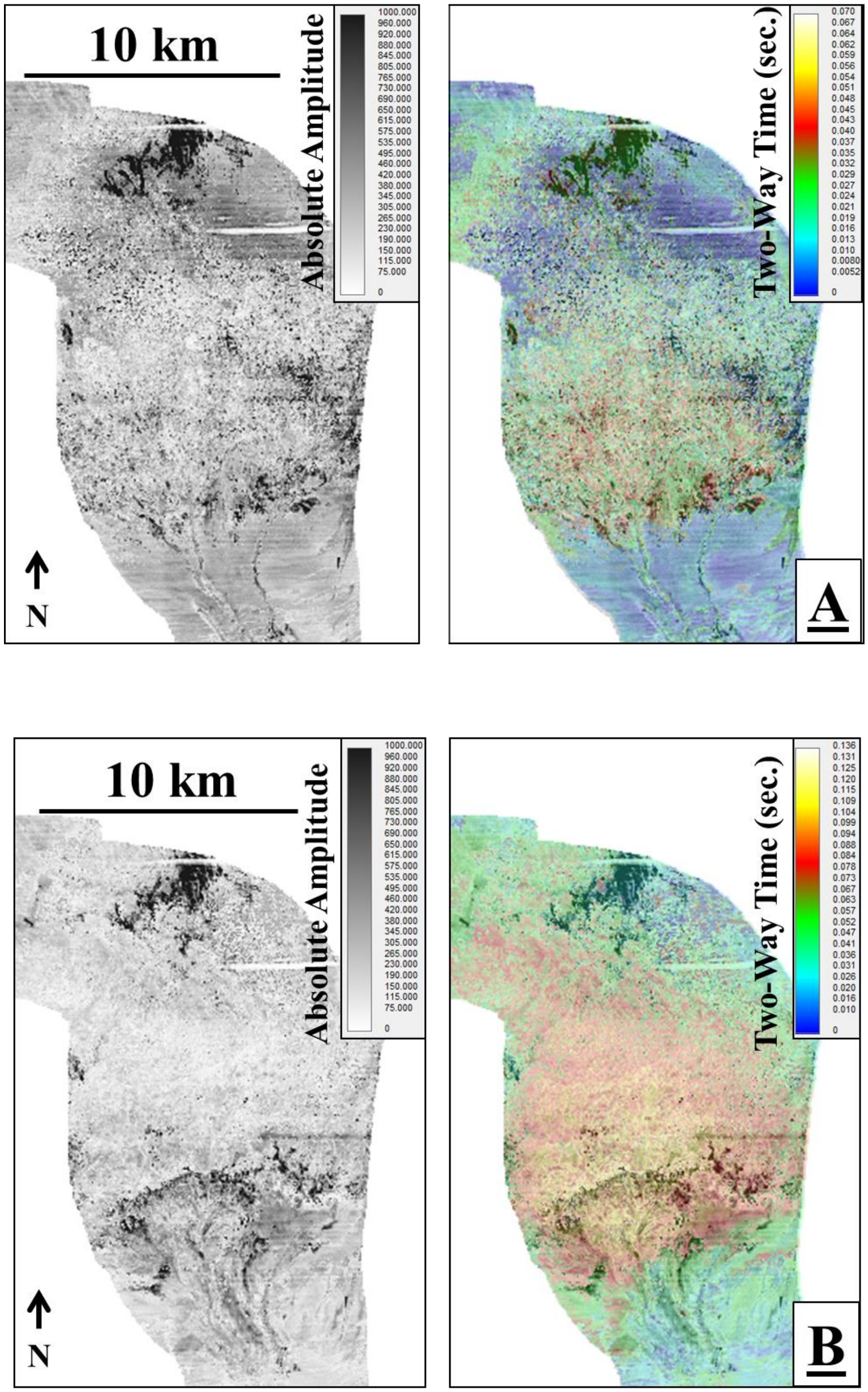

Figure 18. Two horizon slices through Package E with the absolute amplitudes of the slice shown on the left. The right versions show the amplitude overlaid by colored interval thickness maps. A) Horizon slice of the lowest 20% of Package E. B) Horizon slice of the lowest 60% of Package E.

slumps. The increased amount of sediment quickly filled the minibasin, causing the system to form two main slope channels near the slump features.

5.2 Two Deltaic Depositional Styles

The two types of deltas present shed further light on sediment supply and rate. Unstable deltas, associated with a high fluvial influence, form when large amounts of sediment are delivered to the shelf margin and rapidly fill the accommodation space that is available. This rapid deposition coupled with a high sediment supply is the cause of internal syndepositional slope failure and ensuing formation of listric growth faults.

The stable deltas show signs of wave domination. Sediment is constrained and distributed into linear features previously described as strand plains due incoming waves energy preventing the rapid progradation. The concentration of these high amplitude belts can again be seen in Figure 9 B and Figure12 B**.**

The tendency of stable deltas to aggrade rather than prograde is supported by comparing the dips noted by Perov and Bhattacharya (2011), and Lee (2010). Clinoforms contained within Package G had a maximum dip of 2.5°, while unstable clinoforms in Perov and Bhattacharya's work dipped up to 3.2°. The increased dip angle can indicated that in a fluvial- influenced system sediment tends to build basinward while wave influenced, stable systems want to build upwards. This is supported when viewing the shapes that the depocenters of the delta packages take shown in Figure 16. The wave influenced, stable deltas (Package B and Package G) form a shape more parallel to the shelf margin. Fluvial- influenced, unstable deltas (Package E and Package J) take a shape that is oblong towards the basin, or more progradational.

5.3 Shelf-margin Sediment Bypass

Dixon et al., (2012) concluded that by looking at the depositional styles of the deltas located on the shelf edge, one can predict whether or not sediment was transported deeper into the basin. By synthesizing the results of over 20 previous studies which for the most part covered the shelf margin, slope, and deeper basin, they concluded that unstable, fluvial-influenced deltas were an indicator that sediment was being carried deeper into the basin. Wave-influenced, stable deltas were considered ineffective at transporting sediment to the basin.

The unstable deltas in this study, particularly Package E, show very well-developed slope-channel networks that would have served as an effective transport conduits from the staging area on the shelf margin (Figure 18). These channels are deeply incised, and are filled with much higher amplitude reflections as seen in Figure 10 B**,** and Figure 18. The youngest, stable shelf-margin delta in this study, Package B, does show signs of sediment being transported through the shelf margin and deeper into the basin as it contains a well-developed channel network similar to the unstable deltas. This is significant, since wave-dominated, stable deltas rarely show signs of sediment bypass. The slope-channel bypass system likely formed due to the constricting nature of the minibasin. Most stable shelf-margin delta examples are found on open-shelf edges, where as in the Gulf of Mexico, minibasin formation creates a unique setting where delta lobes cannot switch and avulse as easily. Since sediment deposition is constricted to a smaller area, it would take less sediment to fill the available space, and instead of the deltaic system relocating, it can only push sediment farther into the basin via slope channels. Due to the setting, wave-influenced deltas do have the ability to serve as effective mechanisms for coarse sediment to be carried to the deeper basin.

6. Conclusions

The filling of the shelf-margin study area occurred in a cyclic manner with delta deposition occurring during periods of low sea level, followed by muddy wedges backfilling during transgressions, followed by sediment settling out of suspension during periods of high sea- level stand when the shoreline had retreated to the north.

Two forms of shelf-margin deltas are present in the study area, stable, wave-influenced deltas, and unstable, fluvial- influenced deltas. The former are deposited in a series of linear features, or in the case of Package B a single linear feature, classified as strand plains which form parallel to the slope of the minibasin. The shape of the depocenters, combined with their characteristics in cross section, indicate that they tend to favor aggradation over progradation. Unstable, fluvial-influenced deltas favor progradation into the basin over aggradation, and are characterized by frequently occurring syndepositional-listric growth faults. The formation of these features can cause the formation of slumped concentrations of coarser sediment, from which slope-channel networks commonly originate.

While stable, wave-influenced deltas are not usually effective at moving sediment deeper towards the basin, the setting found in the study area, where the depositional area of the delta is limited to the minibasin, presents wave-influenced deltas the opportunity to develop features that allow them to carry sediment into deeper water.

Deformation of sediment can be induced by either the vertical growth of salt diapirs or by high and rapid rates of sediment supply. Deformation due to high rates of sediment supply occurs during the formation of entire delta complexes, and the body deforms as a single unit. Salt diapirism in the area is not only responsible for the shape of the minibasin, but also can create unstable conditions that cause sediment to be redeposited in the form of shallow-water MTCs. The shallow-water MTCs found are similar to their deep-water counterparts, but smaller in size.

References Cited

Abdulah, K.C., Anderson, J.B., Snow, J.N., and Holdford-Jack, L., 2004. The late Quaternary Brazos and Colorado Deltas, Offshore Tecas, U.S.A. – Their Evolution and the Factors that Controlled their Deposition, in J.B. Anderson and R.H. Fillon, eds., Late Quaternary Stratigraphic Evolution of the Northern Gulf of Mexico Margin: SEPM *Special Publications*, v. 79, p. 237 – 269.

Adedayo, A.A., McHargue, T.R., and Graham, S.A., 2005. Transient Fan Architecture and Depositional Controls from Near-surface 3-D Seismic Data, Niger Delta Continental Slope, *AAPG Bulletin*, v. 89, no. 5, 9. 627-643.

Akhun, S., 2013. Evolution of Late Cenozoic Minibasins and Growth Faulting, Green Canyon Area, Northwestern Gulf of Mexico: University of Houston, M.S. Thesis, p. 112.

Anderson, J.B., Rodriguez, A., Abdulah, K.C., Fillon, R.H., Banfield, L.A., McKeown, H.A., and Wellner, J.S., 2004. Late Quaternary Stratigraphic Evolution of the Northern Gulf of Mexico Margin: A Synthesis, in J.B. Anderson and R.H. Fillon, eds., Late Quaternary Stratigraphic Evolution of the Northern Gulf of Mexico Margin: *SEPM Special Publication*, v. 79, p. 1-23.

Berryhill, H.L., Jr., 1987. Late Quaternary Facies and Structure, Northern Gulf of Mexico, *AAPG*, Studied in Geology 23, 289 p.

Bhattacharya, J.P., and Giosan, L., 2003. Wave-influenced Deltas: Geomorphological Implications for Facies Reconstruction, *Sedimentology*, v. 50, p. 187-210.

Bhattacharya, J.P., and Willis, B.J., 2001. Lowstand Deltas in the Frontier Formation, Powder River Basin, Wyoming: Implications for Sequence Stratigraphic Models, *AAPG Bulletin*, v. 85, no.2, p. 261-294.

Bull, S., Cartwright, J., and Huuse, M., 2009. A Review of Kinematic Indicators from Mass-transport Complexes Using 3D Seismic Data, *Marine and Petroleum Geology*, v. 26, p. 1132-1151.

Dixon, J.F., Steel, R.J., and Olariu, C., 2012. Shelf-edge Delta Regime as a Predictor of Deep-water Deposition, *Journal of Sedimentary Research*, v. 82, p. 681-687.

Frey-Martinez, J., Cartwright, J.,and Hall, B., 2005. 3D Seismic Interpretation of Slump Complexes: Examples from the Continental Margin of Israel. *Basin Research*, v. 17, p. 83-108.

Galloway, W.E., Whiteaker, T.L., and Ganey-Curry, P., 2011. History of Cenozoic North American Drainage Basin Evolution, Sediment Yield, and Accumulation in the Gulf of Mexico Basin. *Geosphere,* v. 7 (4), p. 938-973.

Konyukhov, A. I. 2008. Geological Structure, Evolution Stages, and Petroliferous Complexes of the Gulf of Mexico basin. *Lithology and Mineral Resources*, *43*(4), p. 380-393.

Lee, P., 2010. A Comparison of the Geometries of Two Pleistocene Shelf Margin Delta Sequences, Vermilion South Addition and Northeast Garden Banks, Gulf of Mexico: University of Houston, M.S. Thesis, 84 p.

Lisiecki, L.E., and Raymo, M.E., 2005. A Pliocene-Pleistocene Stack of 57 Globally Distributed Benthic ^{18}O Records, *Paleoceanography,* v. 20, p. 1-17.

Lucente, C., and Pini, G., 2003. Anatomy and Emplacement Mechanism of a Large Submarine Slide within a Miocene Foredeep in the Northern Apennines, Italy: a Field Perspective, *American Journal of Science*, v. 303, p. 656-602.

Mitchum, R.M., Vail, P.R., and Sangree, J.B., 1977. Seismic Stratigraphy and Global Changes of Sea Level, Part 6: Stratigraphic Interpretations of Seismic Reflection Patterns in Depositional Sequences, in C.E. Payton, ed., Seismic Stratigraphy: Applications to Hydrocarbon Exploration: *AAPG Memoir*, v. 26, p. 117-135.

Morton, R.A., and Suter, J.R., 1996. Sequence Stratigraphy and Composition of Late Quaternary Shelf-margin Deltas, Northern Gulf of Mexico. *AAPG Bulletin*, v. 80, p. 505-530.

Moscardelli, L., Wood, L., and Mann, P., 2006. Mass-transport Complexes and Associated Processes in the Offshore Area of Trinidad and Venezuela, *AAPG Bulletin*, v. 90, no. 7, p. 1059-1088.

Olariu, C., and Bhattacharya, J.P., 2006. Terminal Distributary Channels and Delta Front Architecture of River-dominated Delta Systems, *Journal of Sedimentary Research,* v. 76 no. 2, p. 212-233.

Owens, L., 2011. Eustatic Controls of Deformed Versus Undeformed Shelf-edge Deltas Within a Salt-withdrawl Minibasin, Northern Gulf of Mexico: University of Houston, M.S. Thesis, 64 p.

Perov, G., 2009. Pleistocene Shelf Margin Delta: Intradeltaic Deformation and Sediment Bypass, Northern Gulf of Mexico: University of Houston, M.S. Thesis, 56 p.

Perov, G., Bhattacharya, J.P., 2011. Pleistocene Shelf Margin Delta: Intradeltaic Deformation and Sediment Bypass, Northern Gulf of Mexico, *AAPG Bulletin*, v. 95, p. 1617-1641.

Pindell, J.L., 1985. Alleghenian Reconstruction and Subsequent Evolution of the Gulf of Mexico, Bahamas, and Proto-Caribbean, *Tectonics*, v. 4, p. 1-39.

Porebski, S.J., and Steel, R.J., 2003. Shelf-margin Deltas: Their Stratigraphic Significance and Relationship to Deep-water Sands. *Earth Science Reviews,* v. 62, p. 283-326.

Porebski, S.J., and Steel, R.J., 2006. Deltas and Sea-level Change, *Journal of Sedimentary Research*, v. 76, p. 390-403.

Posamentier, H.W., and Kolla, V., 2003. Seismic Geomorphology and Stratigraphy of Depositional Elements in Deep-water Settings, *Journal of Sedimentary Research*, v. 73, p. 367-388.

Rubio, S. H., 2010. Enhancing Geologic Interpretations with Seismic Attributes in the Gulf of Mexico. University of Houston, M.S. Thesis, 58 p.

Saller, A.H., Noah, J.T., Ruzuar, A.P., and Schneider, R., 2004. Linked Lowstand Delta to Basin-floor Fan Deposition, Offshore Indonesia: An Analog for Deep-water Reservoir Systems, *AAPG Bulletin,* v. 88, no. 1, p. 21-46.

Salvador, A., 1987. Late Triassic-Jurrassic Paleogeography and origin of Gulf of Mexico Basin, *AAPG Bulletin*, v. 71, no. 4, p. 419-451.

Sangree, J.B., and Widmier, J.M., 1978. Seismic Stratigraphy and Global Changes of Sea- level, Part 9: Seismic Interpretation of Clastic Depositional Facies, *AAPG Bulletin*, v. 62, p. 752-771.

Suter, J.R., and Berryhill, H.L., 1985. Late Quaternary Shelf-margin Deltas, Northwest Gulf of Mexico, *AAPG Bulletin,* v. 69, p. 77-91.

Sydow, J., and Roberts, H. H., 1994. Stratigraphic Framework of a late Pleistocene Shelf-edge Delta, northeast Gulf of Mexico: *AAPG Bulletin***,** v. 78, p. 1276-1312.

Vail, P.R., Mitchum, R.M., Todd, R.G., Widmier, J.M.,Thompson, S., Sangree, J.B., Bubb, J.N., and Hatlelid, W.G., 1977. Seismic Stratigraphy and Global Changes in Sea-level, Part 4: Global Cycles of Relative Changes of Sea-level, in C.E. Payton, eds., Seismic Stratigraphy: Applications to Hydrocarbon Exploration, *AAPG Memoir 26*, p. 49-213.

Wellner, J.S., Sarzalejo, S., Lagoe, M., and Anderson, J.B., 2004. Late Quaternary Stratigraphic Evolution of the West Louisiana East Texas Continental Shelf, in J.B. Anderson and R.H.Fillon, eds., Late Quaternary Stratigraphic Evolution of the Northern Gulf of Mexico Margin: *SEPM Special Publications*, v. 79, p. 217-235.

Wellner, R., Beaubouef, R., Van Wagoner, J., Roberts, H., and Tao, S., 2006. Jet-plume Depositional Bodies the Primary Building Blocks of Wax Lake Delta, *Gulf Coast Association of Geological Societies Transactions*, v. 55, p. 867-909.

Appendix 1. Horizons

Time-structure maps of every picked horizon. The scale is in two-way time (seconds) and the contour invervals vary based on the range of values.

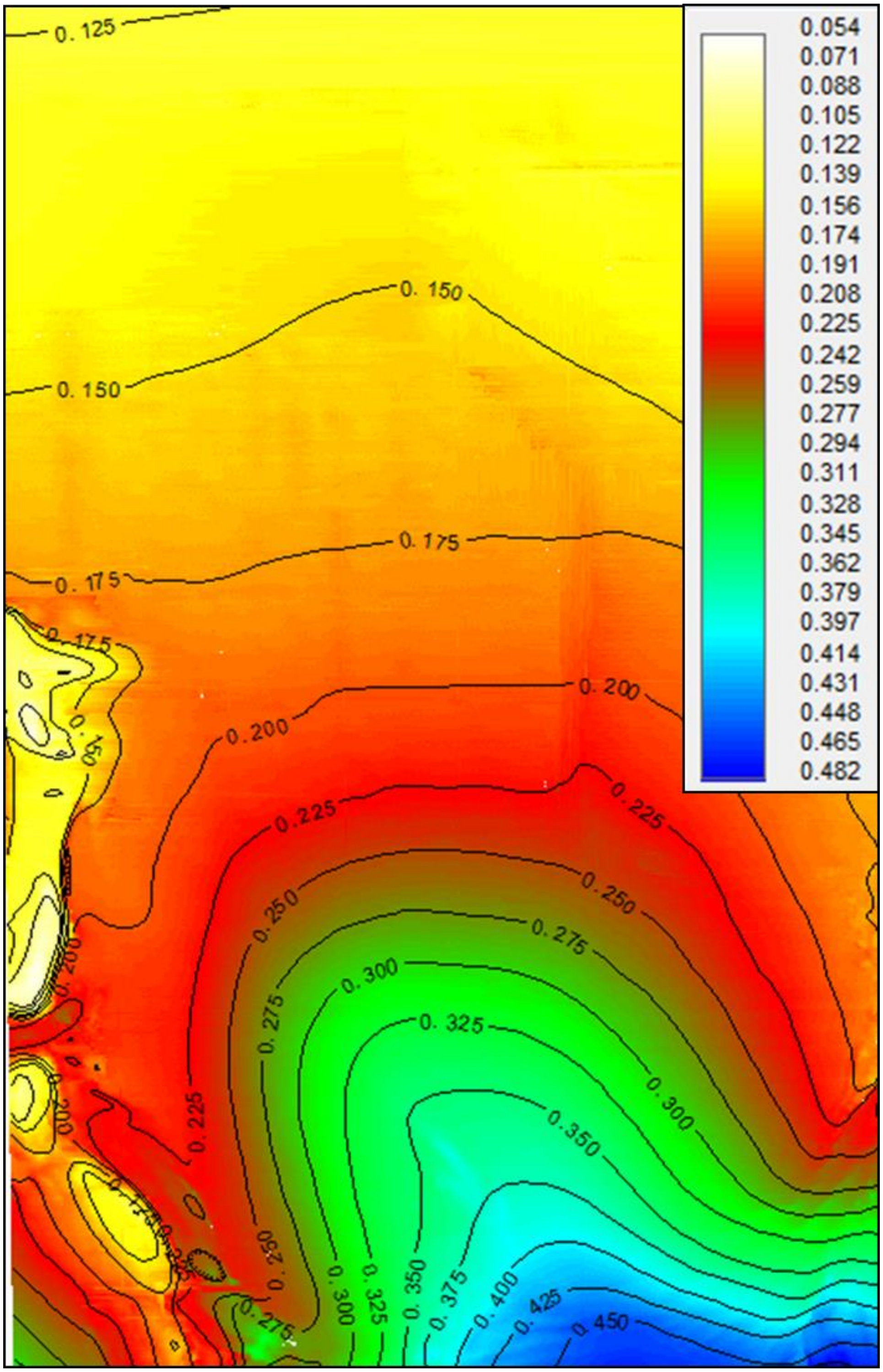

Figure A1-1. Top of Package A (seafloor) measured in two-way travel time (seconds).

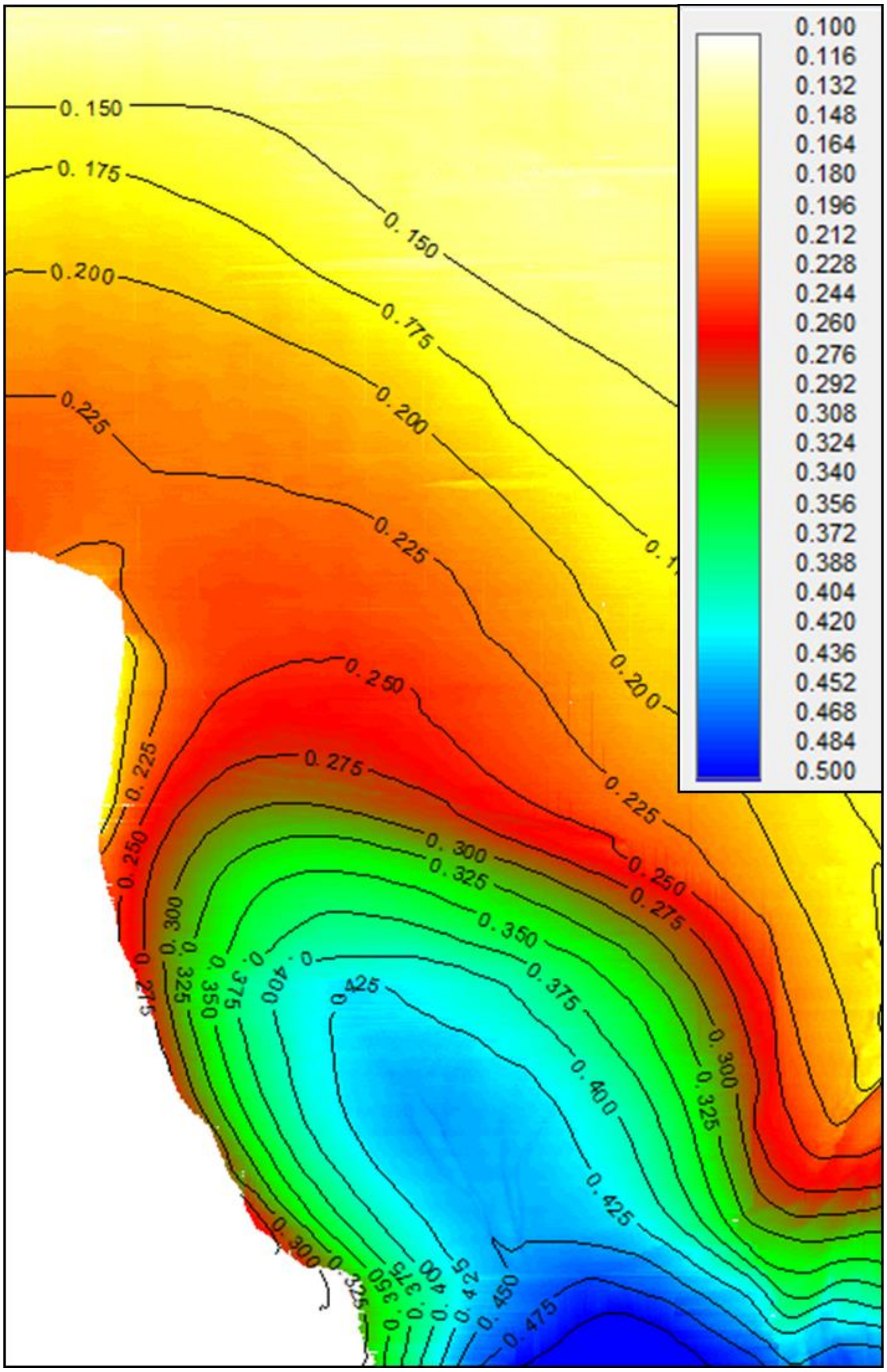

Figure A1-2. Top of Package B measured in two-way travel time (seconds).

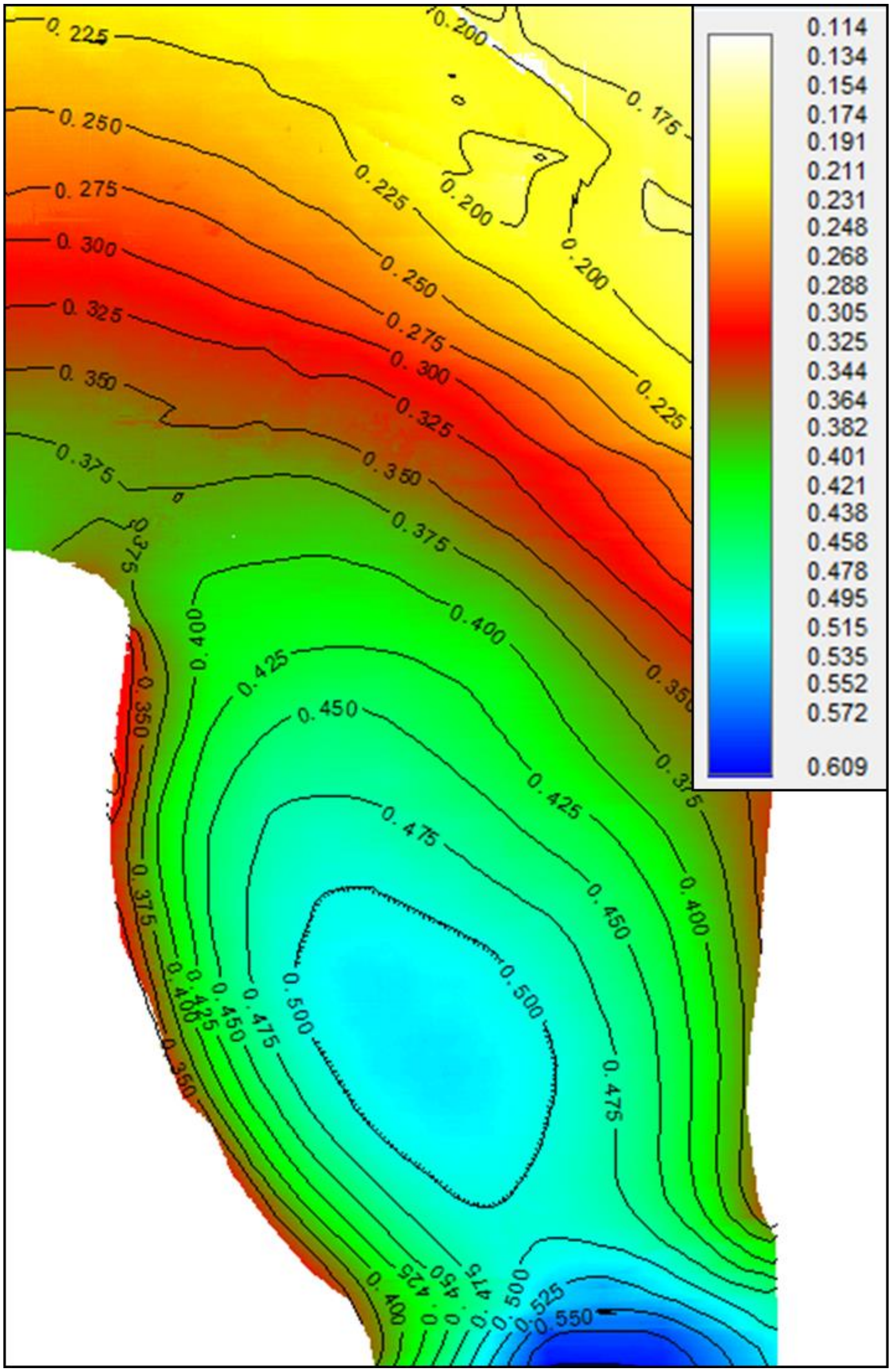

Figure A1-3. Top of Package C measured in two-way travel time (seconds).

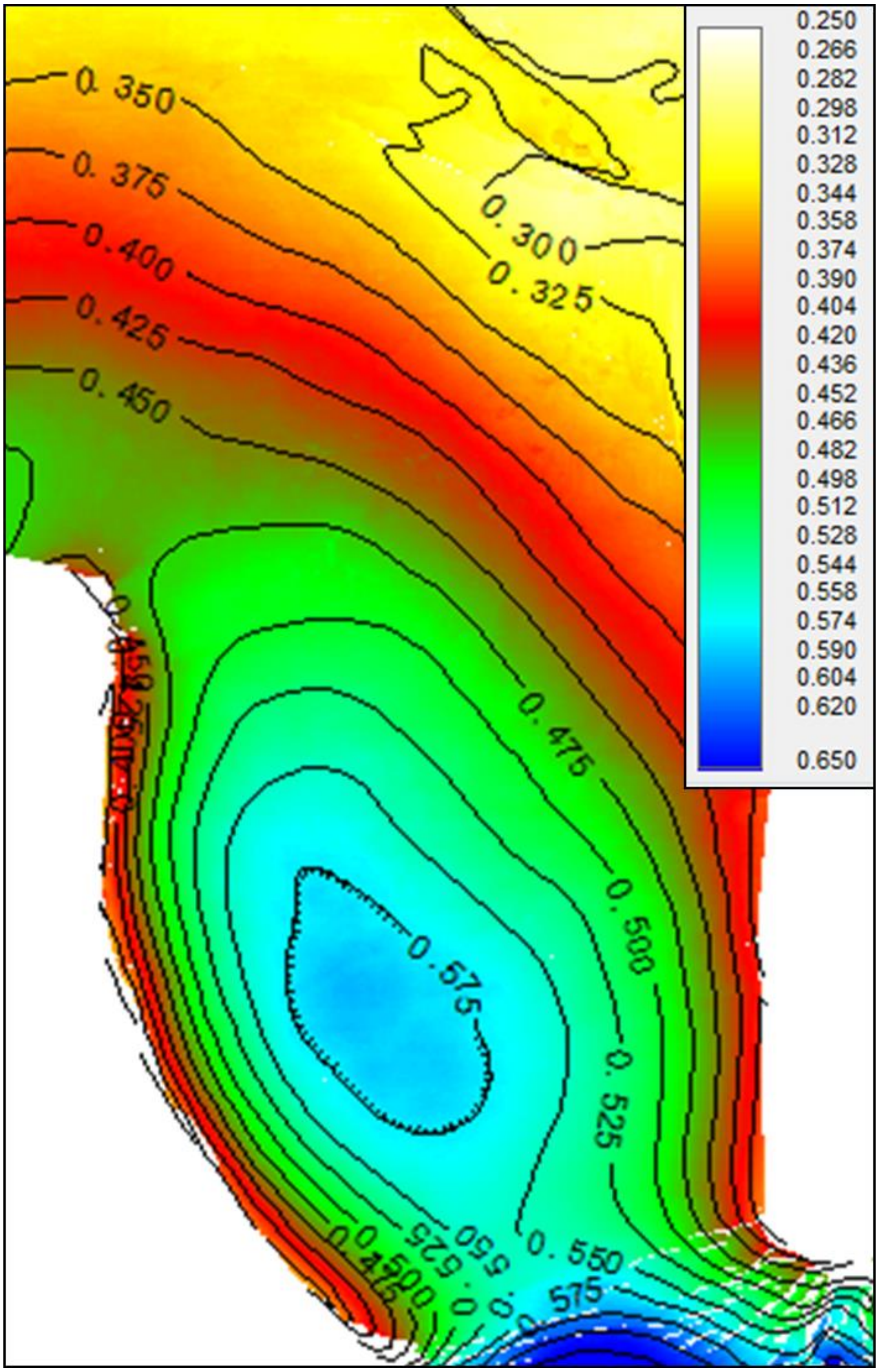

Figure A1-4. Top of Package D measured in two-way travel time (seconds).

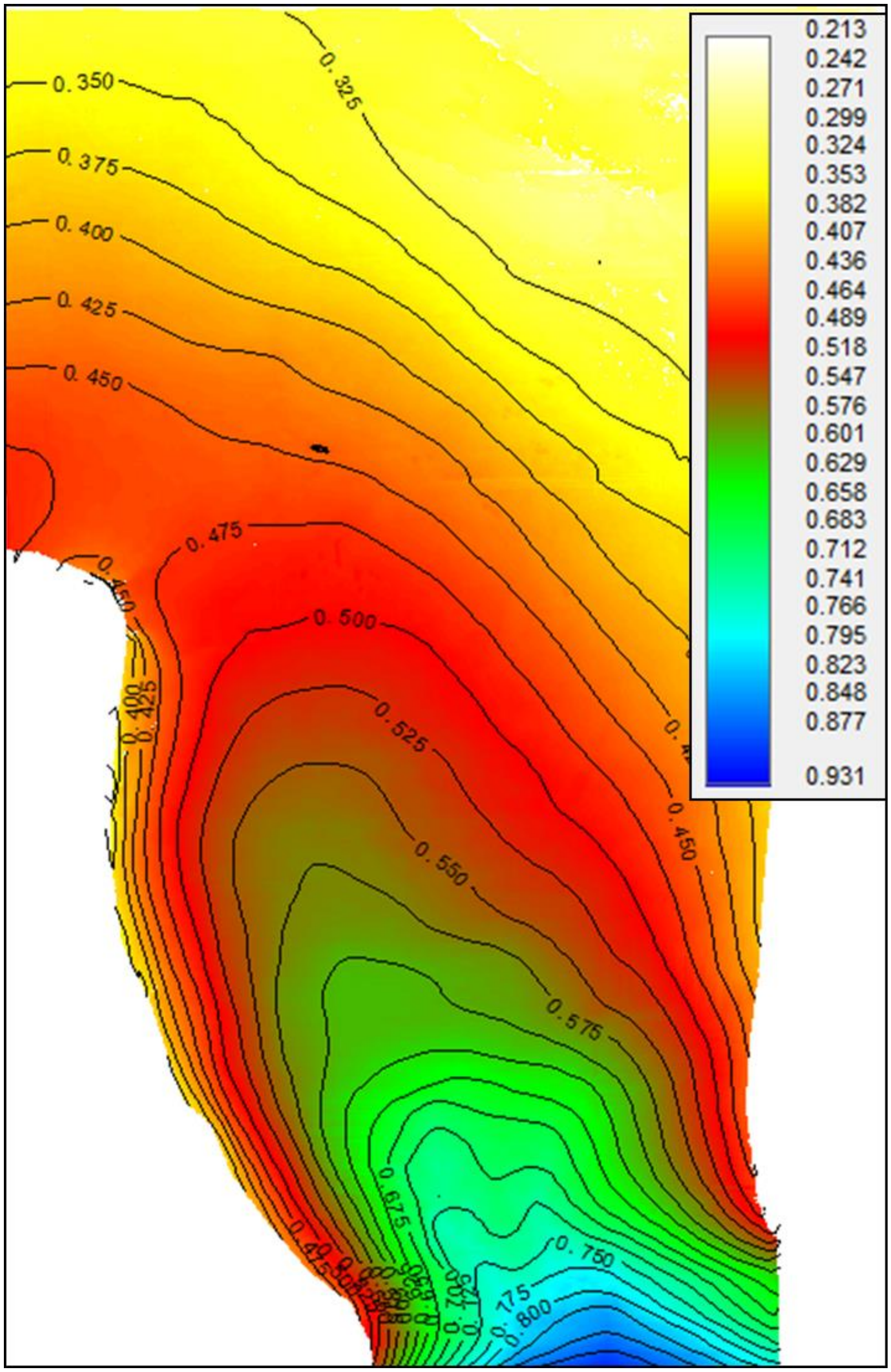

Figure A1-5. Top of Package E measured in two-way travel time (seconds).

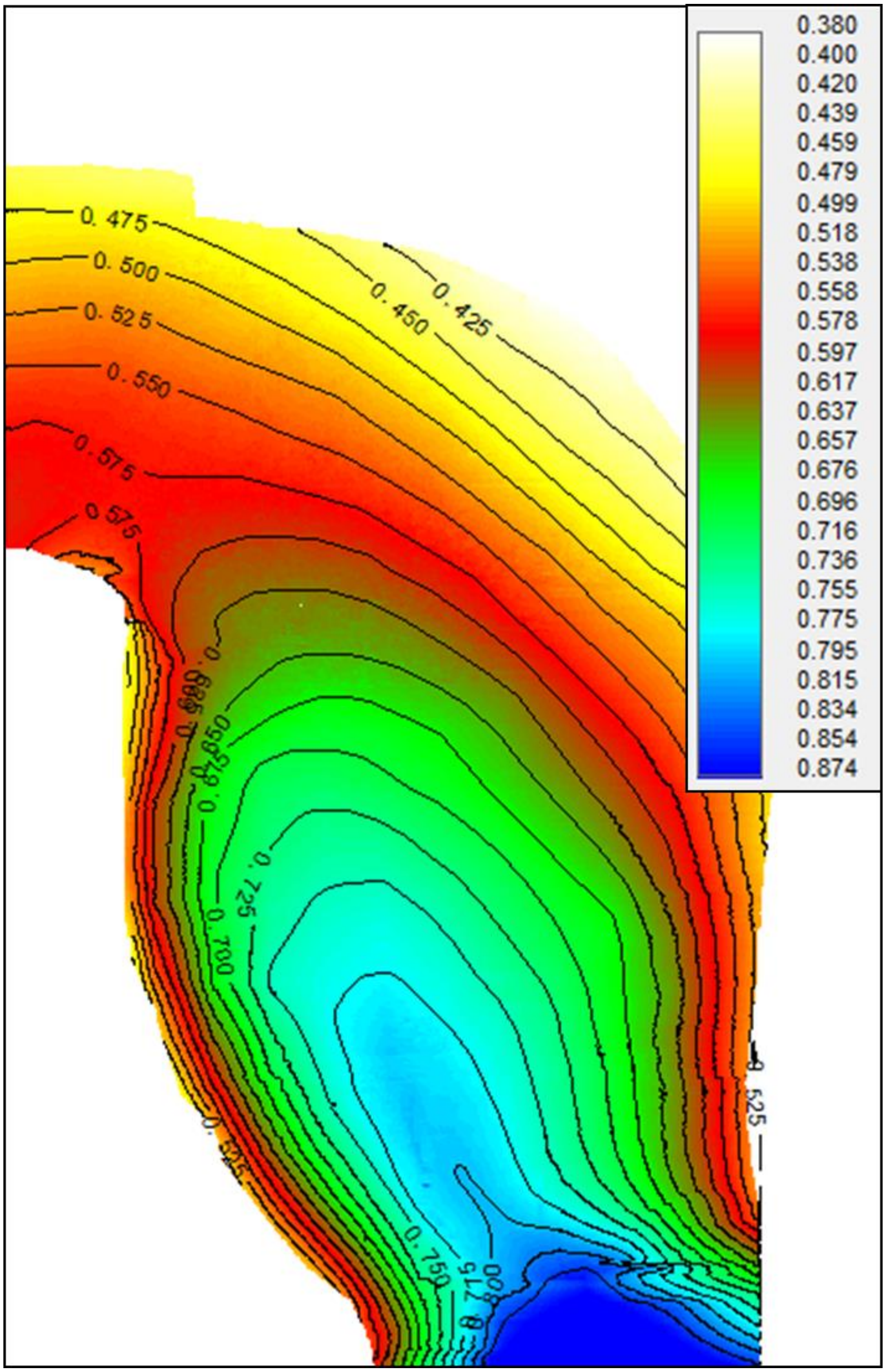

Figure A1-6. Top of Package F measured in two-way travel time (seconds).

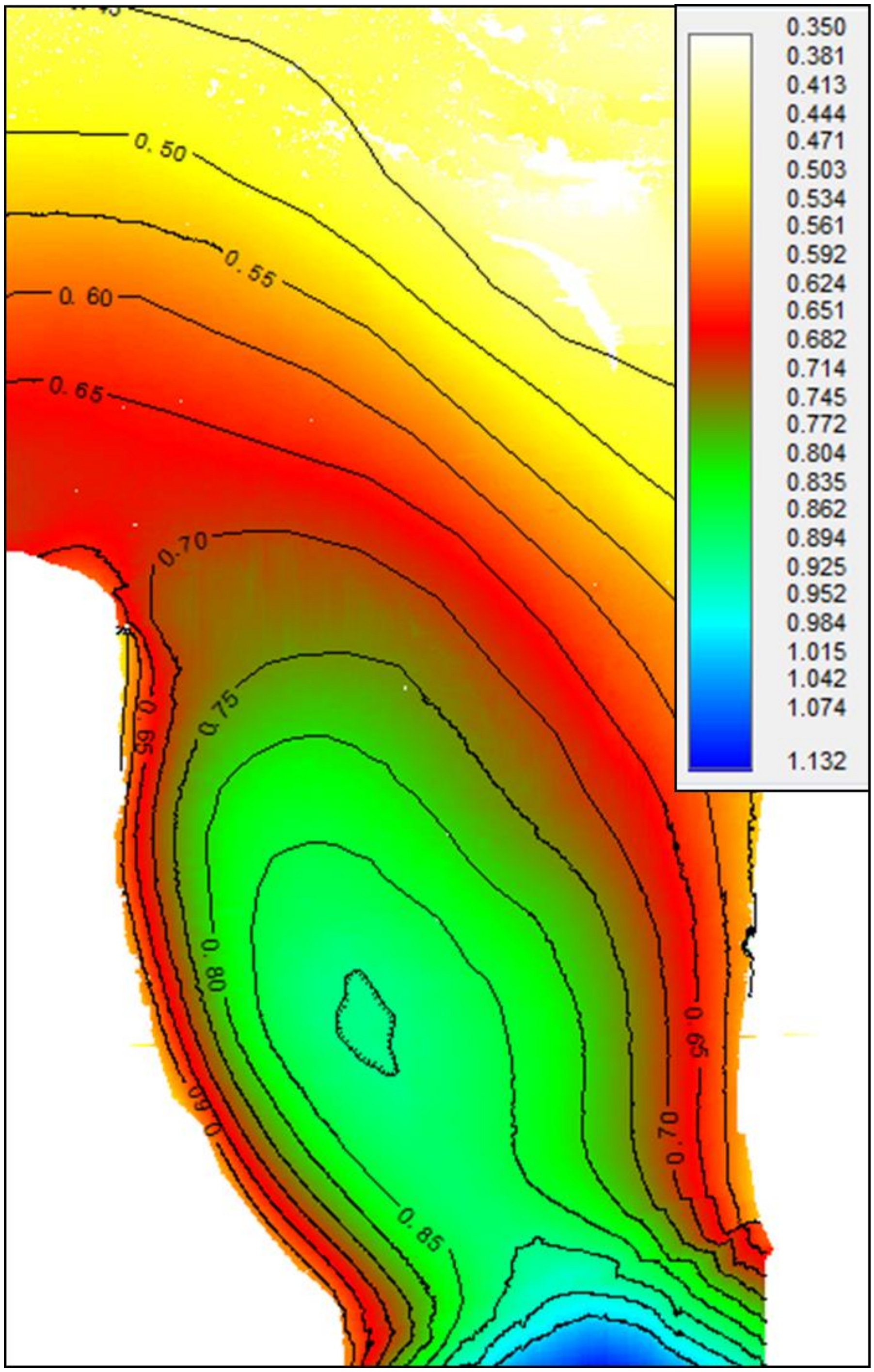

Figure A1-7. Top of Package G measured in two-way travel time (seconds).

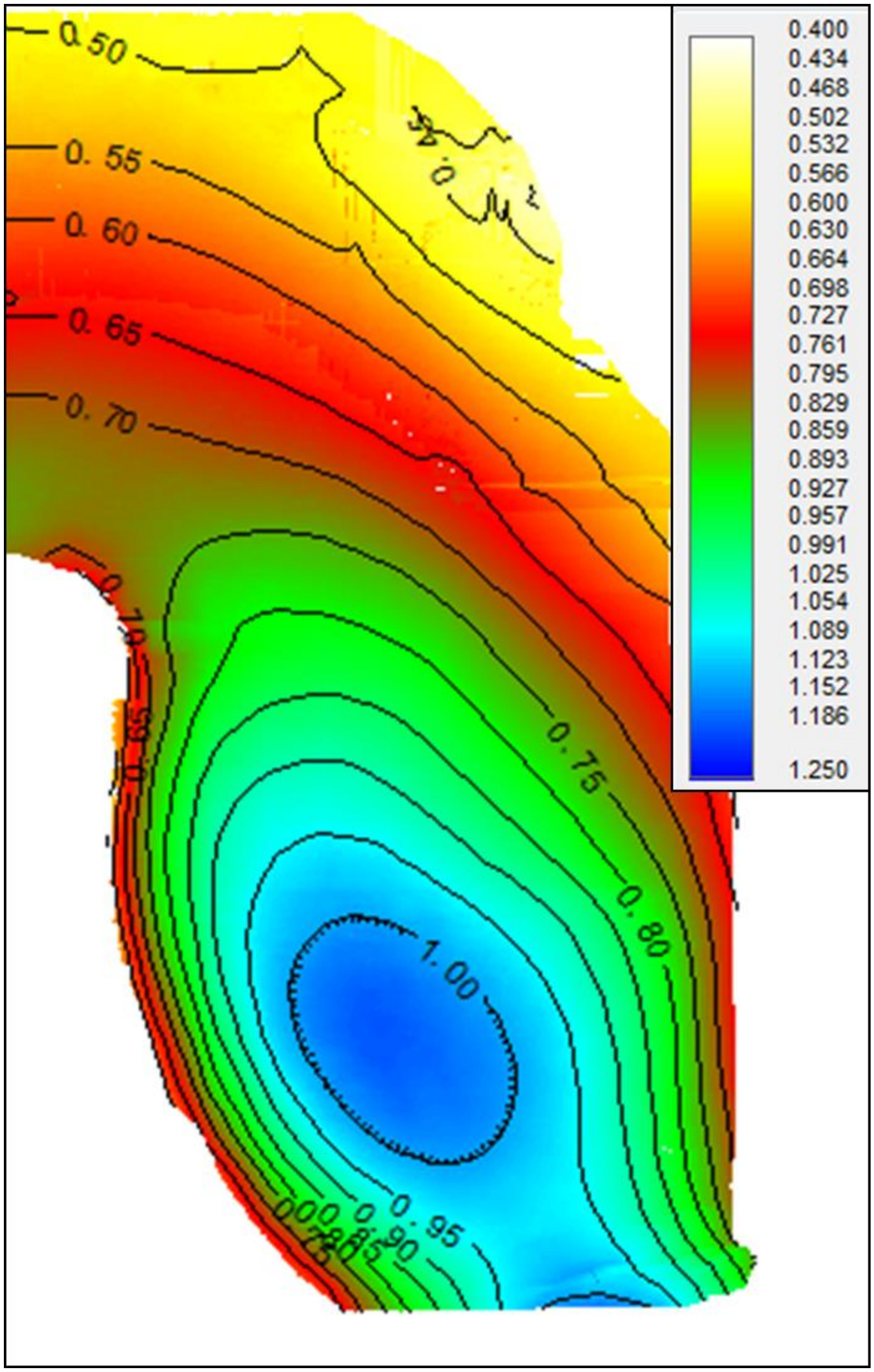

Figure A1-8. Top of Package H measured in two-way travel time (seconds).

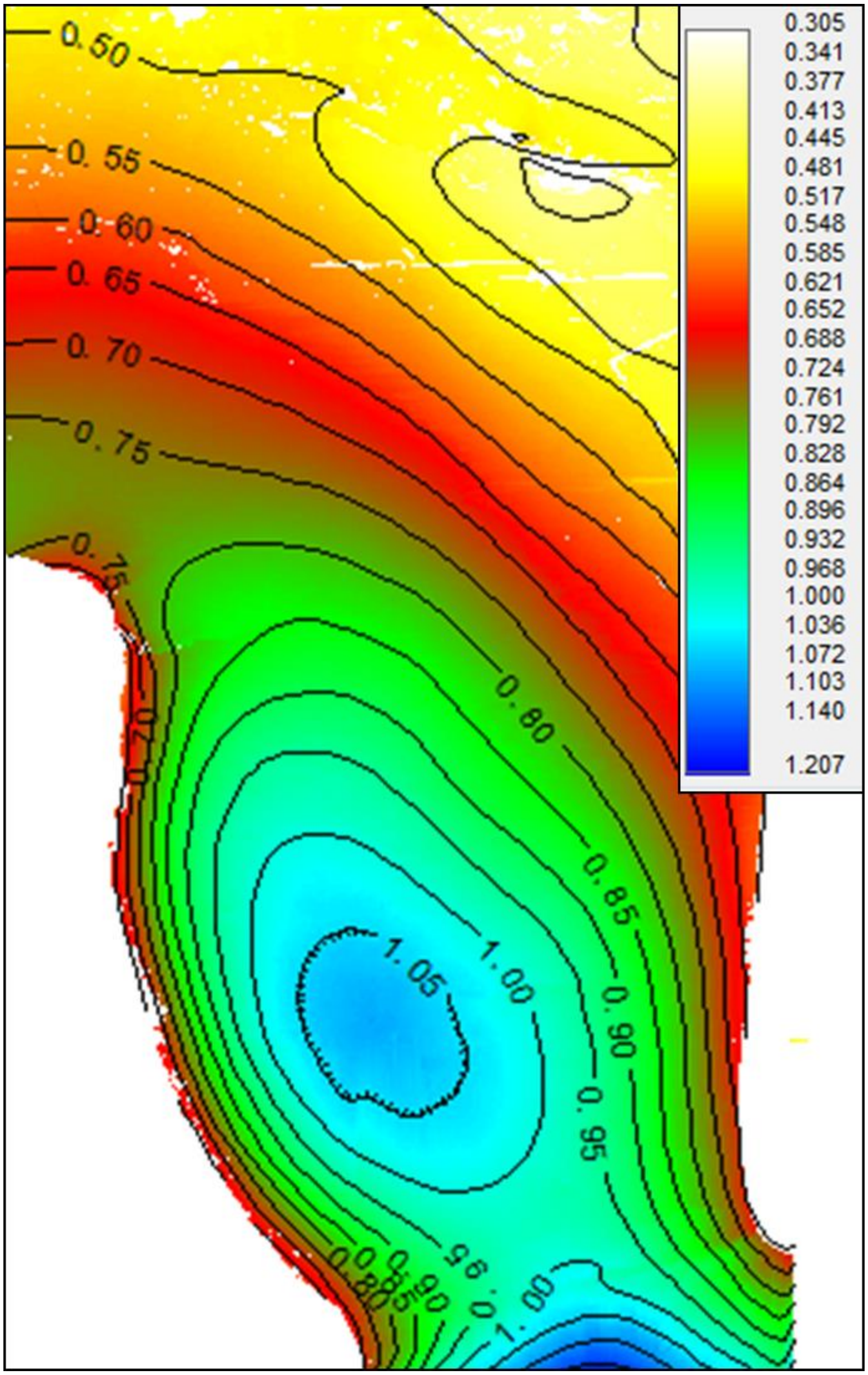

Figure A1-9. Top of Package I measured in two-way travel time (seconds).

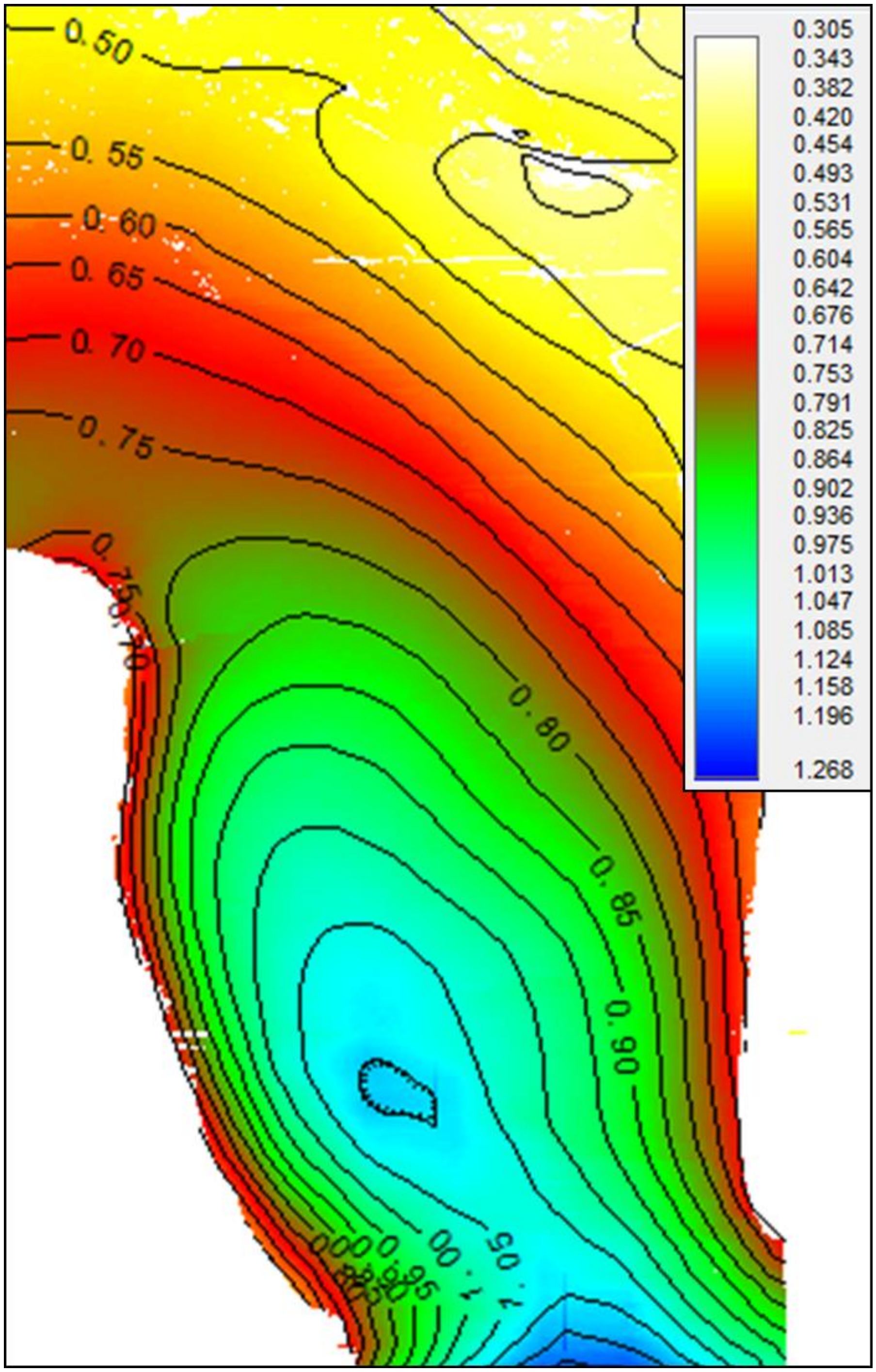

Figure A1-10. Top of Package J measured in two-way travel time (seconds).

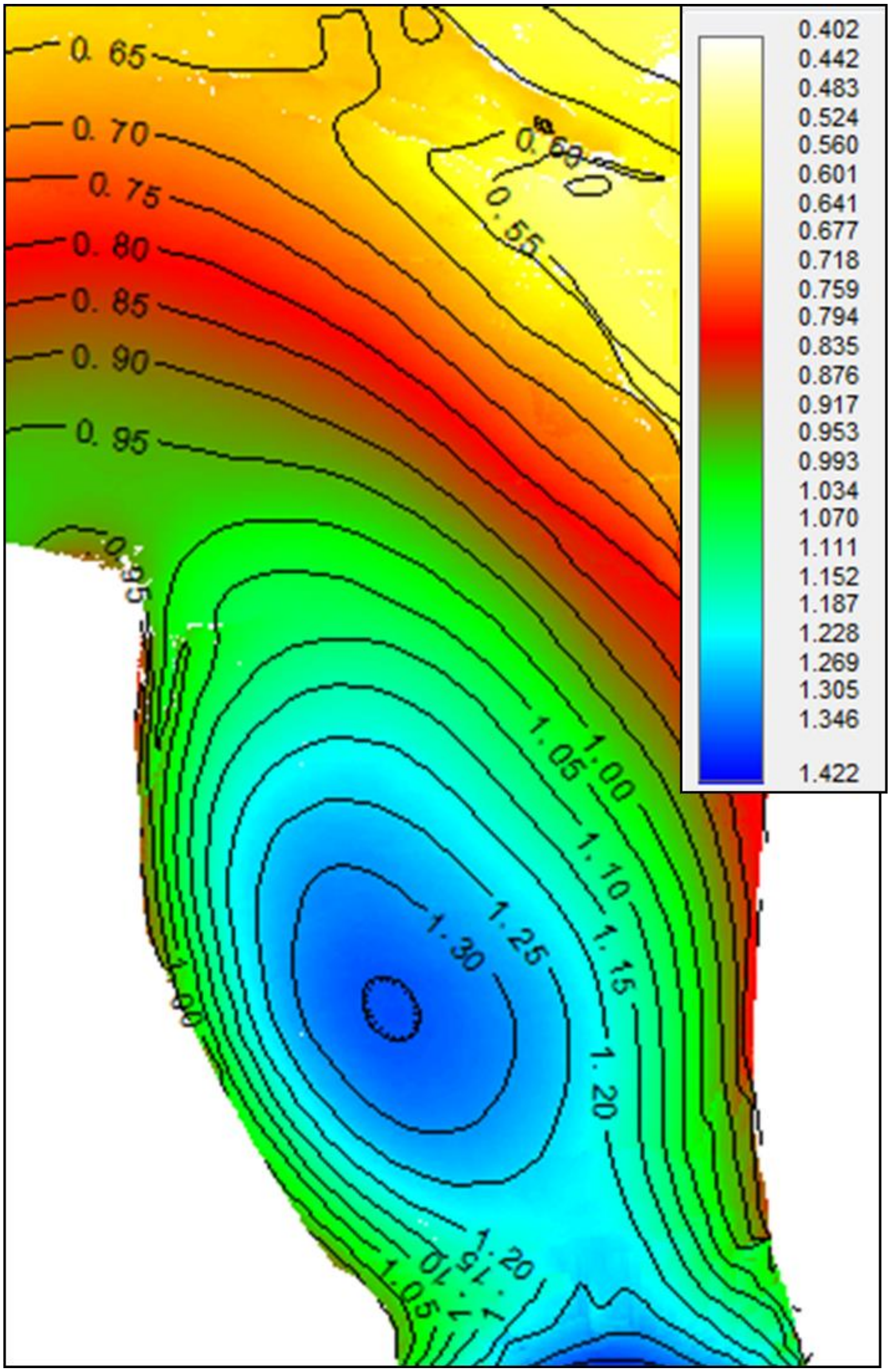

Figure A1-11. Top of Package K measured in two-way travel time (seconds).

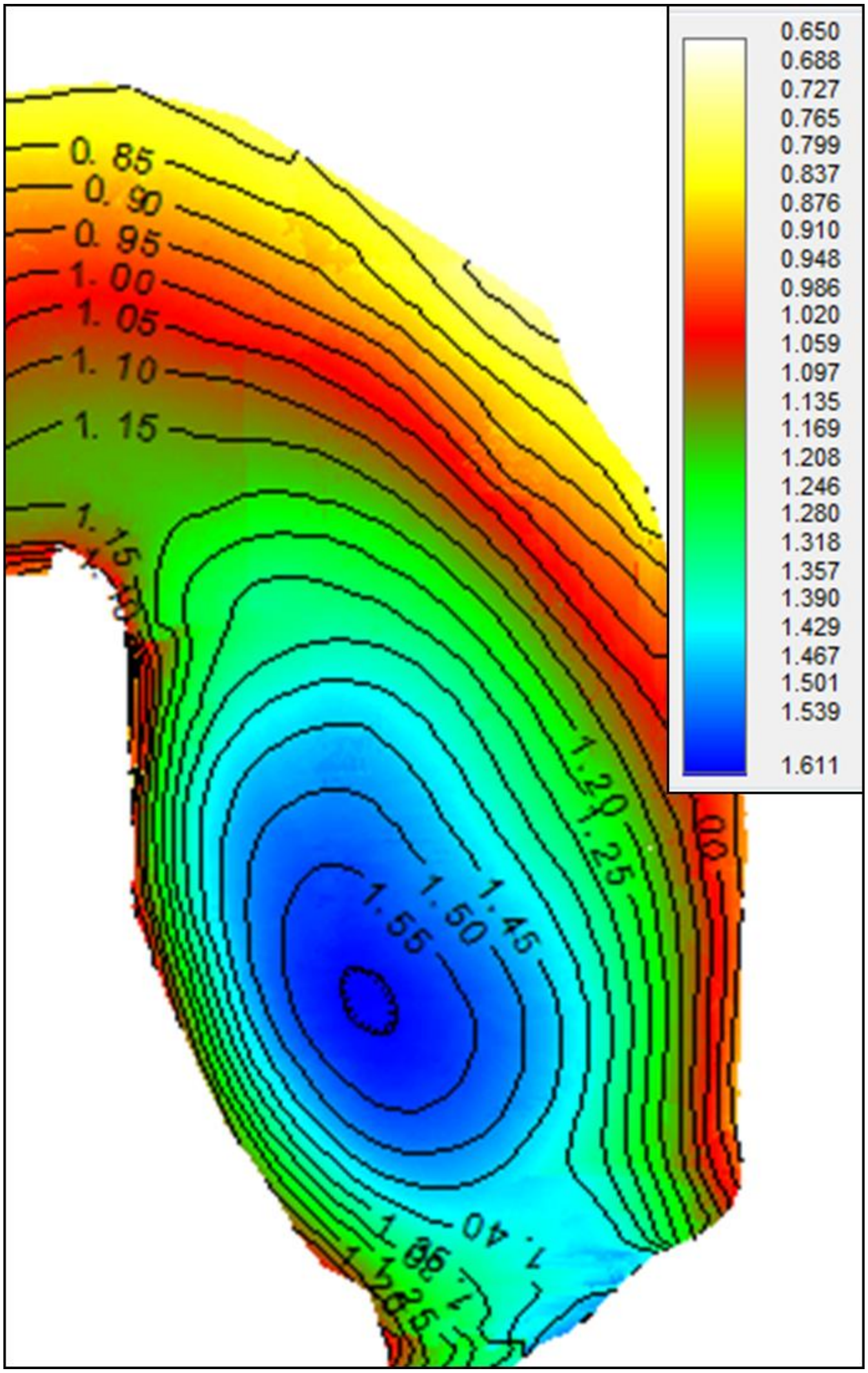

Figure A1-12. Top of Package L measured in two-way travel time (seconds).

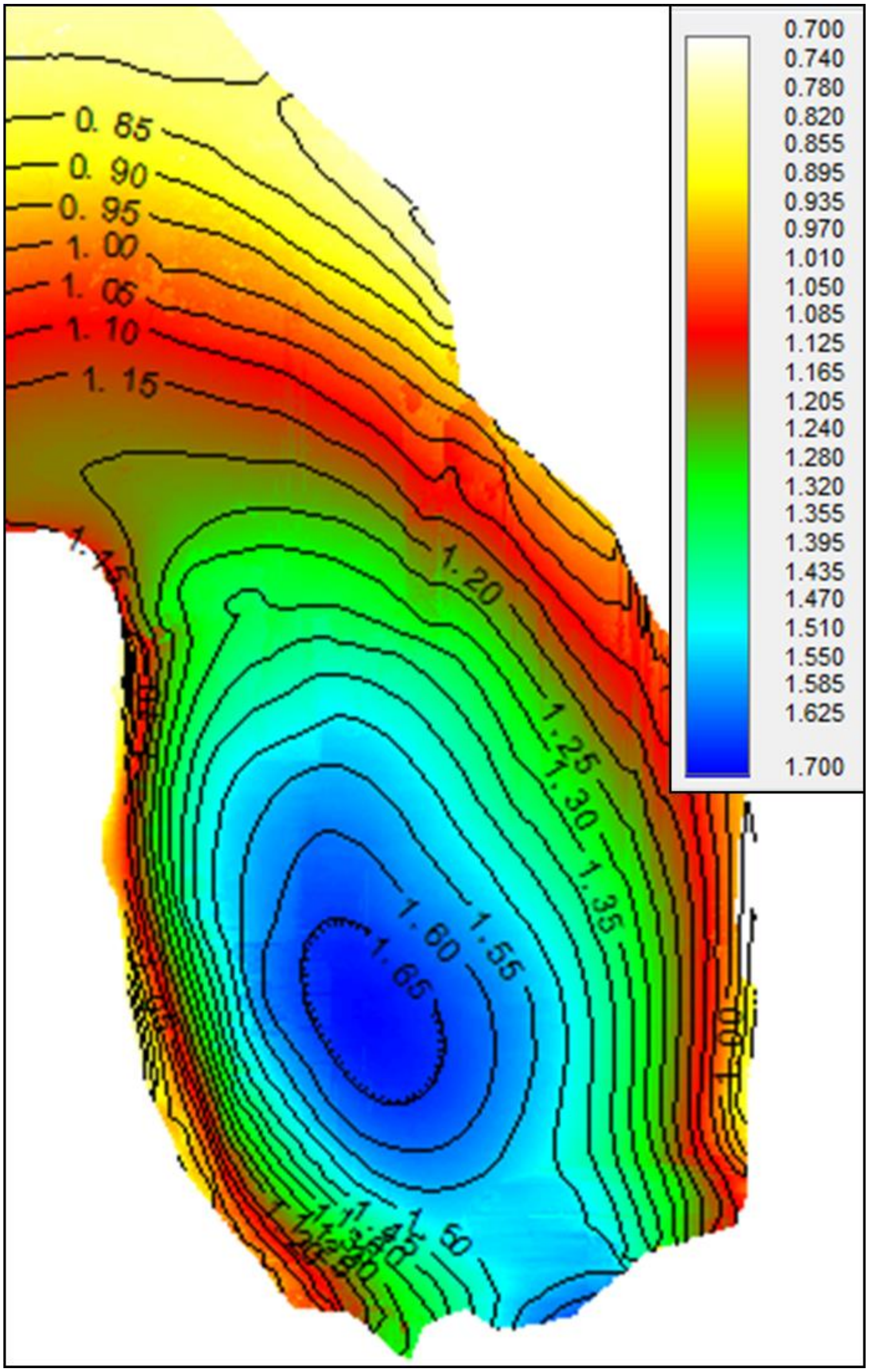

Figure A1-13. Top of Package M measured in two-way travel time (seconds).

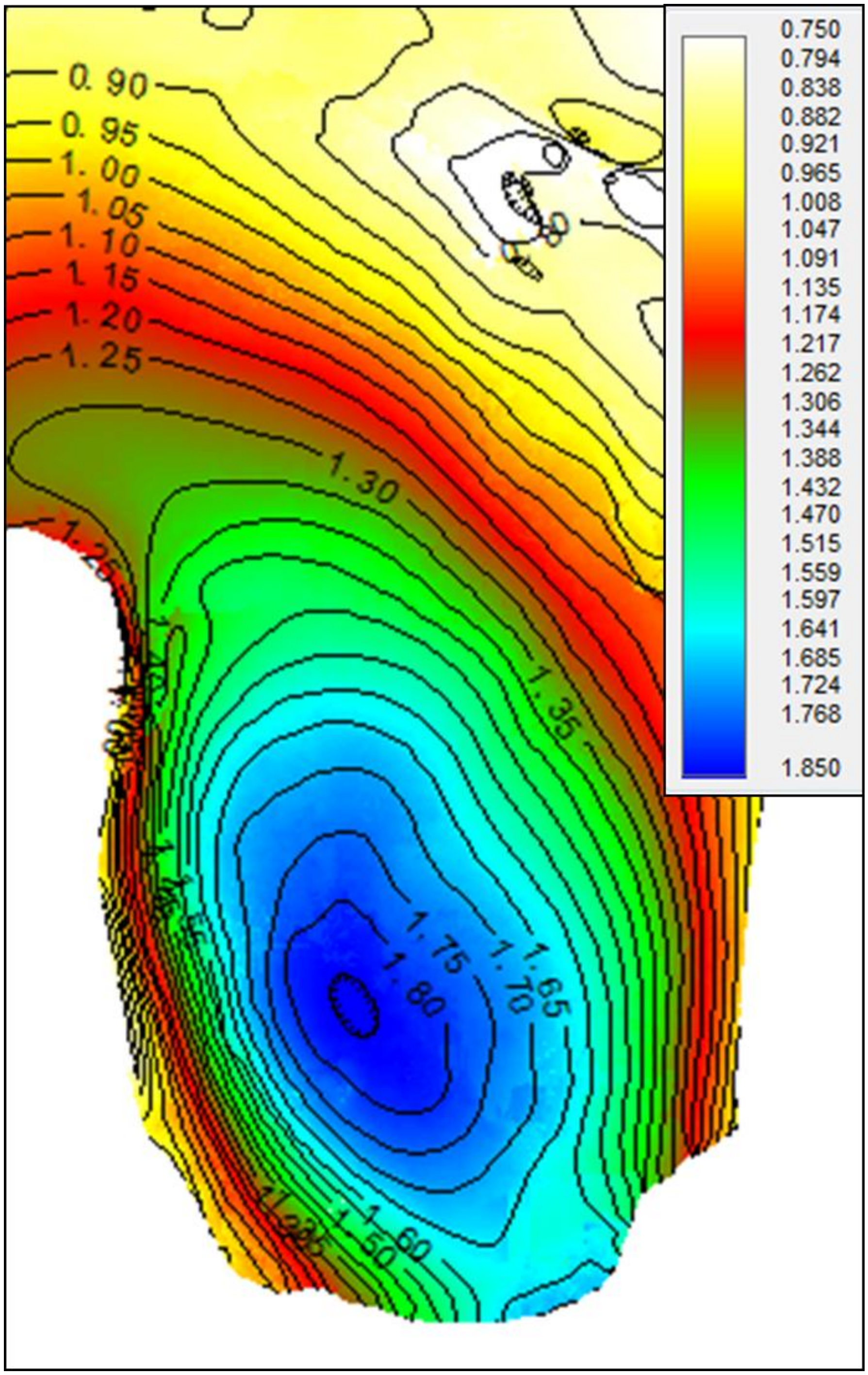

Figure A1-14. Top of Package N measured in two-way travel time (seconds).

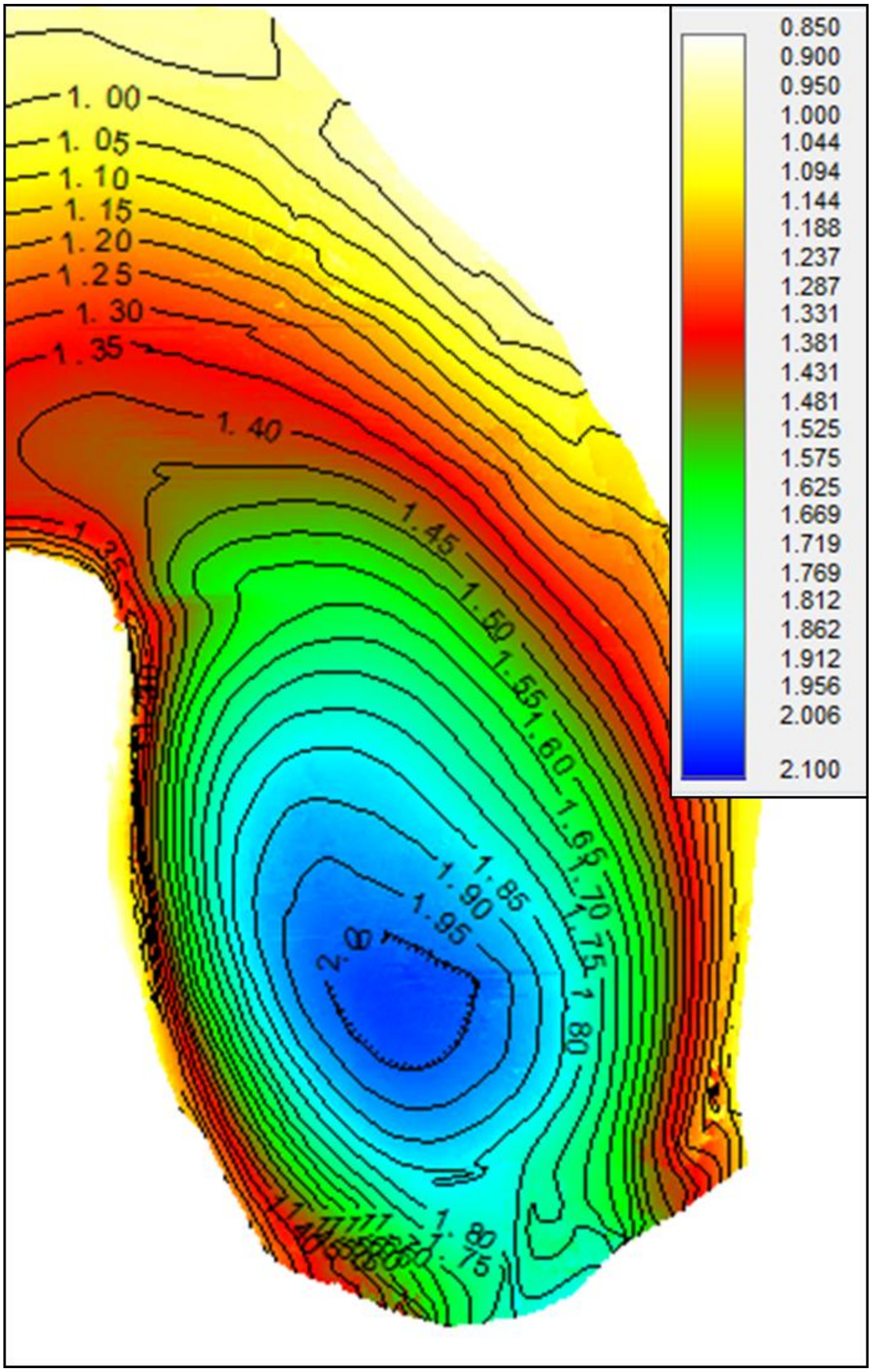

Figure A1-15. Base of Package N measured in two-way travel time (seconds).

Appendix 2. Isochron Maps

Thickness map of most packages defined in the study. The scale is in two-way time (seconds) and the contour intervals vary based on the range of data.

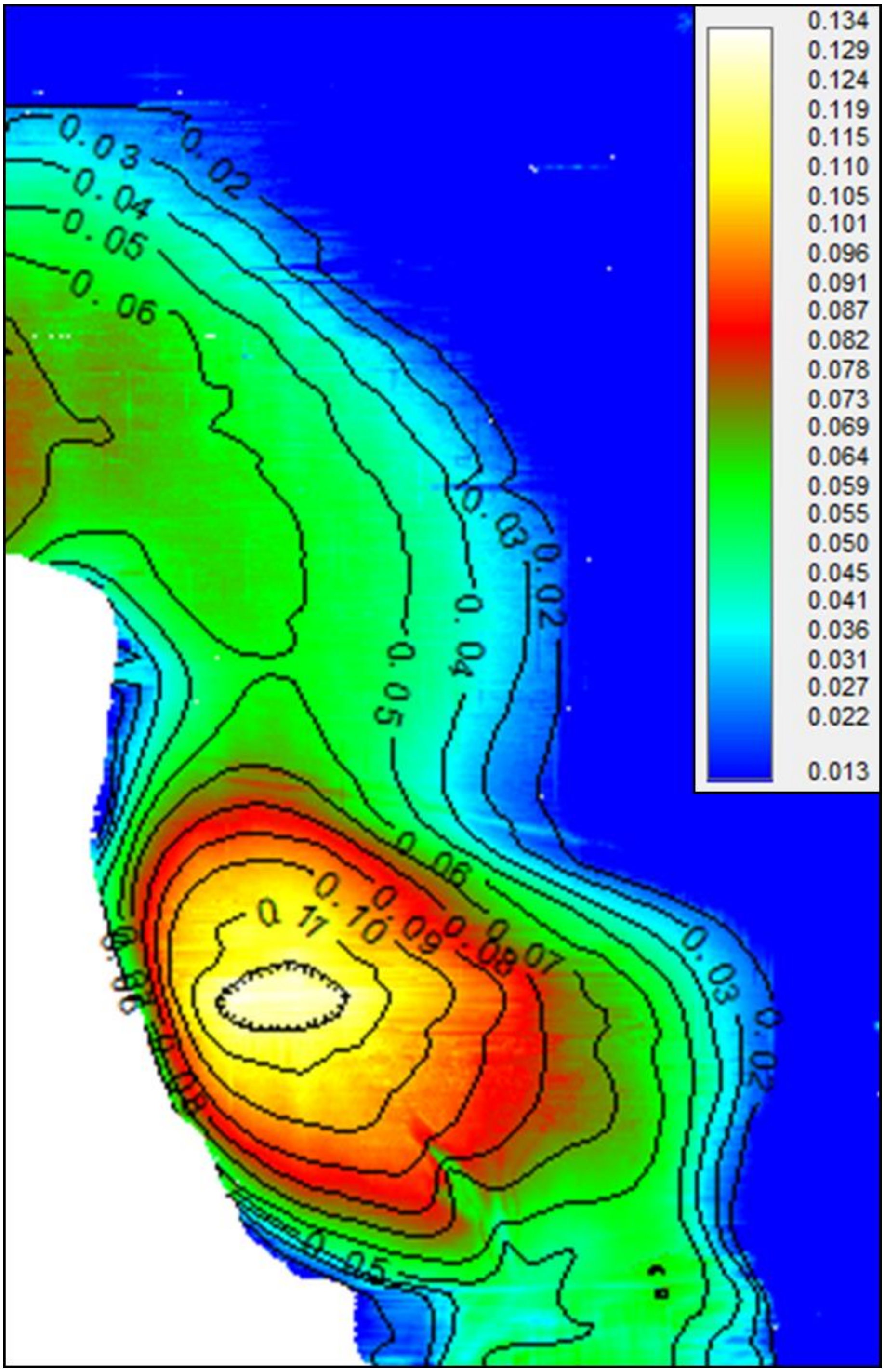

Figure A2-1. Package A Isochron map measured in two-way travel time (seconds).

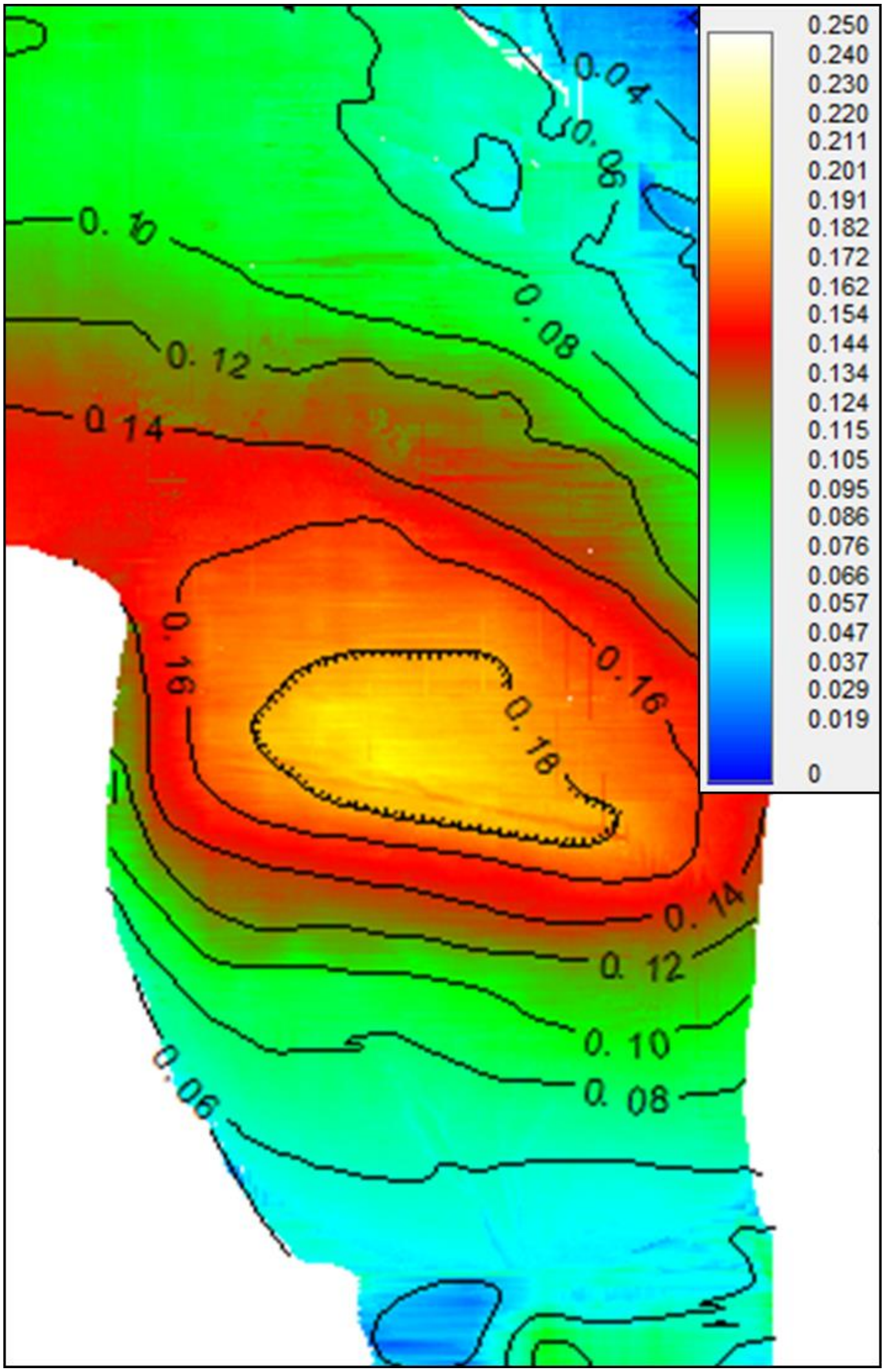

Figure A2-2. Package B Isochron map measured in two-way travel time (seconds).

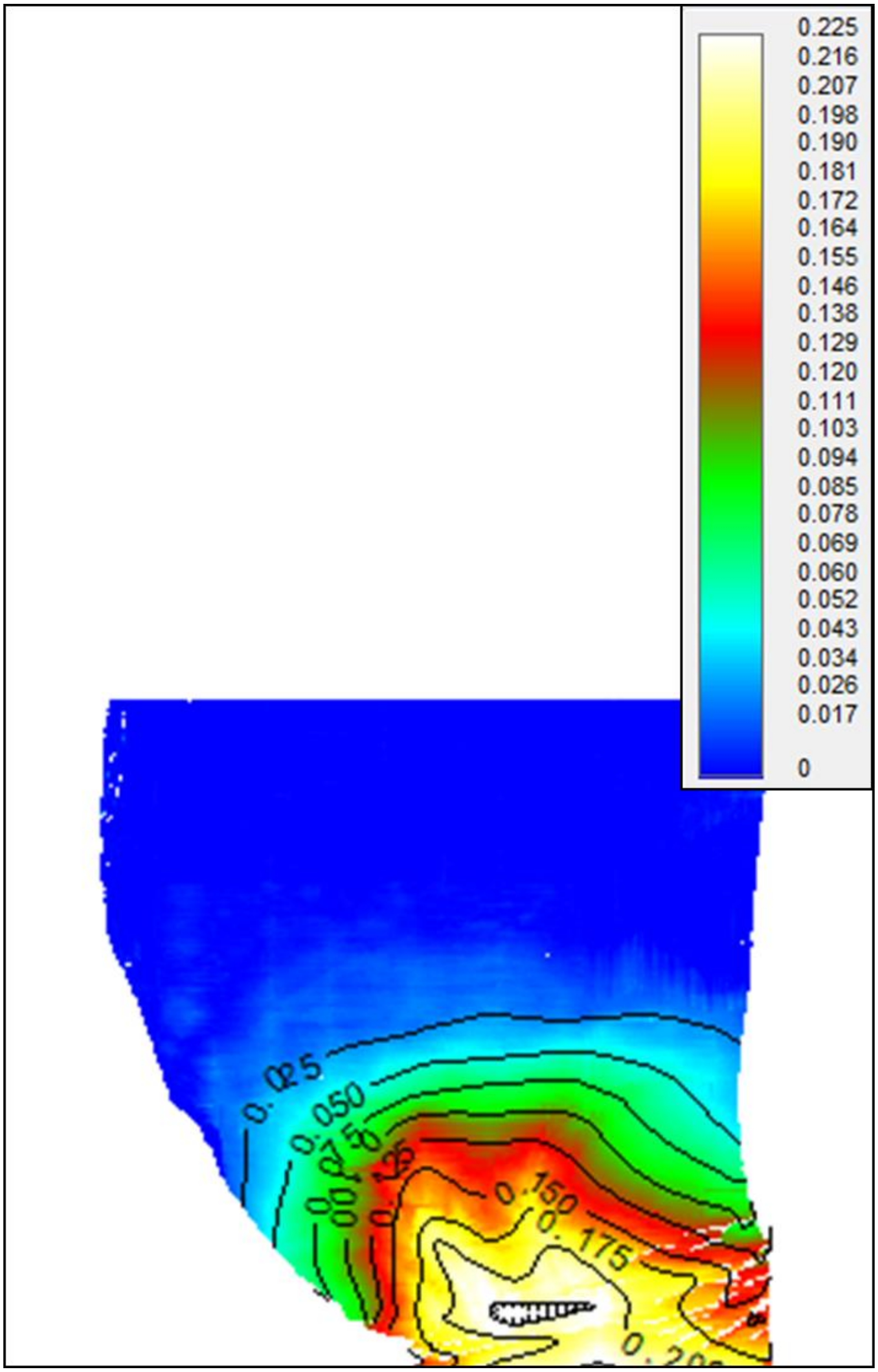

Figure A2-3. Package D Isochron map measured in two-way travel time (seconds).

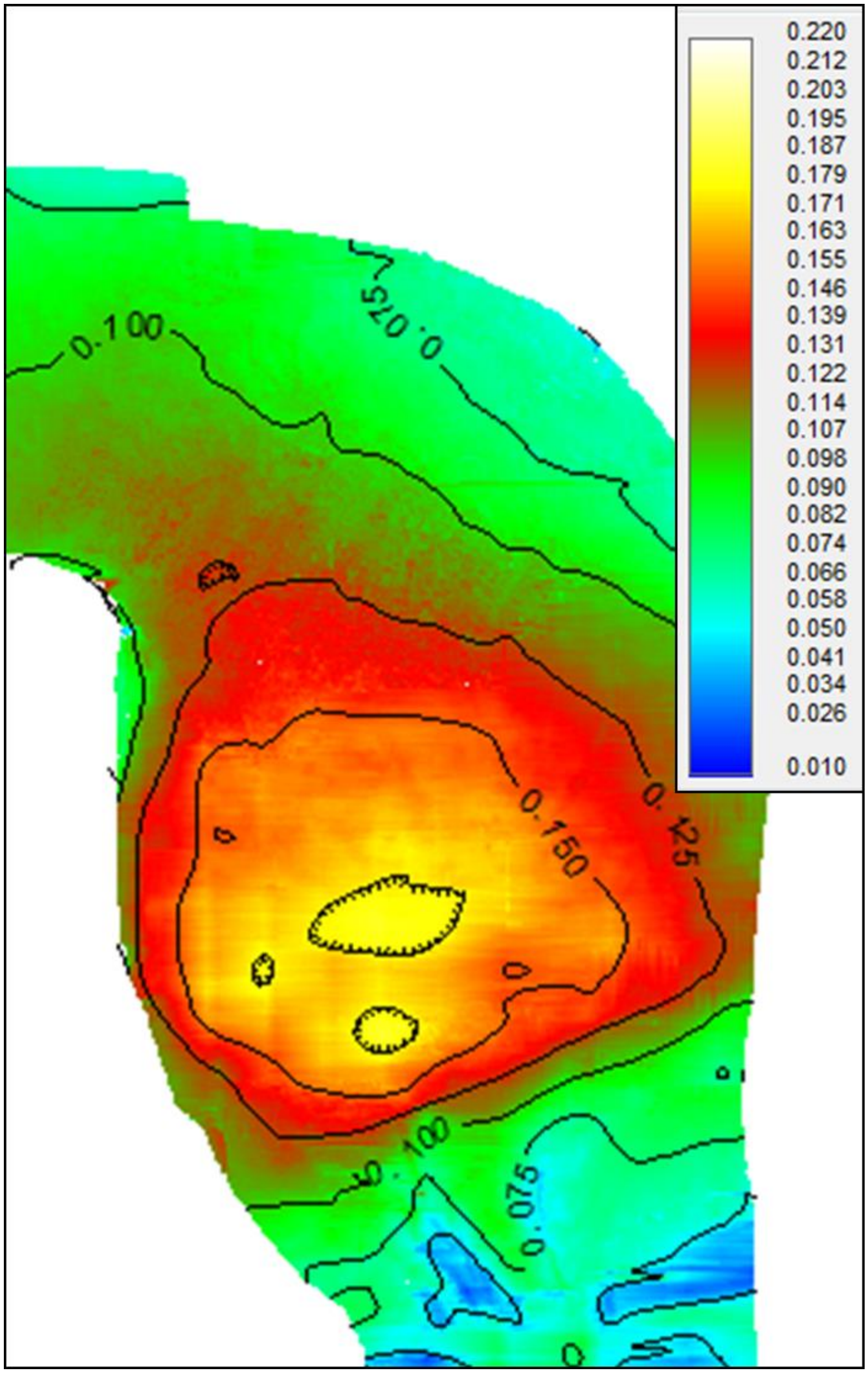

Figure A2-4. Package E Isochron map measured in two-way travel time (seconds).

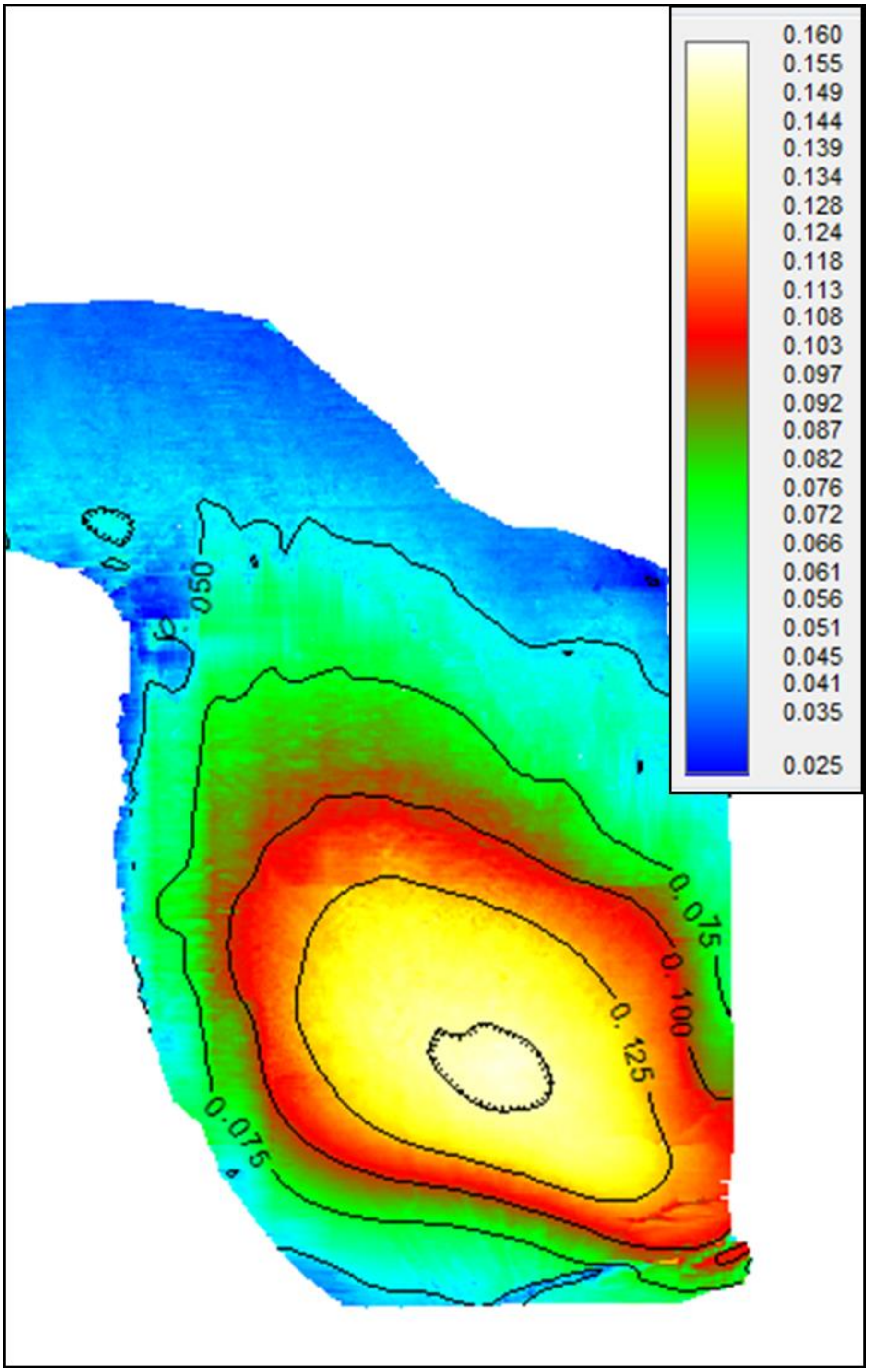

Figure A2-5. Package G Isochron map measured in two-way travel time (seconds).

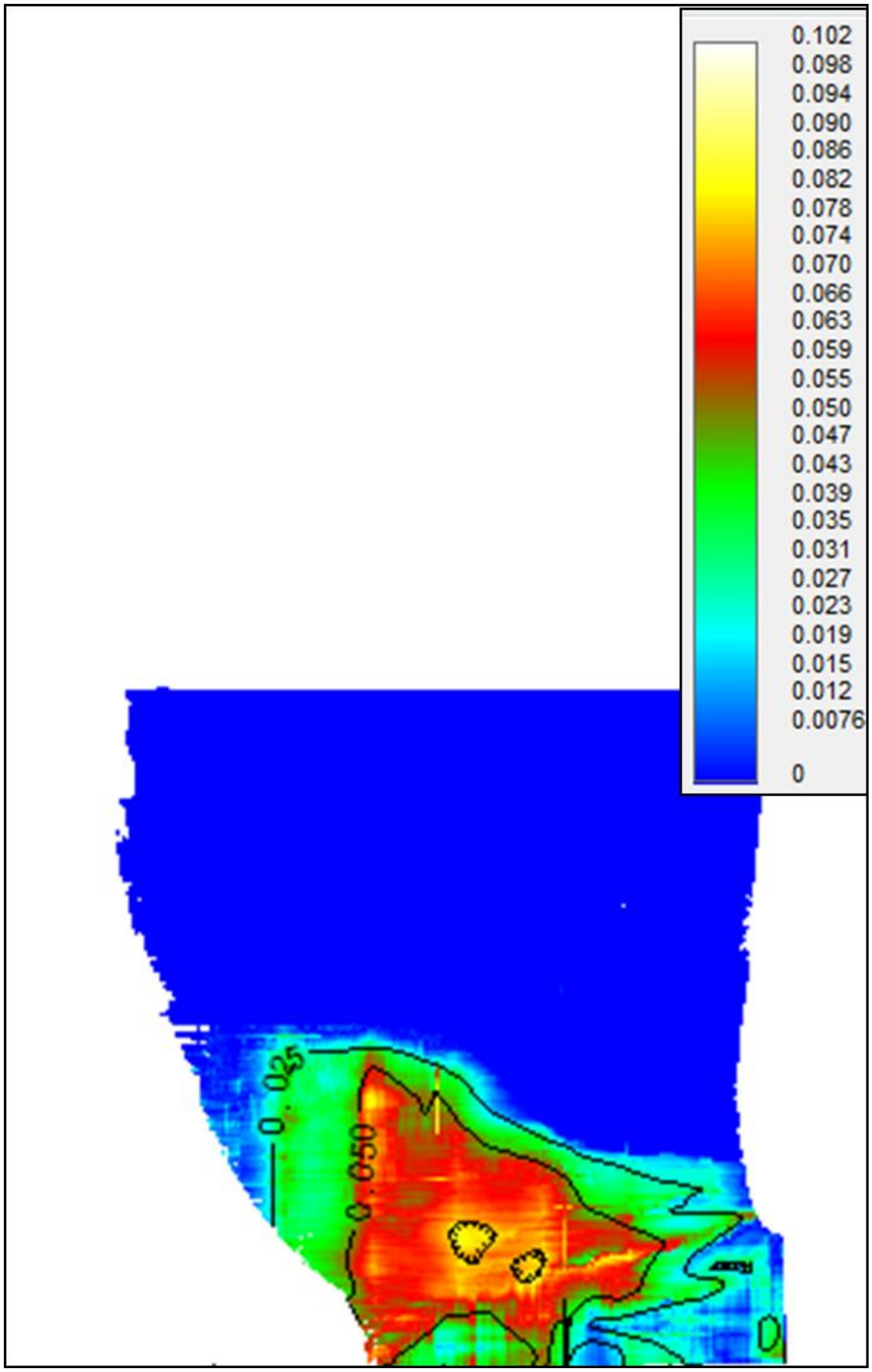

Figure A2-6. Package I Isochron map measured in two-way travel time (seconds).

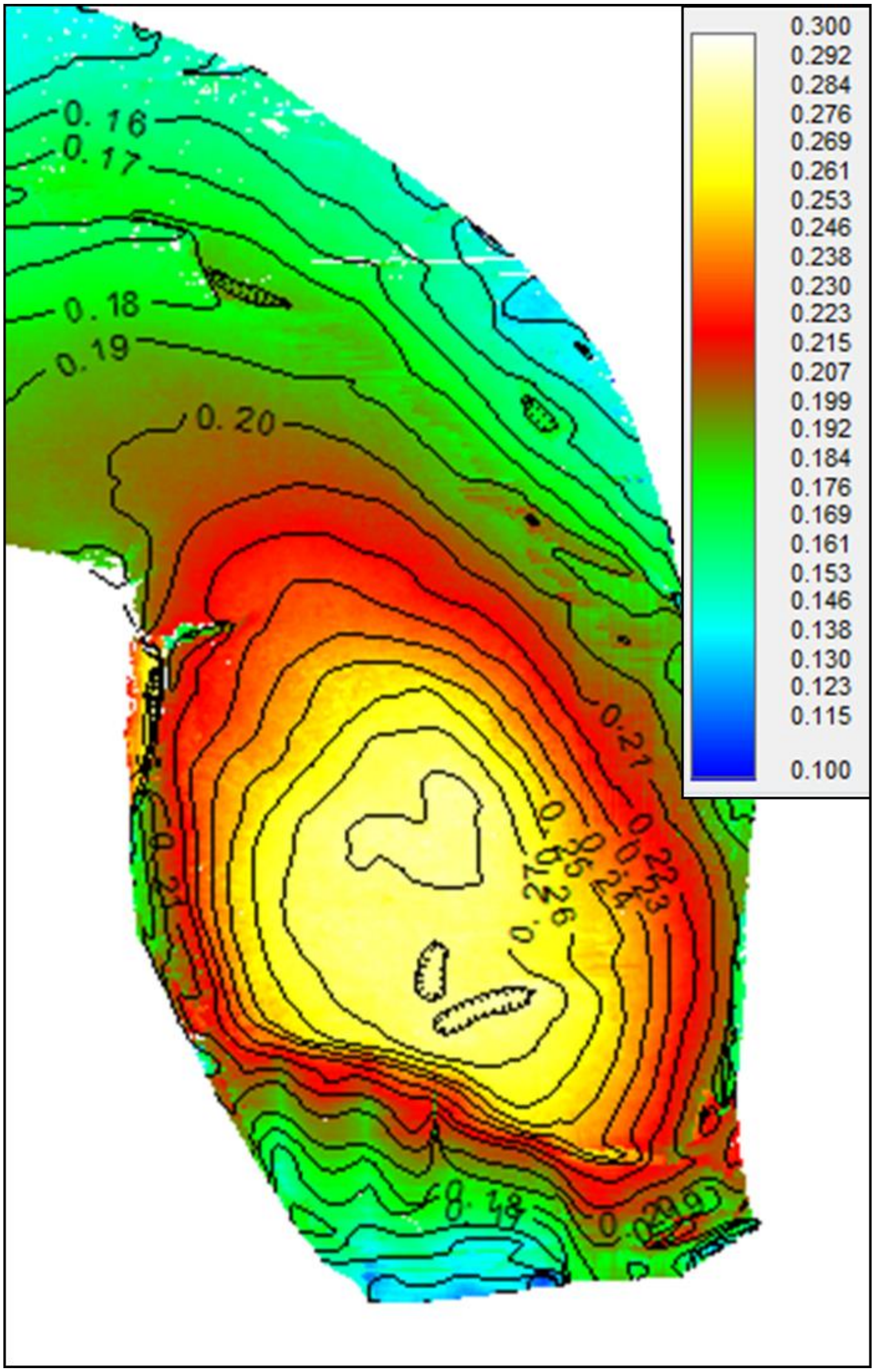

Figure A2-7. Package J Isochron map measured in two-way travel time (seconds).

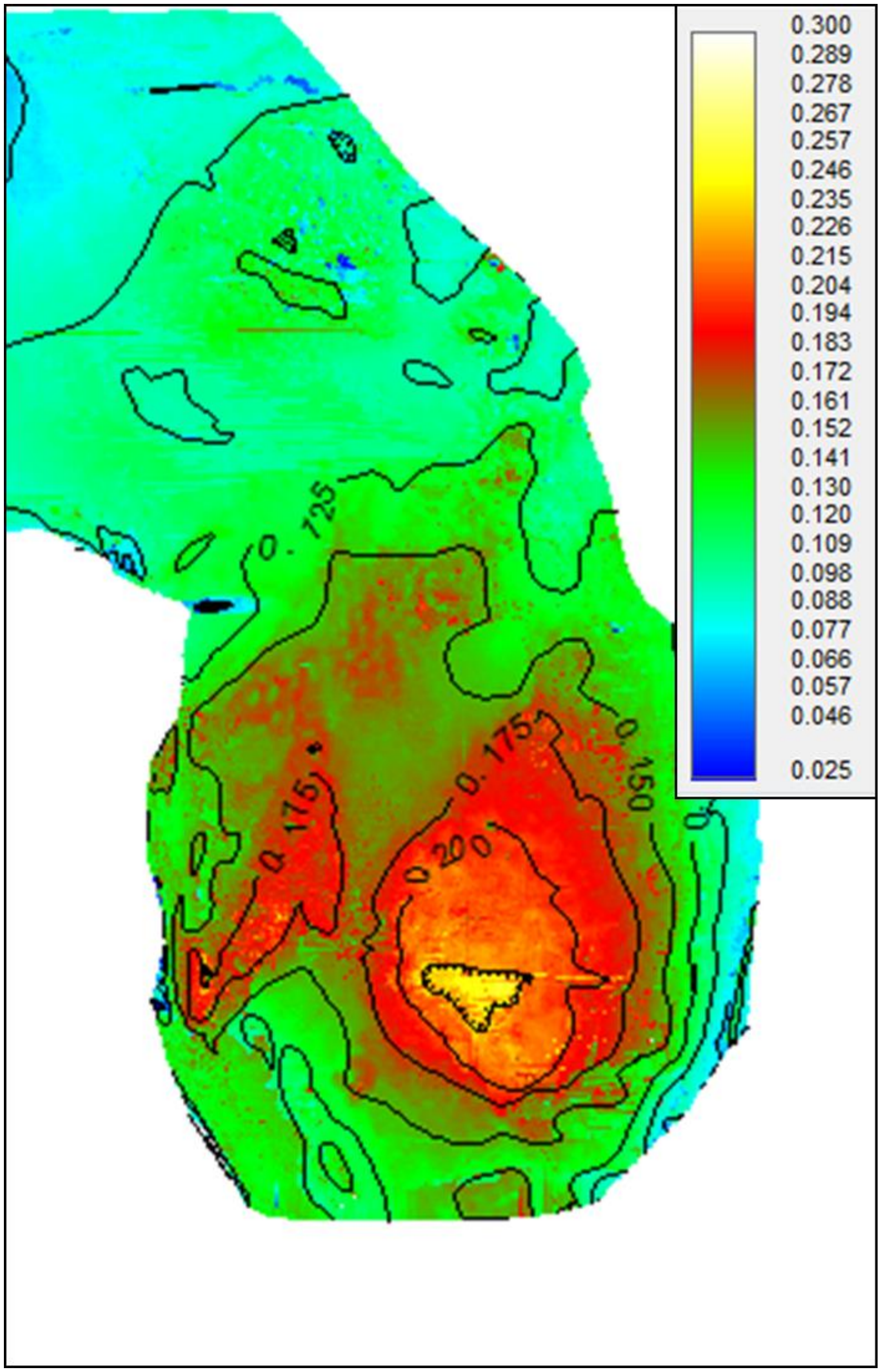

Figure A2-8. Package N Isochron map measured in two-way travel time (seconds).

Appendix 3. Volume Attribute Minimum Amplitude Maps

Minimum amplitude maps of most intervals defined in the study. The scale represents amplitude.

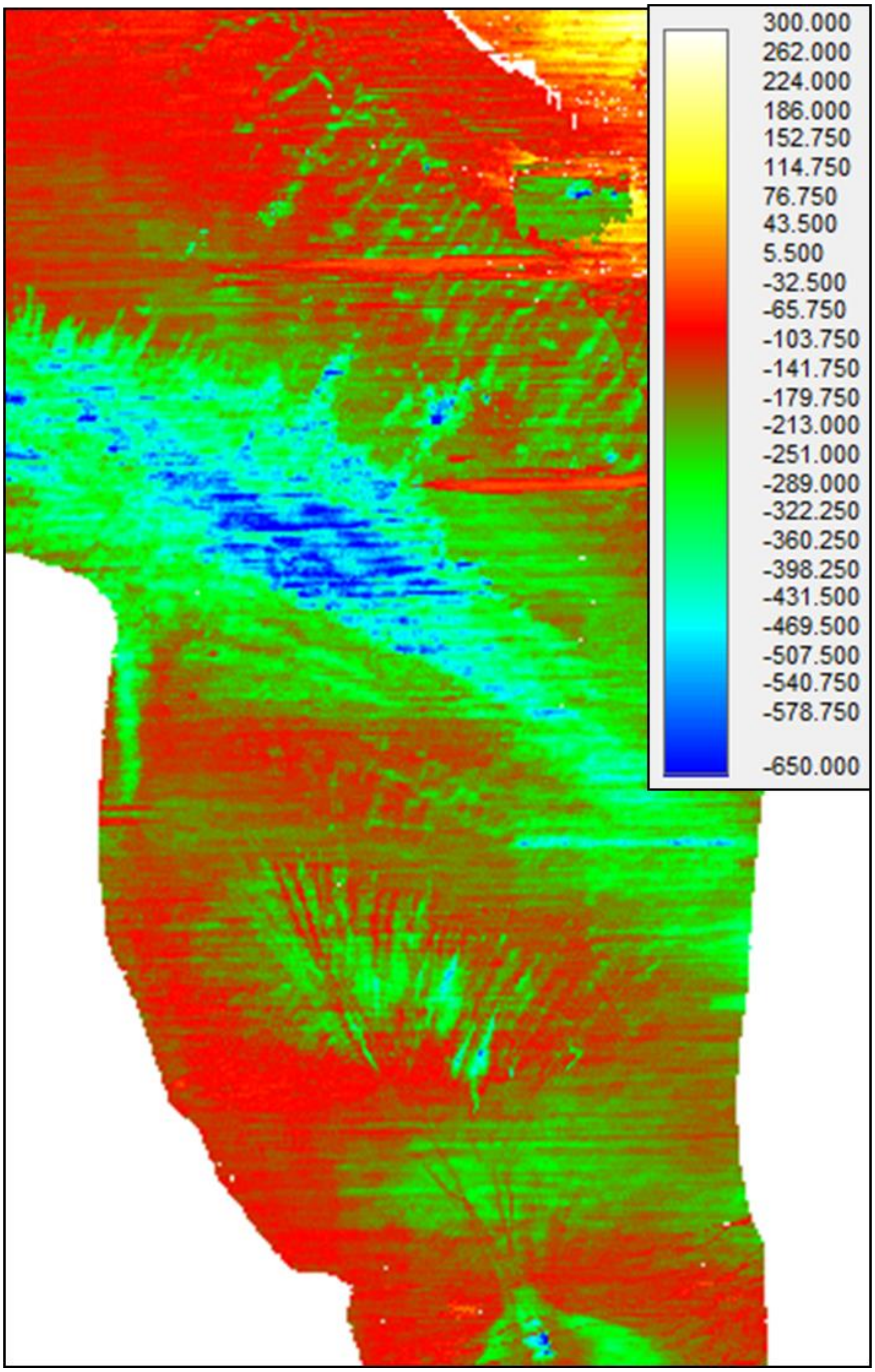

Figure A3-1. Package B VATMIN map measured in amplitude.

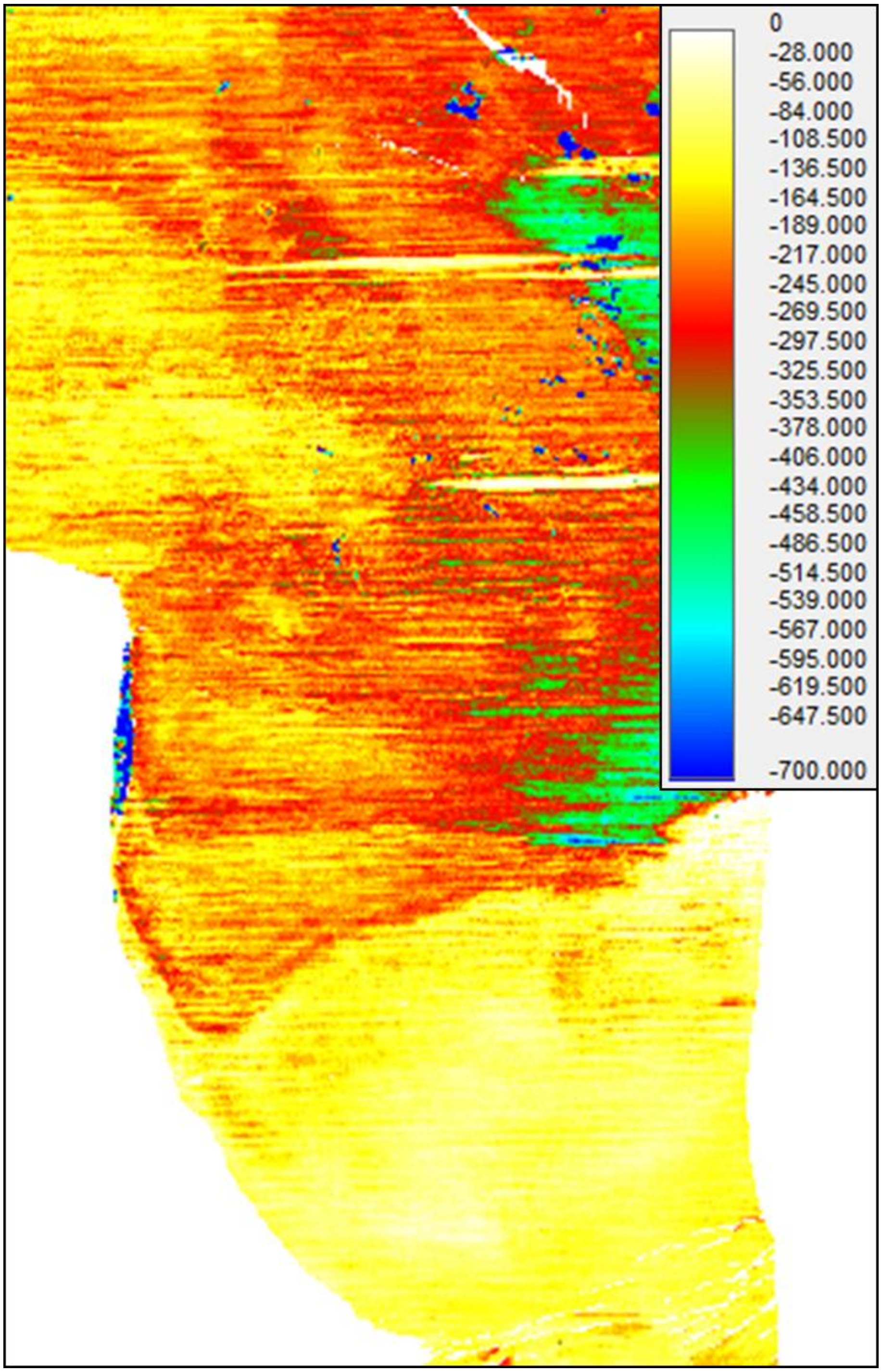

Figure A3-2. Package C VATMIN map measured in amplitude.

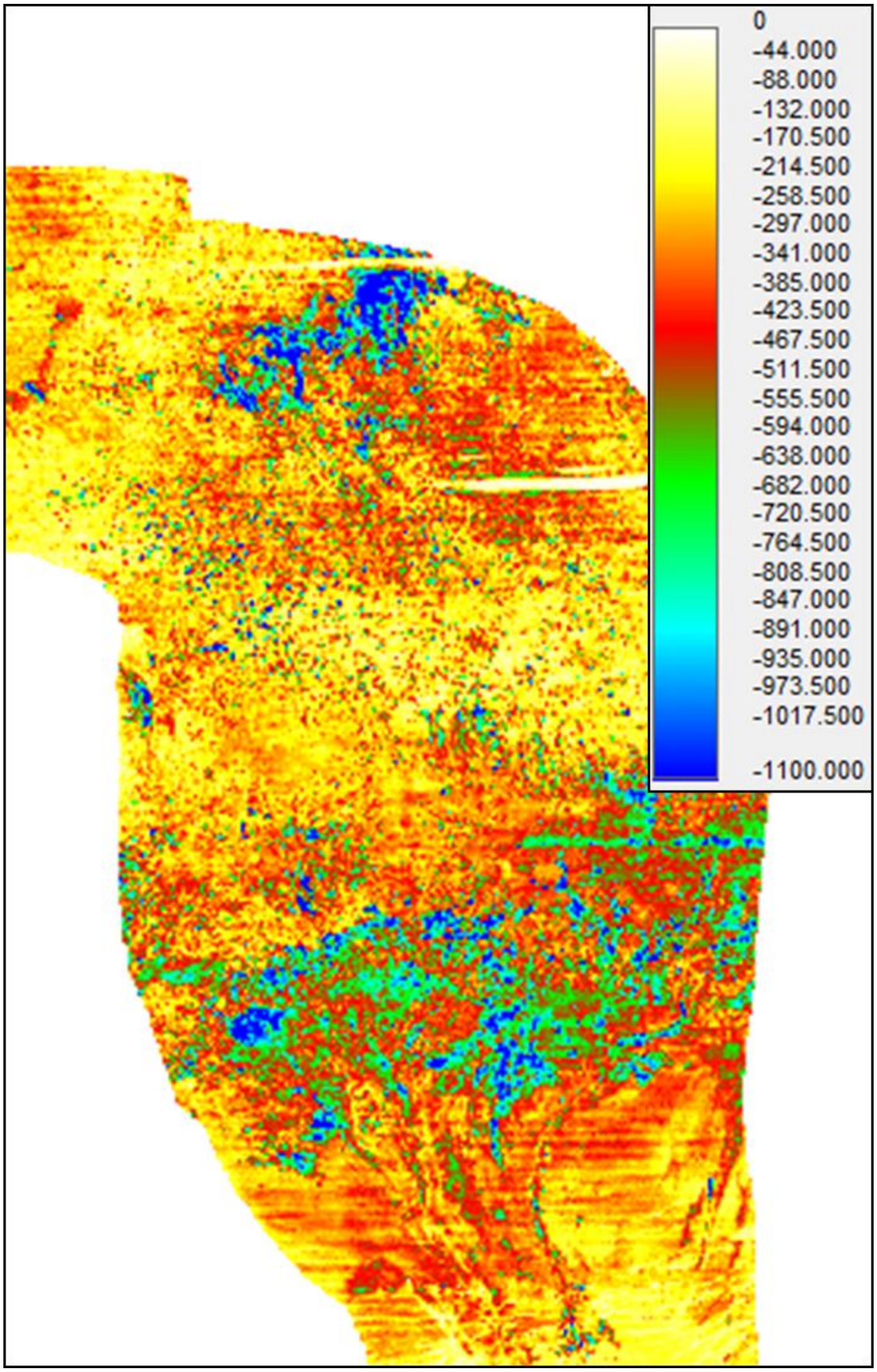

Figure A3-3. Package C VATMIN map measured in amplitude.

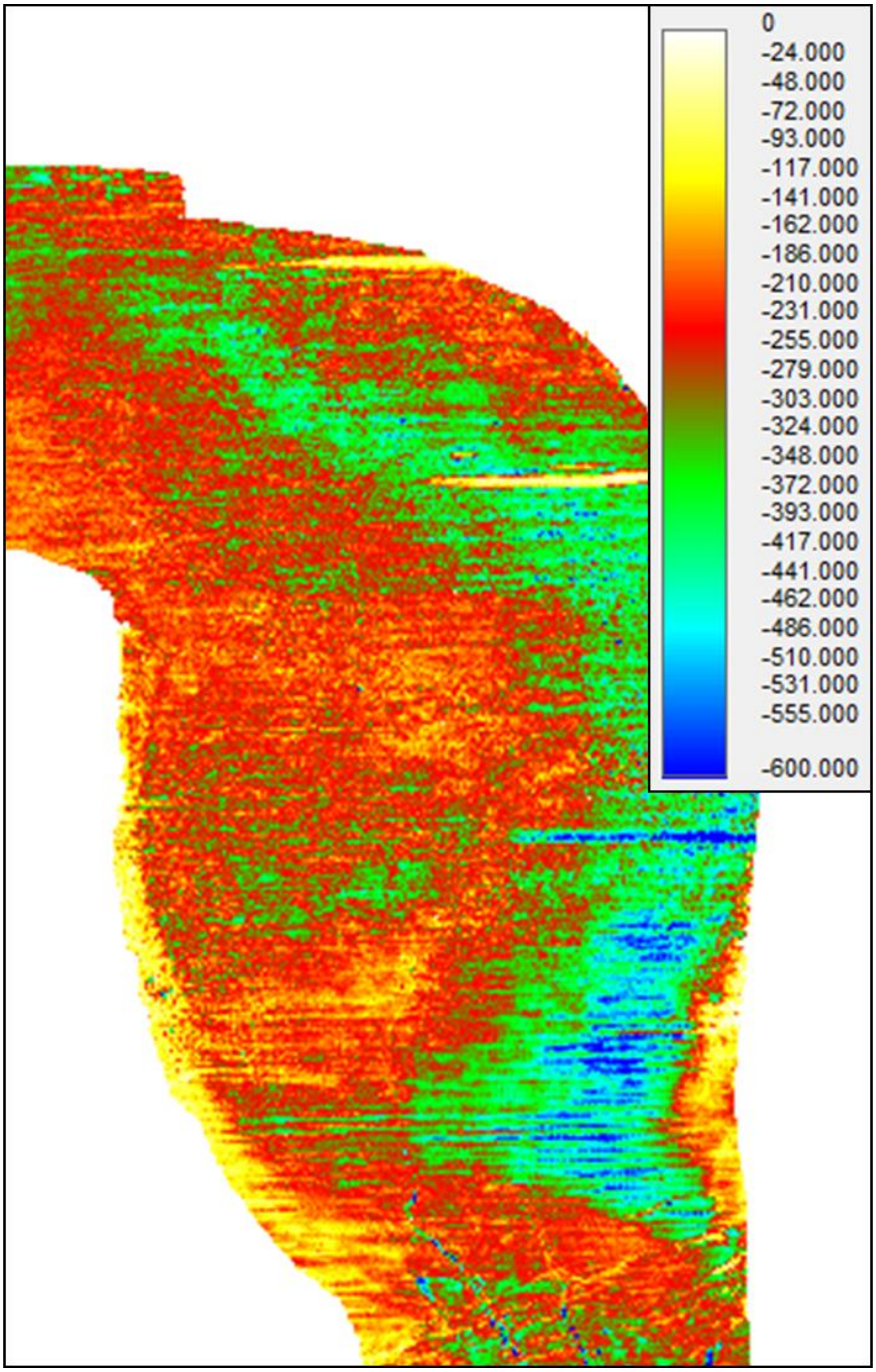

Figure A3-4. Package F VATMIN map measured in amplitude.

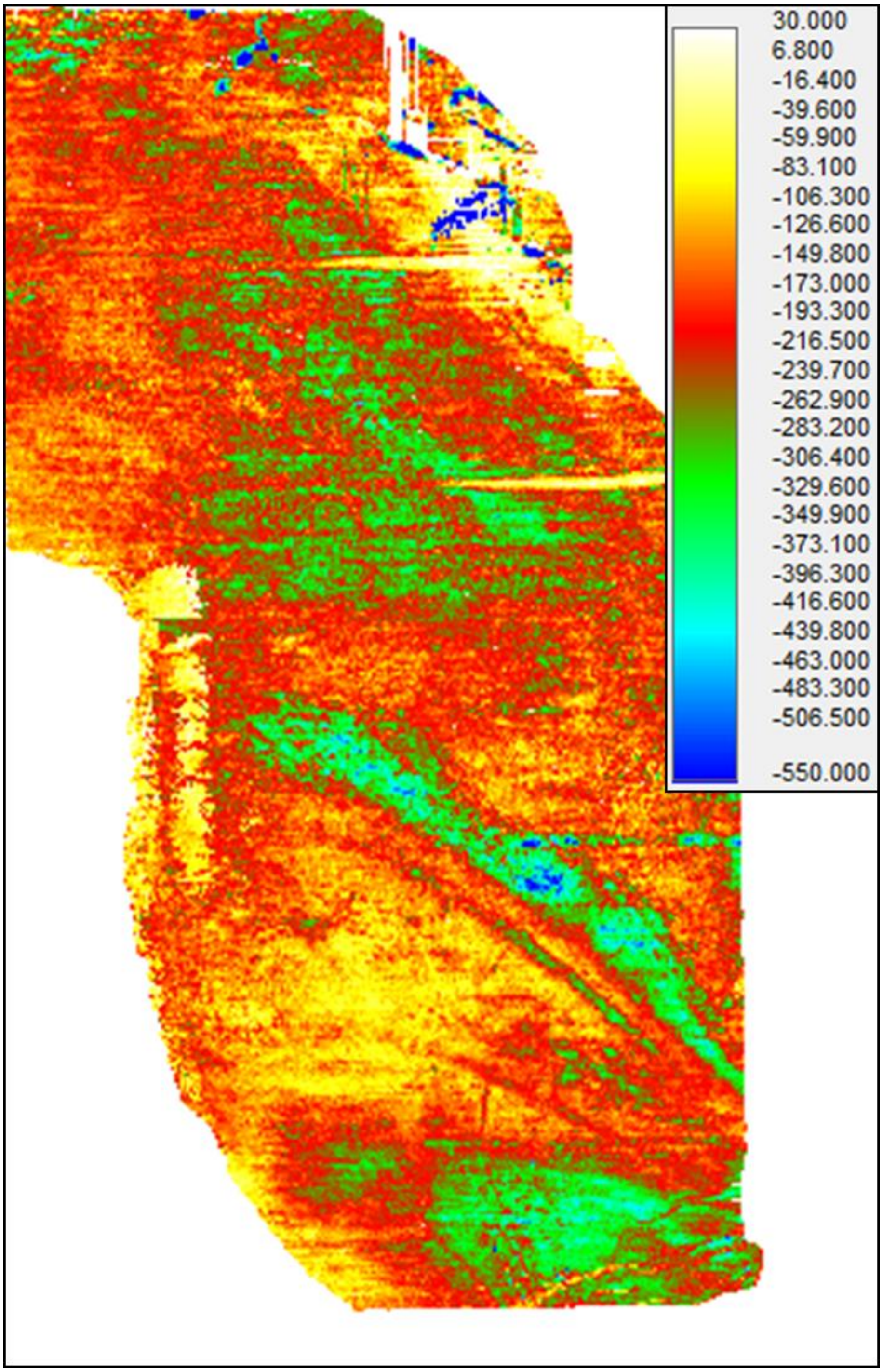

Figure A3-5. Package G VATMIN map measured in amplitude.

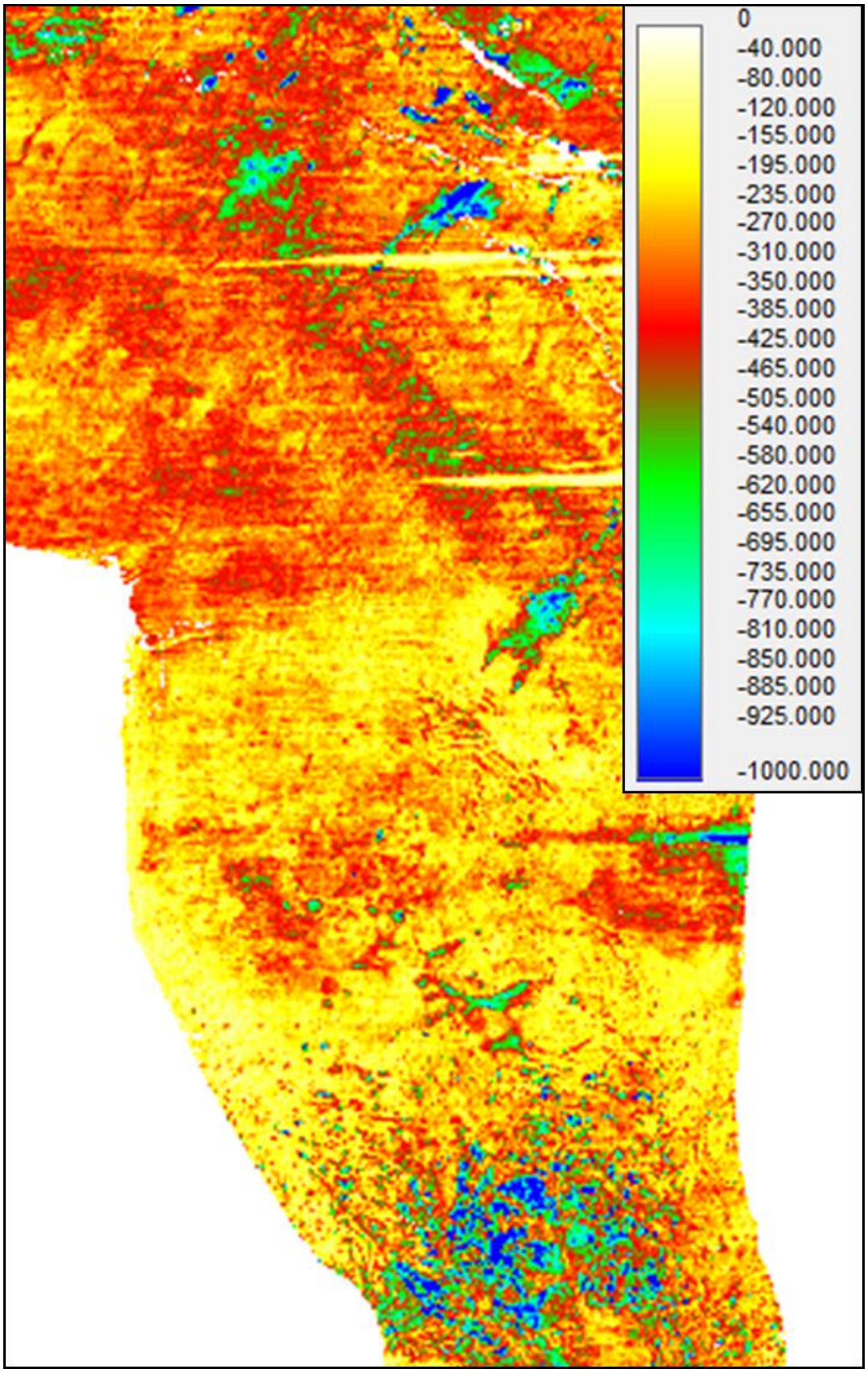

Figure A3-6. Package J VATMIN map measured in amplitude.

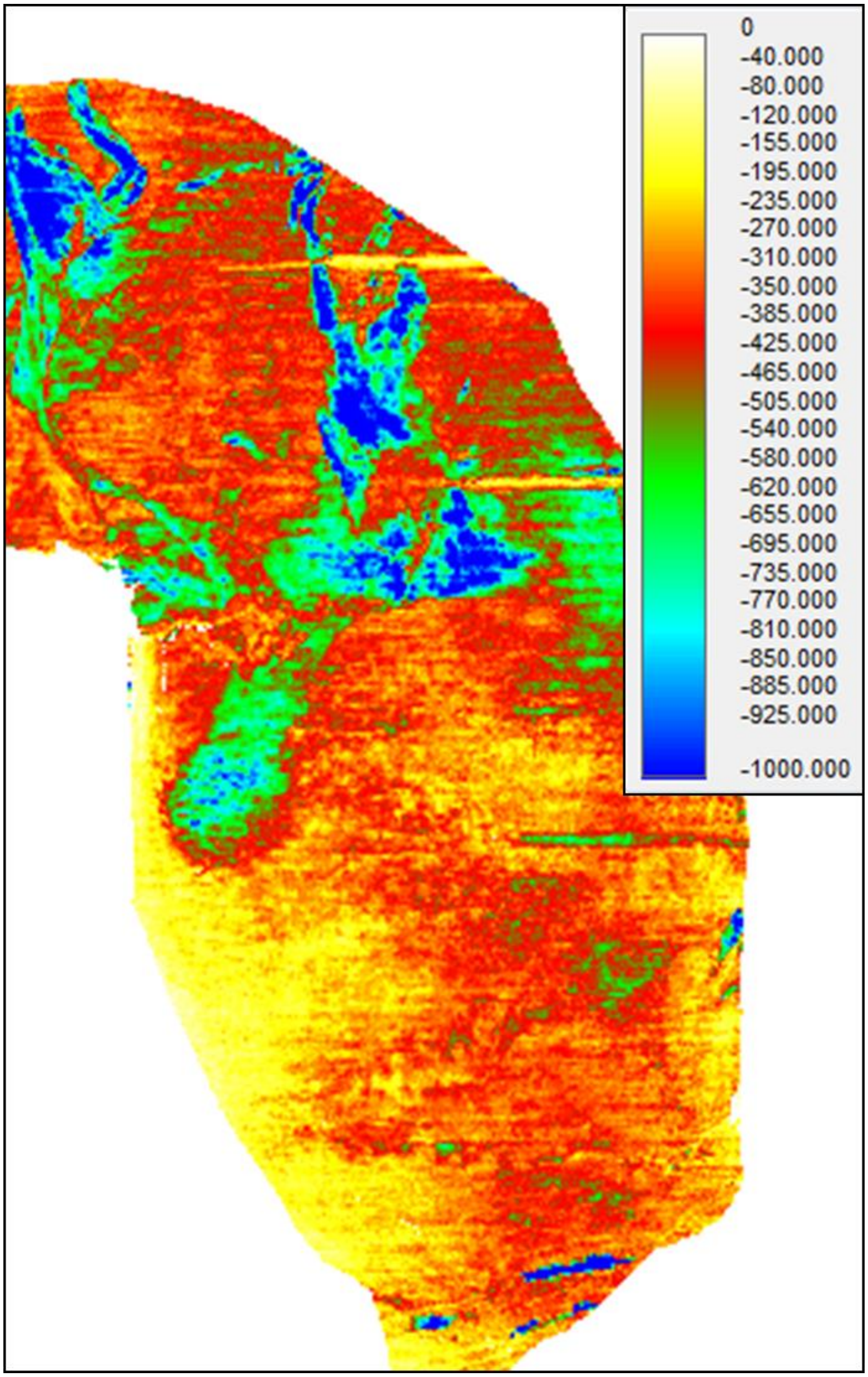

Figure A3-7. Package K VATMIN map measured in amplitude.

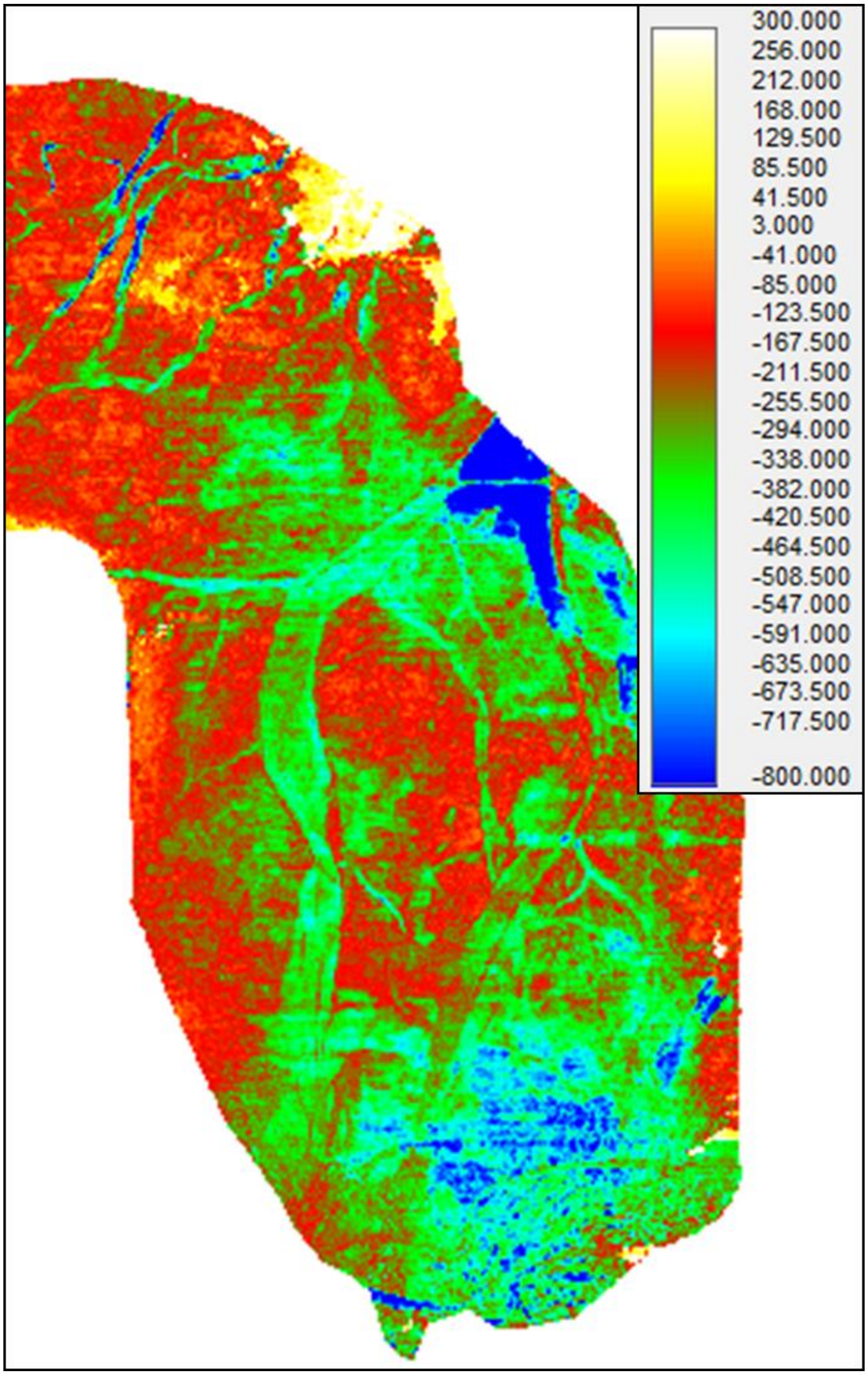

Figure A3-8. Package L VATMIN map measured in amplitude.

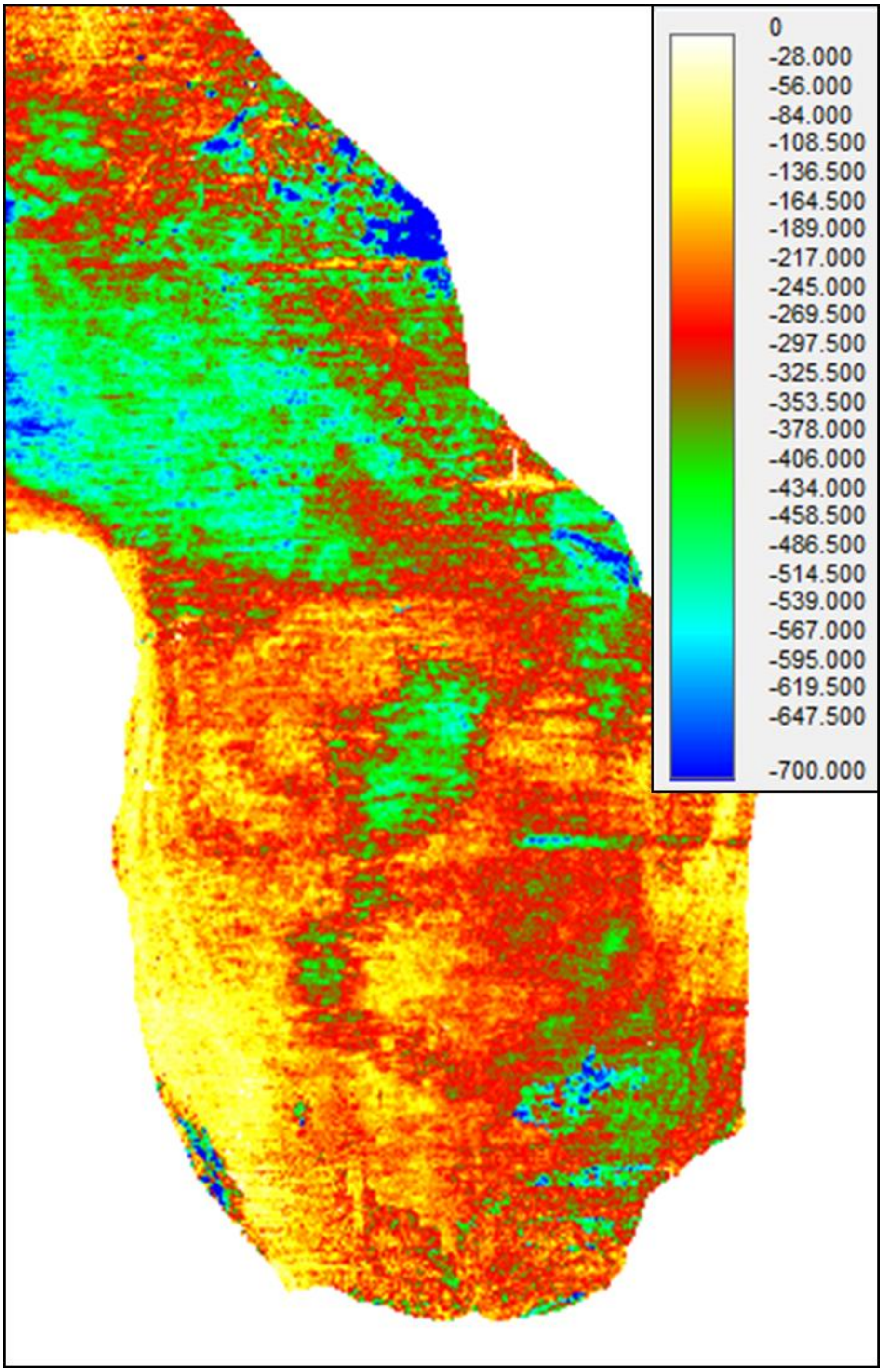

Figure A3-9. Package M VATMIN map measured in amplitude.

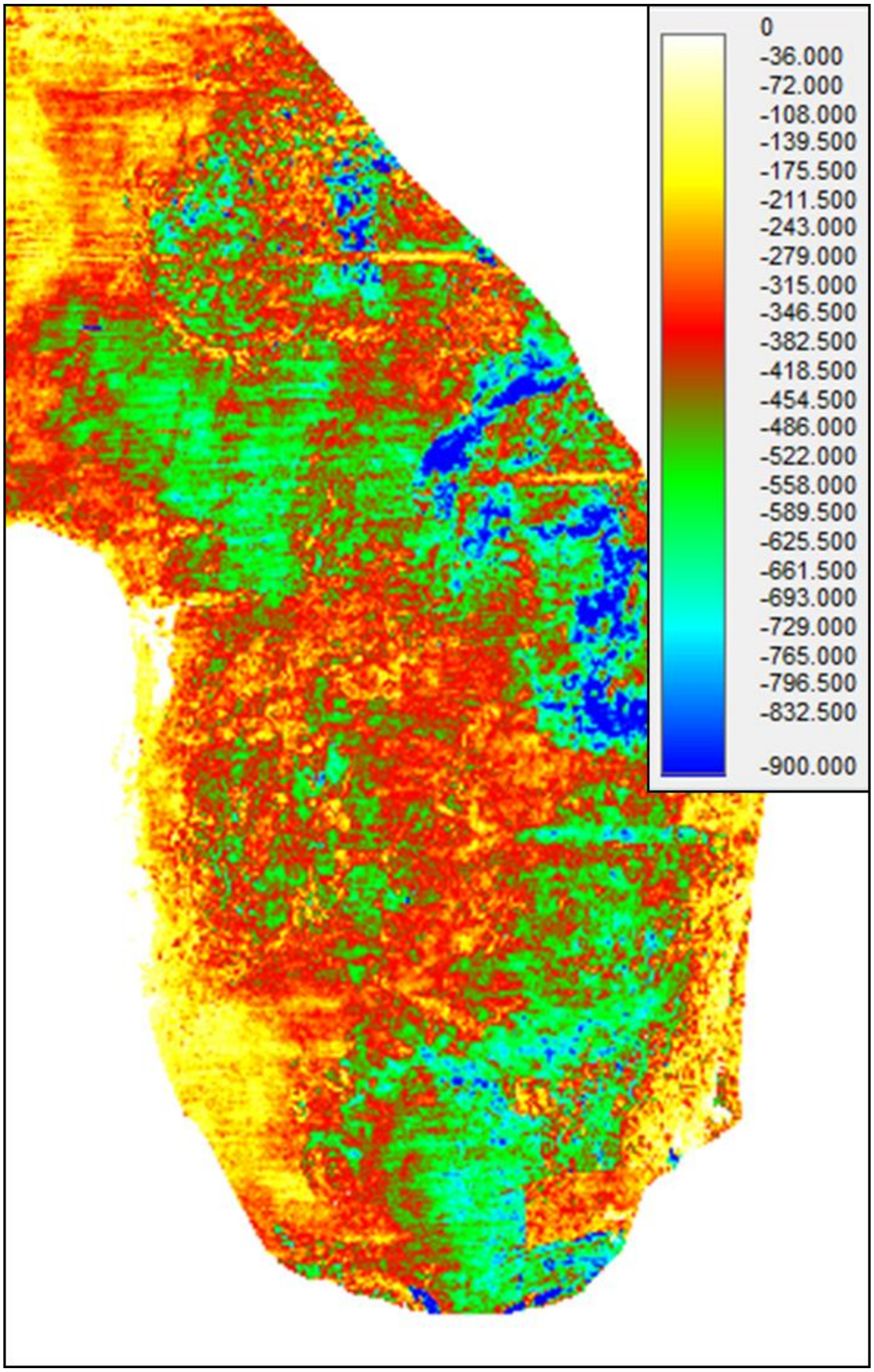

Figure A3-10. Package N VATMIN map measured in amplitude.